The Hong Kong Polytechnic University

Department of Building Services Engineering

Online Optimal Control of Multiple-Chiller Systems in Large Buildings

Sun Yongjun

A thesis submitted in partial fulfillment of the requirements

for the Doctor Degree of Philosophy

September, 2009

CERTIFICATE OF ORIGINALITY

I hereby declare that this thesis is my own work and that, to the best of my knowledge and belief, it reproduces no materials previously published or written, nor material that has been accepted for the award of any other degree or diploma, except where due acknowledgement has been made in the text.

I also declare that the intellectual content of this thesis is the product of my own work, except to the extent that assistance from others in the project's design and conception or in style, presentation and linguistic expression is acknowledged.

_____(Signature)

Sun Yongjun (Name of student)

Department of Building Services Engineering

The Hong Kong Polytechnic University

Hong Kong, P.R. China

September, 2009

ABSTRACT

Abstract of thesis entitled: Online Optimal Control of Multiple-Chiller Systems in Large Buildings

Submitted by : Sun Yongjun

For the degree of : Doctor of Philosophy

at The Hong Kong Polytechnic University in September, 2009

This thesis investigates the online optimal control of multiple-chiller systems in large buildings with enhanced robustness and cost efficiency. The control mainly includes chiller sequencing control, optimal start control and electrical demand limiting control. New strategies in the three subjects are proposed and validated on a dynamic simulation platform as well as using site data.

In the first subject, i.e. chiller sequencing control, three methods are developed to enhance its robustness and reliability. Firstly, the data fusion method is proposed to obtain a more accurate and reliable cooling load measurements by combining the complementary advantages of two different load measurements. Secondly, a simplified model is developed to online compute the varying maximum cooling capacity of individual chiller. Thirdly, an online sensor fault detection and diagnosis (FDD) strategy is developed to ensure that the sensors used in the direct measurement

work healthily.

In the optimal start control, a model-based strategy is proposed for minimizing the energy consumption of the central chilling plant in the morning start period. The model-based strategy is realized in two steps. The first step is to identify a feasible set for the operating chiller number. The second step is to estimate the pre-cooling lead time using the simplified building model for each number inside the feasible range identified, and calculate the corresponding energy consumption.

In the subject of electrical peak demand limiting control, a strategy of minimizing the monthly electricity bill is proposed via utilizing the building thermal mass. Previous studies can not to achieve maximized monthly cost saving because the demand cost reduction may be largely/completely traded off by the energy cost rise. Therefore, a strategy taking full consideration of the relationship is developed. The strategy consists of two phases. The first one is to predict a suitable monthly peak demand threshold. In the second phase, the extended pre-cooling lead time will be determined based on the difference between the demand threshold and the predicted daily peak demand.

The developed strategies are validated through case studies, which show the satisfactory performances.

PUBLICATIONS ARISING FROM THIS THESIS

Journal Papers Published

2008 G.S. Huang, S.W. Wang, Y.J. Sun, Enhancing the reliability of chiller sequencing control using fused measurement of building cooling load, HVAC&R Research 14 (6) 941-958.

2009 G.S. Huang, S.W. Wang, F. Xiao, Y.J. Sun, A data fusion scheme for building automation systems of building central chilling plants, Automation in Construction 18 (3) 302-309.

2009 Y.J. Sun, S.W. Wang, G.S. Huang, Chiller Sequencing Control with Enhanced Robustness for Energy Efficient Operation, Energy and Buildings, doi:10.1016/j.enbuild.07.023.

2009 Y.J. Sun, S.W. Wang, G.S. Huang, Online Sensor Fault Diagnosis for Robust Chiller Sequencing Control, International Journal of Thermal Sciences, doi:10.1016/j.ijthermalsci.10.003.

2009 Y.J. Sun, S.W. Wang, G.S. Huang, Model-based Optimal Start Control Strategy for Multi-chiller Plants in Commercial Buildings, *Building Services Engineering Research & Technology*, in print.

Journal Papers Prepared/Submitted

2009 Y.J. Sun, S.W. Wang, G.S. Huang, A Demand Limiting Strategy for Maximizing Monthly Cost Savings of Commercial Buildings, Prepared.

Conference Paper

2008 S.W. Wang, W.K. Pau, Y.J. Sun, X.H. Xu, Enhanced Measurement of

Cooling Load Using Data Fusion in Air Conditioning Systems, *The 4th International Conference on Intelligent, Green & Energy Efficient Building*, Beijing, China.

2008 S.W. Wang, Y.J. Sun, G.S. Huang, N. Zhu, A Control Scheme of Enhanced Reliability for Multiple-chiller systems Using Fused Building Cooling Load Measurement, *The 8th International Conference for Enhanced Building Operations (ICEBO)* .

2009 G.S. Huang, Y.J. Sun, S.W. Wang, Robust chiller sequencing control for central chilling plant, *The 7th Asian Control Conference,* Hong Kong. [Nominated for the best application paper]

2009 S.W. Wang, Y.J. Sun, G.S. Huang, F. Xiao, Application of Data Fusion and FDD for Improving the Performance of Chiller Sequencing Control, *The 6th International Symposium on Heating, Ventilating and Air Conditioning* , Nanjin, China.

2009 S.W. Wang, Y.J. Sun, G.S. Huang, Online Optimal and Cost-Effective Control of Multiple-Chiller Plants in Large Buildings, *The International Conference in Sustainable Development in Building and Environment*, Chongqing, China.

ACKNOWLEDGEMETNS

My sincerest gratitude goes to my supervisor, Shengwei Wang, Chair Professor, for his patient supervision, stimulating encouragements and continuous support during the course of this research. Also, I would like to express my heartfelt appreciation to my co-supervisors, Linda Fu Xiao, Assistant Professor, for her constructive suggestions and indeed helps. My special thanks go to Dr. Gongsheng Huang for his selfless assistance and friendly cooperation. Without your precious supports, this research may never be finished in time.

I am truly grateful to Mr. Waikeung Pau, Sun Hung Kai Real Properties Limited for his essential support to this research work. I would also like to thank all my colleagues in the research team. Their talents and diligence always inspire and encourage me to be better.

Lastly, I would like to deliver my deepest appreciation to my beloved wife, Jia Zhang, not only for her understanding and encouragement, but also for her taking good care of our acute daughter alone in the past years. I would also like to dedicate this thesis to my parents for their unconditional trust and support in my life.

TABLE OF CONTENTS

Page

LIST OF FIGURES

Page

LIST OF TABLES

Page

NOMENCLATURE

a	Coefficient
A_1	Impeller entry area (m^2)
b	Outlier or systematic error
c	Coefficients
c_p	Specific thermal capacity (kW/kg·K)
C	Capacitance Parameter
CS	Cost saving (HKD)
COP	Coefficient of performance
db	User defined dead band (kW)
e	White noise of measurement
$\hat{e}$	Coefficient
E_m	Threshold to distinguish the outliers (kW)
E_{dr}	Error between the direct measurement and the actual one(kW)
E_{fr}	Error between the fused measurement and the actual one(kW)
$\tilde{E}_f$	Calibration to indirect cooling load measurement (kW)
$\underline{E}_f$	Lower boundary of $\tilde{E}_f$ (kW)
$\overline{E}_f$	Upper boundary of $\tilde{E}_f$ (kW)
EC	Energy consumption (kWh)
F	Fault status

h	Specific enthalpy (kJ/kg)
h_{fg}	latent heat at reference state pressure (kJ/kg)
H	Pump pressure drop (kPa)
I_{global}	Global solar radiation
J	Energy consumption of the chiller plant when
K	Process gain
L_{pipe}	Pipe length (m)
L_{pum}	Number of healthily operating pumps
md	Moffat distance
M	Water flow rate (L/S)
$\tilde{M}$	Reconstruct water flow rate (kg/s)
MCC_0	Maximum cooling capacity of individual chillers (kW)
MCC	Calibrated maximum cooling load (kW)
N_0	Number of currently operating chillers
N_c	Optimal number of operating chillers
N_{pum}	Number of operating pumps
N_w	Length of moving window
Num	Number
p	Pressure (kPa)
P	Power consumption (kW)

P_{com}	Chiller compressor power consumption (kw),
PD	Electrical peak demand (kVA)
PLR	Part load ratio
q_m	Mass flow rate of the refrigerant (kg/s)
q_v	Maximum volumetric flow rate (L/s)
Q	Cooling load or heat transfer rate (kW)
$\vec{Q}$	Cooling load vector
$\tilde{Q}$	Reconstructed cooling load (kW)
R	Gas constant (kJ/K·mol)
RH	Relative Humidity
S	Sum of cooling load measurements (kW)
ST	Switch threshold (kW)
T	Temperature ℃
$\tilde{T}$	Reconstructed temperature (℃)
U	Vane leading edge velocity (m/s)
V	Absolute velocity (m/s)
V_r	Relative velocity (m/s)
W_{Rad}	Wall absorbed radiation
x	Measurement of temperature or relative humidity
$\overline{x}$	Predicted value of x.

$\hat{x}$	Calibrated value of $\overline{x}$.
X	Sum of measurement x.
$\overline{X}$	Predicted value of X
Z	Compressibility factor of the refrigerant
	Subscript
1,2	Inlet, outlet of compressor
a	Air
act	Actual value
amb	Ambient
avg	Average
AC	Air-Conditioning
Bld	Building
cd	Condensing
ct	Cooling tower
cp	Constant speed pump
chi	Chiller
conv	Convection
const	Constant
dm	Cooling load direct measurement
D	Diameter of the impeller (m)

ei	External wall
ev	Evaporating
f	Fused load measurement
fr	Fresh air
fan	Supply fan
g	Gaseous refrigerant
hp	Header pipe
i	i^{th} item
in	Indoor
im	Cooling load indirect measurement
k	Time instant
l	Liquid refrigerant
la	Latent heat
md	Minimum down time
mu	Minimum up time
max	Maximum
mes	Measurement
min	Minimum
mon	Month
nom	Nominal value

opt	Optimal
on,*off*	Online, offline
over	Exceeding the temperature set-point by 0.4 ℃
occup	Occupant
pre	Prediction
prv	Previous
pum	Pump
rf	Roof
rej	Heat rejection
rtn	Return
set	Set point
sol	Solar air
sum	Sum
sup	Supply
sys	System
tot	Total
Thres	Threshold
vp	Variable Speed Pump
w	Water
win	Window

Superscripts

i	i^{th} item,
r	True value of the measurements
*	Calculated value
'	Ideal result

Greeks

α	Loss factor of electromechanical losses
$\hat{\alpha}$	Positive constant
$\widehat{\alpha}, \widehat{\beta}$	Unit prices for electrical demand and energy separately
β	Constant part of electromechanical losses (kW)
β_1	Vane angle (Rad)
δ	User defined constant for the transient interval (kW)
$\hat{\delta}$	Calculation uncertainty or disturbance
δ_h, δ_l	Scale factors
ε	Positive threshold for faulty measurements
$\hat{\varepsilon}$	Wall absorption coefficient;
φ	Nonlinear function
γ	Confidence degree
$\tilde{\gamma}$	Reconstructed confidence degree
η	Efficiency

λ	Calibration factor in the transient interval
μ_1, μ_2	Threshold for confidence degree calculation
ν	Refrigerant specific volume (m^3/kg)
ρ	Density (kg/L)
σ	Standard deviation
$\hat{\sigma}$	Control deviation.
ς	Time delay
τ	Time period
ζ	Calibrating factor for chiller maximum cooling capacity
Δ	Variation or uncertainty
Γ	Time constant
$\hat{\Gamma}$	Error due to the parameter deviation
Λ	Pipe intersect area (m^2)
Ω	model bias (kW)
$\hat{\Omega}$	External wall heat transfer coefficient

CHAPTER 1 INTRODUCTION

1.1 Motivations

The multiple-chiller systems are usually equipped in high rising commercial buildings. The control of them mainly includes the chiller group control, cooling tower control, water pump control, etc. Especially, the chiller group control is of great significance because it is the most sophisticated and power consuming component and its control result is usually taken as an important influential factor for the other related components control [Schneider, 1981]. For example, chiller operating number can simply be used to determine the number of operating cooling towers in practice. In this thesis, the online optimal control of multiple-chiller systems mainly focuses on the control of the chiller group. The control includes chiller sequencing control, chiller optimal start control, and demand-limiting control. Chiller sequencing control aims to switch on an appropriate number of operating chillers for satisfying the varying building cooling load with an energy efficient operation [ASHRAE 2007]. The chiller optimal start control is used to recover the indoor environment to a desired level prior to the occupation of buildings by scheduling the chiller morning start-up operation. The energy consumption can be minimized by choosing an appropriate operating chiller number and related lead time. The demand-limiting control is to restrain the short-term demand peak to an appropriate predefined threshold value for minimizing monthly electric bill. In this case, the operating chiller number is required

to be controlled for charging and discharging the cooling stored mass, *e.g.* building thermal mass.

Thanks to the comprehensive building automation systems (BASs) equipped in the large commercial buildings, the possibility of enhancing and optimizing the operation and control of multiple-chiller system is allowed. In the last two decades, tremendous efforts have been made to develop optimal control strategies for multiple-chiller systems thanks to the growing scale of BAS integration and the convenience of collecting a huge amount of online operation data by the application of BASs [Ma, 2008]. A number of research papers and technical articles/reports have been yielded due to these efforts [Zaheer-uddin and Zheng 2000; Lu et al. 2005; Nassif et al. 2005; Sun and Reddy 2005; Braun 2007]. The conclusions drawn in these studies demonstrate that a substantial amount of energy/costs in multiple-chiller systems can be saved when optimal control strategies are used. Even a small overall increase in the operating efficiency would result in significant energy or cost savings. Other benefits can also be achieved including enhanced control robustness, improved thermal comfort of occupants, reduced maintenance costs, etc. However, most of existing optimal control strategies are either too mathematical or lack generality since the requirements and constraints of practical applications, *i.e.* control reliability, computational cost, memory demand, etc, were not cautiously considered during the development of these optimal control strategies [Wang and Ma 2008].

Inappropriate control and operation of multiple-chiller systems can cause substantial energy and cost waste. For example, if chillers being switched online are more than necessary, they will operate at a low efficiency due to the low part load ratio and result in significant energy and cost waste. Besides the energy and cost waste, improper chiller plant control and operation may cause serious system reliability problems as well as great indoor thermal comfort sacrifice. For instance, the developed building load based chiller sequencing control strategies usually perform poorly in terms of robustness. The major reason is that the building cooling load usually cannot be accurately measured due to the small temperature difference between chilled return and supply water (e.g. 5 ℃ or even less), which causes cooling load measurement vulnerable to temperature measurement uncertainties. 0.5 ℃ uncertainty in each temperature measurement can result in 20% relative error of overall cooling loads measurement if temperature difference is taken as 5℃. No reliable chiller sequencing control can be expected based on such great load deviation. Meanwhile, the insufficient supplied cooling will cause serious occupants complaints when less than necessary chillers operate due to inaccurate cooling load measurements.

In practice, proper and energy efficient operation of multiple-chiller system is a difficult engineering issue. Due to the increasing number of high-rise buildings and growing concerns on building energy consumptions/operating costs, the configurations and design philosophies of chiller plants are becoming more and more sophisticated. The difficulties related to optimal control and operation of these

complex multiple-chiller systems are therefore increased accordingly [Ma, 2008]. How to achieve reliable and energy efficient control and operation of multiple-chiller system to minimize their energy inputs/operating costs while providing the robust control performance is one of the major challenging issues encountered by building professionals and building operators nowadays.

Therefore, the research in this thesis will focus on developing online optimal control strategies for chiller sequencing control, optimal start control, and demand limiting control, which are intended to be applied to a complex central chilling system equipped in the International Commerce Center (ICC) in Hong Kong. These online applicable strategies are expected to produce more efficient and reliable operations as well as cost savings with acceptable indoor thermal comfort. The implementation guidelines for applying the developed strategies are also provided.

1.2 Aim and Objectives

Online optimal control strategies of multiple-chiller systems in large buildings play important roles in reducing the overall energy consumption, in electricity bill of buildings, and in well satisfying the indoor thermal comfort requirements. However, the previous related studies in this field are far from sufficient. Therefore, the development and validation of online optimal multiple-chiller system control strategies with satisfying performance in terms of energy consumption, operation cost, and control accuracy and reliability is the main aim of this research. The aim can be accomplished by addressing the following major objectives:

(a) Develop and validate an algorithm for solving the long lasting inaccuracy problem in practical cooling load measurement by adopting data fusion technique. It is expected to obtain more accurate and reliable fused cooling load measurements after the temperature measurement uncertainties are alleviated or removed. Meanwhile, the quality of the fused cooling load will be evaluated systematically.

(b) Develop and validate a chiller sequencing control strategy for control robustness enhancement and energy efficiency. The proposed strategy is intended to satisfy the requirements and constraints of practical applications (i.e., control accuracy, control reliability, computation load, etc.) and can be easily implemented.

(c) Develop and validate a sensor fault detection and diagnosis (FDD) method which can promptly and effectively isolate faulty sensors in cooling load direct measurements. The healthy sensor operation can guarantee the high quality of fused cooling load measurements and further enhance the robustness of cooling load based chiller sequencing control.

(d) Propose and validate an optimal chiller start control strategy for energy efficiency. The strategy intends to include chiller operating number as an influential factor as well as the outdoor and indoor temperatures. It targets at generating the optimal operating chiller number and its related lead time which cause the least energy consumption in this start period.

(e) Develop and validate a demand limiting strategy which is used to minimize

the monthly electricity bill. The strategy will fully consider the relationship between the cost rise from the extra energy consumed for limiting the electrical peak demand and the cost saving from the related demand reduction.

(f) Develop the associated software tools and provide the implementation guidelines for online application of these developed optimal control strategies.

1.3 Organization of the Thesis

The whole thesis is divided into 10 chapters. The main content of each chapter is presented as follows.

Chapter 1 outlines the motivation of the research by presenting the need of online optimal control of multiple-chiller systems to enhance the energy or/and cost efficiency, the HVAC system control robustness and the indoor thermal comfort. The main aims and objectives are also included in the chapter.

Chapter 2 presents a brief review of the previous related works about developments and applications of online optimal control strategies of multiple-chiller systems, and describes the research gaps which are intended to be bridged in this thesis. The analysis and evaluation of the main methods of online optimal control for multiple-chiller systems and optimization techniques developed and/or utilized in the HVAC field are provided.

Chapter 3 describes a super high-rising building and its complex central chilling system. Based on this complex central chilling system, a dynamic simulation platform is constructed. The major component interconnections to construct this dynamic simulation platform are presented. The following developed online optimal control strategies are tested on this dynamic simulation platform to analyze and evaluate their performances in terms of control robustness and energy efficiency. These validated control strategies are intended to be programmed into dynamic link libraries (DLLs) that will be used in the building automation (BA) system of the under construction ICC commercial building.

In chapter 4, the data fusion technique has been adopted for solving the inaccuracy problem of cooling load direct measurement in practice. The two different cooling load measurements and their characteristics are analyzed respectively. The detailed mathematical processes for merging these two load measurements are provided when different sensor measurement uncertainties (i.e. noises, outliers and systematic errors) occur. The algorithms for calculating the associated confidence degree are as well illustrated. In the case study, the performance of the developed data fusion method is evaluated. A dedicated section is used to discuss the application issues including the main steps for practical usage and approach of parameters fitting.

Chapter 5 presents a robust chiller sequencing control strategy in which the fused cooling load and calculated chiller maximum cooling capacity (MCC) are used instead of cooling load direct measurement and constant chiller rated capacity. The

development of a simplified model for online calculating the chiller MCC is introduced. The approach of using the confidence degree from the data fusion process to calibrate the computed MCC for energy saving is also provided. The related case studies are conducted to validate the proposed chiller sequencing control strategy and its related application issues are also discussed in the chapter.

Chapter 6 focuses on developing and validating a sensor fault detection and diagnosis (FDD) approach. The FDD approach is used cooperating with the cooling load fused measurement algorithm. For faults occurring in different sensors (i.e. flow meter and temperature sensors), different diagnosing criteria are proposed. In case studies, typical faults including slow drafts and step changes are investigated in testing the efficiency of the developed strategy. The validation results are presented as well.

In Chapter 7, a model-based optimal start control strategy is proposed. Two control variables, including the recovery capability (i.e. number of operating chillers) and pre-cooling lead time (i.e. the time from the moment of chiller start up to the moment that indoor temperature lower down to a desired level), are optimized to minimize the entire system energy consumption in the chiller start period. A case study is conducted to validate the proposed optimal start control strategy. The validation results and related application issues are provided in the chapter as well.

Chapter 8 presents a demand limiting strategy of minimizing the building monthly electricity bill. In this strategy, approach for predicting a suitable monthly peak

demand threshold is firstly proposed. A new algorithm for lowering down the daily peak demand to a predetermined threshold by using the building thermal mass is developed. Case studies are performed to validate the proposed strategy.

Chapter 9 presents the software tools and implementation guidelines for applying the proposed optimal control strategies in practice. An overview of the application software system to implement the online control software packages of the proposed strategies is provided.

Chapter 10 summarizes the work conducted in this thesis, and gives recommendations for future research in the related areas.

CHAPTER 2 LITERATURE REVIEW

A typical control schedule for multi-chiller systems is illustrated as Fig. 2.1, which consists of three modes: optimal start control in pre-cooling period, sequencing control as well as demand limiting control in occupied period and off-working control. Hence, this chapter gives literature reviews of the research and developments related to the controls mentioned above and identify associated research gaps need to be bridged. The fills of these research gaps help in developing more effective control strategies.

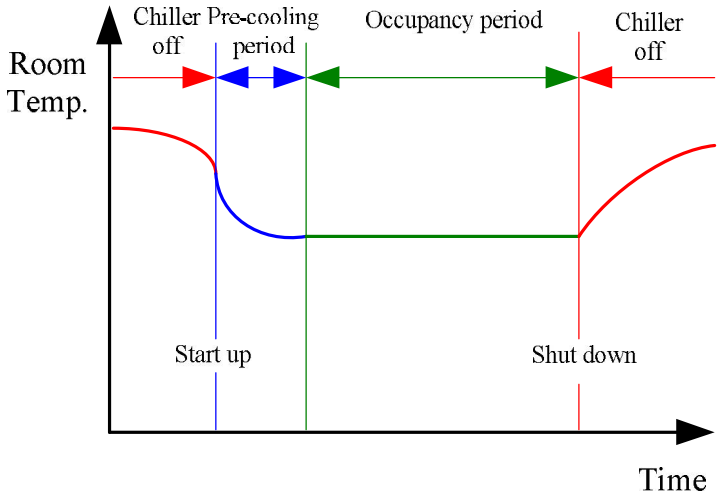

Figure 2.1. Chiller plant operation schedule

Section 2.1 specifies a long lasting application problem for cooling load measurement and presents a fusion technique which is used to solve the problem. A review of data fusion technique is as well provided. In Section 2.2, the previous studies of chiller sequencing control including their strengths and limitations are reviewed and a robustness enhanced chiller sequencing control strategy is provided.

In Section 2.3, the main fault diagnosis methods are categorized and their advantages and disadvantages for practical application are analyzed. In this section, an intention of developing a new online sensor fault diagnosis approach for strengthening the chiller automatic control performance is presented based on data fusion result introduced in section 2.1. Section 2.4 provides a review of optimal start control strategies in HVAC system. The main drawback of the existing studies is analyzed and therefore a new model-based optimal start strategy is proposed for overcoming the limitation. In Section 2.5, a review of the previous demand limiting control strategies in the passive and active commercial buildings is provided. A brief assessment of the existing strategies is analyzed and the main shortcoming of them is presented. Thus, a novel demand limiting strategy based on the cooling load prediction is proposed for minimizing the monthly electricity bill. A summary of this chapter is given in Section 2.7.

2.1 Cooling Load Measurement

Accurate and reliable building load measurement is essential for robust chiller sequencing control, building air-conditioning system performance monitoring and optimization [Wang and Cui 2005; Xu and Wang 2008]. However, the automatic chiller sequencing control of multiple-chiller systems in practice is often switched to manual control due to inaccurate and unreliable measurement of building total cooling load [Kwan, 2001]. Measurement noises, outliers and systematic errors have a significant influence on the measurement of the building cooling load since the

differential temperature is usually small, e.g. 3 or 4°C. The small temperature measurement uncertainties may lead to a large deviation of total cooling load calculation, usually up to 30% [Kwan, 2001]. Reliable building air-conditioning system performance monitoring and control optimization were seriously affected if measurement errors exist [Yu and Chan, 2002; Wang et al., 2002, Du and Jin 2007]. Therefore, accurate and reliable measurement of building cooling load is of tremendous significance in system performance monitoring and control optimization.

Available information about the cooling load can be obtained from two different sources: "direct measurement" and "indirect measurement". "Direct measurement" is obtained simply by measuring the differential temperature of chilled water return and supply temperature and the total water flow rate, *i.e.* $Q = c_{pw}\rho_w M_w \left(T_{w,rtn} - T_{w,\text{sup}}\right)$. "Indirect measurement" uses a simplified inverse model of chillers, which establishes a relationship function between the cooling load and the instantaneous chiller electrical power input and the chiller operation condition variables. Both direct and indirect measurements might not be reliable or accurate in practice due to uncertainties associated with the measurement instruments and the chiller inverse model. In this case, data fusion technique is adopted to improve the total building cooling load measurement of building automation systems.

Data fusion is a method which combines data derived from independent/different information sources such that the resulting information is more accurate, complete or dependable than when these sources were used individually [Ruhm, 2006].

Measurement data are easily corrupted by two types of uncertainties: random errors and outliers or systematic errors (systematic errors are a kind of outliers but last for a longer time). The essential objectives of data fusion are to remove the outliers and systematic errors and to reduce the influence of noises. General schemes for data fusion and evaluation of the uncertainties associated with the final merged data can be described as follows [Urbanski and Wasowski, 2003]: 1) description and estimation of the uncertainties associated with each individual information source, 2) construction of appropriate aggregation operations to combine the outputs from different information sources, and 3) evaluation of the joint uncertainty of the different information sources and the propagation of uncertainty through merging processes.

Current fusion methods are mainly based on statistical theory. Different estimators within the framework of statistics are available for data fusion. The most popular ones are: Minimum Variance Estimator (MVE), Maximum Likelihood Estimator (MLE) [Ozyurt and Pike, 2004], and estimator based on Bayes' rule [Grewal, 2001]. These methods of statistical data fusion always lead to a weighted average of the observations from different sources. The presence of outliers and systematic errors sometimes invalidate the theoretical basis for statistical data fusion procedures, and thus it is essential that they are eliminated before the application of statistical data fusion [Abu-el-zeet and Becerra, 2002]. For this reason, a number of methods have been proposed to detect the presence of outliers and reduce their impact on the rest of the data or remove them completely [Soderstrom, Himmelblau and Edgar, 2001].

2.2 Chiller Sequencing Control

Chiller sequencing control has been widely used in centralized chilling plants with multiple-chillers, which aims to provide economical loading/unloading of chillers, i.e. to make the operating chillers to achieve an overall coefficient of performance (COP) as high as possible while fulfilling the demanded cooling load [Hackner et al. 1984; Honeywell 1997; Chang et al. 2005]. It determines how many and which chillers are to be put into operation according to instantaneous building cooling load. Since over one third of total energy consumption in most of air-conditioned commercial buildings is used by chillers in the climate like in Hong Kong [Lam 2000], chiller sequencing control plays an important role for the energy efficiency in building automation systems.

Various chiller sequencing control strategies have been developed for different buildings with different complexity in terms of control parameters and equipments. The differences in these strategies mainly lie in how the instantaneous building cooling load is measured or estimated. Four typical methods are commonly adopted in application, including return chilled water temperature-based sequencing control, bypass flow-based sequencing control, direct power-based sequencing control and total cooling load-based sequencing control [Honeywell 1997]. In principle, the total cooling load based sequencing control is the best approach for chiller sequence control [Honeywell 1997]. In this method, the optimal number of the chillers, which

are put into operation, is mainly determined by the building cooling load measurement and the chiller maximum cooling capacity

$$N_{chi} = \varphi\left(Q, Q_{\max}\right) \tag{2.1}$$

The building cooling load is generally measured using the chilled water flow rate and the differential temperature between the chilled supply water and the return water, i.e. cooling load direct measurement. Because the differential temperature cannot be measured accurately, the cooling load direct measurement-based sequencing control does not operate properly in practical applications [Kwan 2001].

The improvement of building cooling load measurement will surely enhance the reliability of the chiller sequencing control. Data fusion has therefore been used to improve the measurement of building cooling load. The fusion algorithm is to combine the complementary advantages of the cooling load direct measurement with those of the cooling load indirect measurement. The details of the fusion algorithm will be illustrated in Chapter 4. The quality of the fusion algorithm has been systematically evaluated using a confidence degree of the fused measurement, which can also be used to identify measurement outliers or systematic errors in the direct measurements. The concept of chiller sequencing control is illustrated in Figure 2.2.

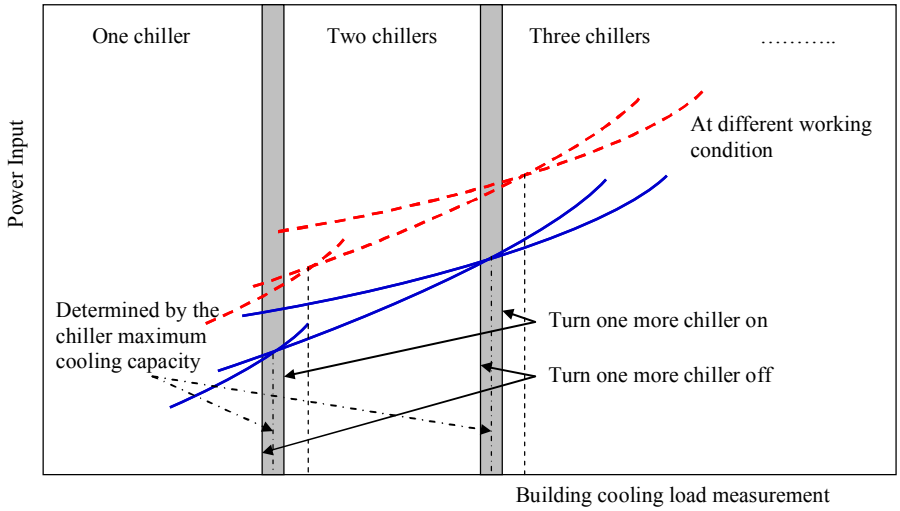

Figure 2.2. Total cooling load based chiller sequencing control

Traditionally, the chiller maximum cooling capacity is assumed to be constant in chiller sequencing control, being equal to the chiller rated cooling capacity. However, the chiller maximum cooling capacity may vary greatly with the chiller operating conditions [Gordon et al. 2000; Ding and Fu 2005], such as the chiller evaporating temperature, the chiller condensing temperature, the suction temperature of chiller compressor etc. Therefore, even if the cooling load is measured exactly, it is still possible that the number of the chillers in operation given by the chiller sequencing controller is not appropriate due to the use of an inaccurate chiller maximum cooling capacity. As a consequence, the number will be either less than necessary (the cooling is deficient resulting in occupants' thermal discomfort) or more than necessary (the cooling is excessive resulting in energy waste).

In this thesis, a new strategy is proposed to improve the reliability of the chiller sequencing control and energy consumption efficiency. In addition to the use of the fused measurement of the building cooling load, a simple but reliable model of

chillers is developed to online identify the maximum cooling capacity of individual chillers. The chiller maximum cooling capacity is calibrated when the direct measurement suffers from systematic errors.

2.3 Online Sensor Fault Detection and Diagnosis

As mentioned in Section 2.1, the direct measurement of cooling load is usually corrupted by noises, outliers and systematic errors or other types of sensor faults. These faulty measurements may lead to inaccurate or even unreasonable cooling load calculation which finally severely influences the accuracy and reliability of chiller automatic control (e.g. chiller sequencing control). Therefore, it is of great significance for the building automation systems (BAS) to rapidly detect and diagnose these sensor faults for a better chiller automatic control performance in terms of supplying sufficient cooling with less energy consumed.

For detecting and diagnosing various faults of facilities and sensors in HVAC systems, many studies [Piette et al 2001; Comstock et al. 1999; Peitsman 1996; Rossi 1997; Yoshida et al, 1996, Ngo, 1999, House et al, 2001, Dexter, 2001 and Lee et al,1997] developed different kinds of strategies which, generally speaking, can be grouped into two categories, i.e. model based and model free. For the model based fault detection and diagnosis (FDD) methods, one major limitation is the complex process to set up an explicit model [Wang and Cui, 2005]. The model may be physical models, data driven models (black box models) or semi-physical model (grey box models). Although physical model can obtain the best final results of FDD, some

approximations need to make for solving the differential equation in the dynamic ones. These approximations will corrupt their accuracy. Further more, it is not convenient for the user to fit the required parameters due to the incomplete data offered by the device manufactures. Data driven models eliminate the complexity of building physical model, but the final results can not always ensure sufficient reliability and accuracy due to non-physical nature. More often, the semi-physical model need to be used for balancing the complexity of model construction and reliability of FDD results.

Model free methods do not utilize an explicit mathematical model of the target system, e.g. physical redundancy for the sensor FDD. But its applications usually are limited by the cost, space and complexity of installing of redundant sensors. Even so, several model free FDD strategies have been proposed. For instance, the limit checking method has been proved to be effective in univariate quality control [Haves, 1999]. But it will not be able to detect the fault measurements that are within the limits but do not follow the normal correlation among the variables.

For the faults occurring in sensor measurements, many methods have been specifically developed. For example, the systematic comparison and optimization method (SCOM) was proposed by Jiang and Zhu [Jiang et al, 1999] for detecting the slow drifts in sensors. Wang et al. [2002] developed a law-based strategy for sensor faults detecting, diagnosing and validating. The sensor validation and reconstruction

based on Principal Component Analysis (PCA) was developed by Wang and Chen [2004].

However, the studies about the sensor FDD strategies for online implementation are still inadequate especially for those sensors (e.g. chilled water supply/return temperature sensor) whose performance can greatly influence the final result of optimal control strategies (e.g. chiller sequencing control). Therefore, an online sensor FDD strategy for promptly diagnosing the unhealthy sensors is essential to ensure satisfactory chiller automatic control performance.

The strategy developed in the thesis presents an online sensor FDD method based on the cooling load fused result (Section 2.1) to detect and diagnose the faults occurred in the chilled water flow rate, supply and return temperature sensors. Chapter 4 specifically utilize a data fusion technique to fuse two kinds of cooling load measurement (i.e. direct measurement and indirect measurement based on a simplified inverse chiller model) into a more reliable and accurate one with an associated confidence degree indicating the quality of fused cooling load. When certain sensor faults, such as complete/partial failure or systematic errors, occur to the flow meter and/or temperature sensors, the confidence degree will stay low until the they are removed. The low confidence from the DF process is a reliable indicator of the faults occurring but without knowing which sensor suffering from faulty measurement. Therefore, an online sensor FDD method based on the generated confidence degree was proposed to further diagnose the faulty sensor measurements.

2.4 Optimal Start Control

It has been recognized that the recovery ability, outdoor temperature and indoor temperature are three most influential factors in the pre-cooling period for energy efficiency [Seem, et al., 1989]. The recovery ability refers to the amount of cooling supplied to a building and it is mainly determined by the operating chiller number. Previous related studies have demonstrated that substantial energy and cost savings can be achieved by optimizing the pre-cooling operation [Jackson, 1976; Liptak, 1975; Seem, et al., 1989]. The simplest optimal start strategy is to use two different constants of the pre-cooling lead time for hot and cold seasons individually, and these two constants are manually tuned in typical operating conditions [Levenhagen and Spethmann, 1992]. However, daily cooling load in a season may change significantly and this simple method cannot achieve satisfactory performance. The pre-cooling lead time may be too short for a high daily load or too long for a low one. To overcome this problem, advanced methods have been developed in the last decades. For example, an adaptive control strategy was proposed in [Flórez, 1987], which calibrated the length of the pre-cooling lead time using a simple semi-empirically-derived relationship function according to the current indoor and outdoor temperature measurements. Seem et al. [1989] compared seven different methods for predicting the pre-cooling/heating lead time from night setback using TRANSYS simulation, and concluded that a quadratic relationship between the pre-cooling lead time and the initial room temperature can obtain a better prediction of lead time. Capitalizing on its great representational power, artificial neural

networks (ANN) were also utilized to predict the optimal start time. For example, Yang et al [2003] developed an optimal back-propagation ANN model to determine the optimal start time for a heating system.

The recovery ability, however, was not considered in most of previous studies although it has been considered as an influential factor for energy efficiency. The reasons are probably (i) the case building is equipped with few numbers of chillers (i.e. only one or two chillers); (ii) the relationship among operating chiller numbers, the pre-cooling lead time and the indoor and outdoor temperatures is difficult to identify based on empirical studies. The influence of the recovery ability on pre-cooling is illustrated in Fig. 2.3. Larger recovery ability can speed up the pre-cooling process but with higher power consumption due to more operating chillers; while smaller recovery ability needs a longer pre-cooling lead time but with lower power consumption because of less operating chillers. The energy consumption, denoted by the shadowed area, will be different for different options.

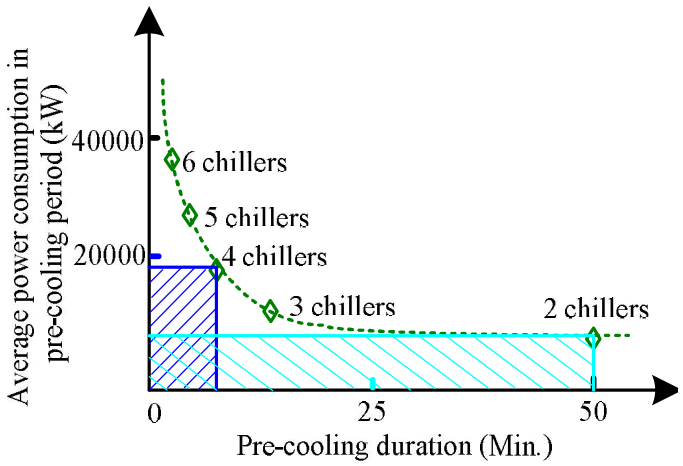

Figure 2.3. The average power consumption of a chiller plant as chiller number varies

In order to consider the recovery ability in pre-cooling operation, this thesis proposes a model-based chiller optimal start strategy for high-rise commercial buildings equipped with multi-chiller plants. The strategy is realized in two steps. The first step is to identify the appropriate range of the operating chiller number in which the building cooling load is predicted based on a simplified building model. The second step is to calculate the pre-cooling lead time and the associated periodical energy consumption for each possible operating chiller number (i.e. the number located in the range determined by the first step) using the supplied cooling and the simplified building model. The proposed strategy is able to properly select the chiller operating number and compute the corresponding pre-cooling lead time, which result in the least energy consumption. Comprehensive case studies are implemented to validate the proposed optimal start control strategy.

2.5 Demand Limiting Control

With more and more electrical equipment is used in commercial buildings, the commercial building electricity bill payment is usually large and becomes a great burden to the owner. The bill mainly consists of two parts. One is the charge for the monthly electrical peak demand which refers to the maximum energy consumed in a demand interval (e.g. 30 minutes) for a complete month; the other one is the cost for the overall energy consumption in the month. Although the price structures of different power companies are diverse, the monthly peak demand cost of a commercial building always contributes a great part to the bill, sometimes even more

than 50% [Seem, 1995]. The interest in developing efficient demand limiting control strategies for minimizing the total bill payment grows rapidly.

For reducing the monthly peak demand, different strategies have been proposed for both active and passive commercial buildings. An active building refers to the building equipped with thermal storage devices, such as chilled-water or ice storage tank. For these buildings, an additional water loop for charging and discharging the storage tank is required. In contrast, the one without such storage facilities is referred as passive building in which only the building thermal mass can be utilized for cooling storage.

For the demand limiting in active buildings, Henze et al. [1997] developed a predictive optimal controller for ice storage system. The predicted load and weather information were fed to the optimal controller for determining the optimal storage charging and discharging rate in discrete time steps. It was found that significant daily cost savings can be achieved due to the tradeoff between a slight cost increase of energy consumption and a significant cost reduction of daily peak demand under the real-time electricity price structure. Massie et al. [2004] developed a neural-network (NN) based optimal controller for ice storage systems. The controller firstly learned equipment responses to the environment and determined the necessary control settings, e.g. chilled water temperature set-points and primary loop three-way valve position. Then, it determined the control actions involving the chiller operation and ice tank charge/discharge rates that minimize total cost over a certain interval, e.g. half an hour.

A similar conclusion was drew on the daily cost saving. In [Drees and Braun, 1996], a rule-based control strategy was proposed by Drees and Braun. The near-optimal strategy was based on simple heuristics that were developed from daily or monthly simulations of central chilling systems with internal melt, area-constrained ice storage tanks. Great utility cost savings can be expected with the implementation of this strategy.

For the demand limiting in passive building, Xu et al. [2006] conducted a site study in a medium-weighted building to demonstrate the good performance of a simple demand limiting strategy for reducing the daily peak demand. The strategy involved maintaining zone temperatures at the lower comfort limit during the off-peak period. When it came to the on-peak period, the zone temperatures floated up to the upper thermal comfort limit. In order to make the set-point varying strategy more practical and applicable, Lee and Braun [2008a] proposed three different approaches, i.e. semi-analytical (SA), exponential set-point equation-based semi-analytical (ESA), and load weighted-averaging (WA) methods. They were used to estimate the building zone temperature set-point trajectories which determined the discharging rate of the cooling stored in building thermal mass for lowering down the daily peak thermal load. All three methods had been evaluated in the companion paper [Lee and Braun, 2008b], and they performed well in terms of peak cooling load reduction. However, it had not mentioned about whether the daily energy consumption increased or how much it increased after the implementation of such demand limiting strategies. The increased energy consumption needed to be taken into consideration because it may

compromise the benefits from the peak demand reduction in practice. Xu et al. [2005] developed another demand limiting approach that combined Lagrangian relaxation, neural networks (NN), stochastic dynamic programming, and heuristics to predict system dynamics and uncontrollable load and to optimize the set-points of heating, ventilation and air conditioning (HVAC) systems. In addition, Chen [2001] proposed a real-time predictive supervisory optimal operation to minimize the daily energy consumption and the daily operation cost with taking into account a number of practical constraints.

For the combined usage of the passive and active building thermal storages, both Guo et al. [2005] and Henze [2005] had conducted different site investigations separately. The parametric analysis in [Guo et al., 2005] was performed to assess the effects of building mass, utility rate, building location and season, thermal comfort, central plant capacities, and economizer on the cost saving performance of demand limiting controls for active and passive building thermal storage inventory. And several key findings were presented. The analysis in [Gregor and Henze, 2005] indicated that the utility cost savings were significantly larger than either active or passive storage, but less than the sum of the individual and the peak demand of on-peak period was able to be reduced greatly.

However, most of the previous studies did not sufficiently explore the relationship between monthly electrical demand cost reduction and the related cost rise of the overall energy consumption after the proposed demand limiting strategies

implemented. They either solely focused on the daily electrical demand reduction without considering the related energy rise or only explored the relationship between demand reduction and energy rise on a daily basis. In this case, these strategies are not capable of achieving optimized monthly cost savings. The main reason is that the demand cost reduction may be largely/completely traded off by the associated overall energy cost rise.

Therefore, a strategy aiming to optimize the monthly cost saving under the electricity price structure from the power company China Light and Power (CLP) is proposed in this paper. The strategy firstly predicts a suitable monthly peak demand threshold and further determines whether a specific demand limiting control needs to be implemented for a particular day by comparing the determined threshold and the predicted daily peak demand.

Secondly, the strategy estimates an extended pre-cooling duration in which the required amount of cooling will be stored in advance and the trajectory of room temperature set-point for limiting the daily peak demand in occupation period is provided as well. In the case studies, the proposed strategy will be validated and the results are presented.

2.6 Summary

This chapter provides the literature reviews of the previous studies related to online optimal multiple-chiller system control strategies including chiller sequencing

control, optimal start control and demand limiting control. The basic assessments of the existent studies have been presented. It is clearly showed that the related research on multiple-chiller system online optimal control is still inadequate in the following aspects: (1) Many strategies were developed from the viewpoint of academic research which are not suitable for online applications because practical constraints, problems, and requirements of realistic applications, such as control stability, computation performance, etc., were not seriously considered during the development of these optimal control strategies; (2) the existing optimal strategies may be developed for simple and typical air-conditioning systems. There still seems be no sufficient optimal control strategies available for complex air-conditioning systems consisting of multiple-chillers. It is still a long way for building HVAC scientists and professionals to propose updated multiple-chiller system online optimal control strategies which have more desirable and satisfactory performance in practical application. These proposed strategies with improved performance will further enhance the reliability and energy efficiency of the entire HVAC system.

CHAPTER 3 THE BUILDING SYSTEM AND ITS DYNAMIC SIMULATION PLATFORM

The dynamic simulation platform, denoted as a virtual building system in this thesis, is a real-time simulation of a building and its HVAC system. It is mainly used to analyze and test the developed optimal strategies in terms of control, thermal comfort and energy performances under dynamic operating conditions. Based on the test results, a control strategy with satisfactory performance is selected for the control and operation of HVAC systems prior to its site implementation. It also provides convenience for testing the performances of the developed diagnosis strategies.

Many well-designed commercial simulation software packages, e.g. EnergyPlus [Crawley et al. 2000], DOE-2 [Lawrence Berkeley Laboratory 1982], etc., are readily available for constructing such dynamic platform. However, the difficulties of integrating the building load calculation, water distribution system and air distribution system into a single one prevent them from being used to build the dynamic platform. In addition, the system configurations, i.e. the water system and air system configurations, in these simulation packages are very complicated and time-consuming or even frustrating. Therefore, limited help can be provided by these software packages for detailed dynamic simulation tests of proposed control strategies. In contrast, TRNSYS, HVACSIM+ and other simulation packages based on modelica

are more suitable for such dynamic simulation. In this study, TRNSYS was chosen to build the dynamic simulation platform.

A dynamic simulation platform for a central chilling system equipped in a complex building is described in this chapter. The platform is the basis for studying the system stability and energy performance. The performance of the developed control strategy will be tested and evaluated on the constructed platform as well.

Section 3.1 briefly introduces a super high-rise commercial building and its complex central chilling system concerned in this research. Based on this complex central chilling system, a dynamic simulation platform with necessary simplifications is constructed in Section 3.2.

3.1 Building and System Description

3.1.1 Building Description

Figure 3.1 is the schematic profile of the International Commerce Center (ICC) building. This building is super high-rising of 490 meter high above the ground with about 440,000 m^2, including a basement of four floors, a block building of 6 floors and a tower building of 112 floors. The basement, about 24,000 m^2, is mainly used for car parking. The block building, from the ground floor to 5th floor, mainly serves as commercial center involving restaurants, shopping markets and exhibition halls. The gross area is about 67,000 m^2. For the tower building, the 6th and 7th floors serve as mechanical floor (M1) to accommodate chillers, cooling towers, pumps etc. The 8th floor is a refugee floor. From the 9th to 98th floors, there are commercial office floors.

Each floor is with the length of 66 m and the width of 65 m. Among the commercial office floors, the 41st and 77th floors are used as refugee floors, and the 42nd (M2), 78th (M3) and 99th (M4) floors are used as mechanical floors to accommodate mechanical equipments such as heat exchangers, pumps, PAU and fans etc. A six-star hotel is located from the 100th to 118th floors.

The whole building is being constructed primarily of reinforced steel concrete. The external walls are mostly made of steel glass curtain with the heat transfer coefficient of 1.32 $W/m^2℃$. The floor structure is about 125 mm slab of reinforced steel concrete. The transportation systems and AHU plants are located in the core of each floor with a quasi-rectangle of 45 m by 41 m. The blocking building is being in construction. The first phase from basement to 41st floor (Phase I) has been put into use at the end of 2008.

Figure 3.1. Profile of International Commerce Center

3.1.2 Zones and System Description

The building is divided into different zones considering the water pressure and human evacuation in case of a fire. The hotel, from the 100th floor to 118th floor, is a separated zone served using separate air-cooled chillers. Other floors of the tower building and the block building constitute four zones served using the chilled water sources provided by water-cooled chillers on the floor M1. To transfer cooling energy from lower zone to the upper zone, heat exchangers are used and act as a means of booster and installed at the mechanical floors of M2 an M3.

The floors below the 6th floor are Zone 1. Zone 2 includes the floors from the 7th floor to 41st floor. Zone 3 is from the 43rd to 77th floor and Zone 4 is from the 79th to 98th floor. The schematics of the central chilling system of these four zones are illustrated in Figure 3.2.

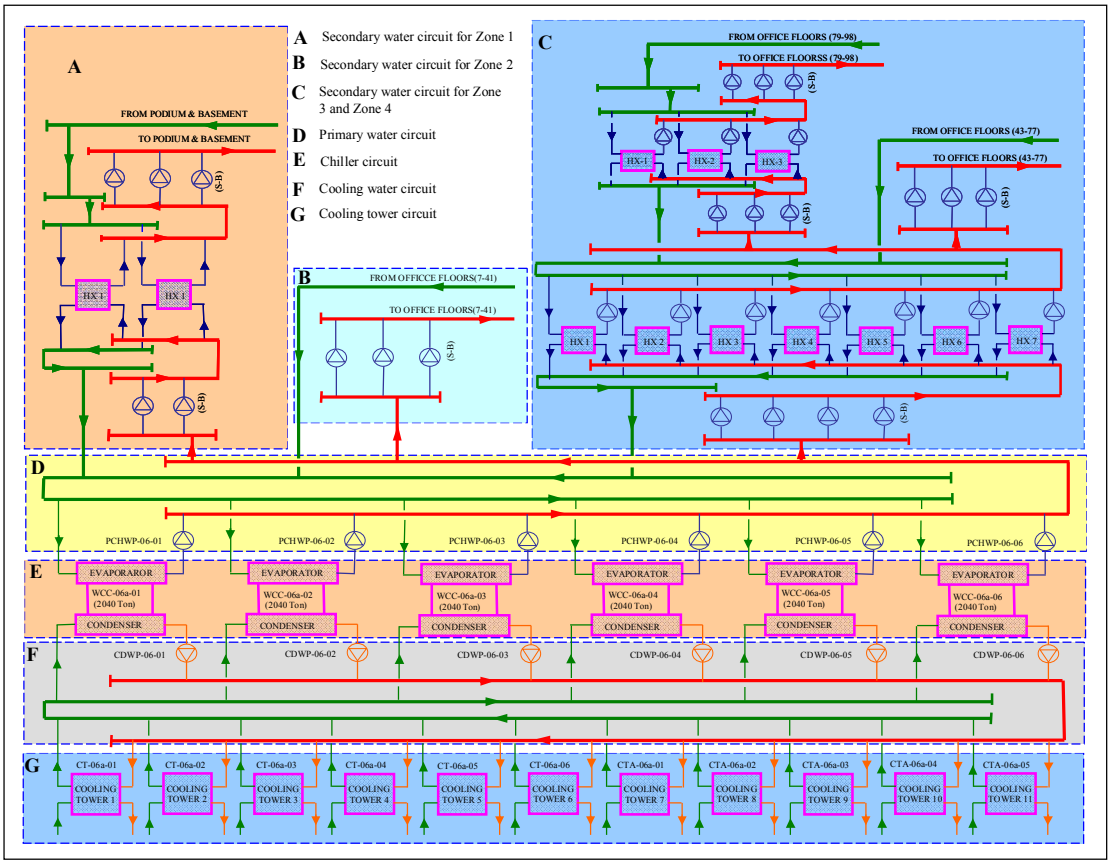

Figure 3.2 Schematics of the central chilling system.

In the central chilling system, six identical single stage centrifugal chillers have been equipped to supply cooling. The rated capacity of them is 7,230kW with 10,000 V high operating voltage. The nominal power consumption of each chiller is 1,346 kW at the full load condition. Each chiller is associated with one constant condenser water pump and one constant primary chilled water pump. The chilled water supply temperature set-point is 5.5℃. The heat generated by the chiller compressor is mostly taken away by the refrigerant. The heat dissipated from the chiller condensers is rejected by eleven evaporative water cooling towers with a design capacity of 51,709 kW. Taking into consideration plume abatement, two different types of cooling towers (named CTA and CTB, respectively) are used in this building. CTB refers to the

cooling towers with a heating coil installed at the air exhaust of each tower. CTA are the towers without heating coils. Each of the CTA towers (six in total) has a heat rejection capacity of 5,234 kW and a nominal power consumption of 152 kW at the design condition. The rated water flow rate and air flow rate of each CTA tower are 250 L/s and 157.2m^3/s, respectively. Each of the CTB towers (five in total) has a heat rejection capacity of 4,061 kW and a nominal power consumption of 120 kW at the design condition. The rated water flow rate and air flow rate of each CTB tower are 194 L/s and 127.0m^3/s, respectively. All cooling towers located in the sixth floor are of crossover flow type.

In the secondary chilled water system, only Zone 2 (indicated as B in Figure 3.2) is supplied with the secondary chilled water directly; while the heat exchangers are used in the other three zones to transport the cooling energy from low zones to high zones to avoid the high water static pressure. The designed cooling load of Zone 2 is about 30% of the total cooling load. Zone 1 (denoted as A in Figure 3.2) is supplied with the cooling from the heat exchangers located on the sixth floor. The chilled water flows through the heat exchanger and serves as the cooling source. The designed cooling load of this zone is about 19% of the total one. The designed inlet and outlet water temperatures at the secondary side of heat exchangers are 11.3°C and 6.3°C, respectively. Zone 3 and Zone 4 (indicated as C in Figure 3.2) are supplied with the cooling from secondary chilled water of the first stage heat exchangers (HX-42 in Figure 3.2) located on the 42nd floor. The designed inlet and outlet water temperatures at the secondary side of the first stage heat exchangers are 11.3°C and

6.3°C, respectively. Part of the chilled water after the first stage heat exchangers is directly delivered to Zone 3 by the secondary chilled water pumps (SCHWP-42-01 to 03) located on the 42nd floor. The rest chilled water is distributed to the second stage heat exchangers (HX-78 in Figure 3.2) located on the 78th floor by the secondary chilled water pumps (SCHWP-42-04 to 06) located on the 42nd floor. The designed inlet and outlet chilled water temperatures at the secondary side of the second stage heat exchangers are 12.1°C and 7.1°C, respectively. The water system after the second stage heat exchangers is the conventional primary-secondary chilled water system. All pumps in the chilled water system are equipped with variable frequency drivers (VFD) for energy efficient operation except those primary chilled water pumps dedicated to chillers. In addition, the water piping system of this building is a reverse-return system.

Most of air-conditioning terminals are AHUs except that some fan coil units are used in the block building. For each floor of the tower building, two AHUs equipped in the core are used to handle the mixture of fresh air and re-circulated air from offices. The fresh air is delivered to each AHU through the shaft in the core by PAUs, which are located on mechanical floors. The PAUs cool down the outdoor air to 16.5°C at the machine dew point. All fans in AHUs and PAUs are equipped with VFDs allowing the energy efficiency operation. The major specifications of main HVAC equipment, such as chillers, cooling towers, water pumps, AHU fans and PAU fans, are summarized in Table 3.1.

Table 3.1 Specifications of main equipment in the air-conditioning system

Chillers		N	$M_{w,ev}$ (L/s)	$M_{w,cd}$ (L/s)	MCC (kW)	P (kW)	P_{total} (kW)
WCC-06-01 to 06		6	345.0	410.1	7,230	1,346	8,076
Cooling Towers		N	M_w (L/s)	M_a (m^3/s)	Q_{rej} (kW)	W (kW)	W_{tot} (kW)
CTA-06-01 to 06		6	250.0	157.2	5,234	152	912
CTB-06-01 to 05		5	194.0	127.0	4,061	120	600
Pumps		N	M_w (L/s)	$Head$ (m)	η (%)	W (kW)	W_{tot} (kW)
CDWP-06-01 to 06		6	410.1	41.60	83.6	202	1,212
PCHWP-06-01 to 06		6	345.0	31.60	84.5	126	756
SCHWP-06-01 to 02		1	345.0	24.60	82.2	101	101
SCHWP-06-03 to 05		2	345.0	41.40	85.7	163	326
SCHWP-06-06 to 09		3	345.0	30.30	84.2	122	366
SCHWP-06-10 to 12		2	155.0	39.90	78.8	76.9	153.8
PCHWP-42-01 to 07		7	149.0	26.00	84.9	44.7	312.9
SCHWP-42-01 to 03		2	294.0	36.50	87.8	120	240
SCHWP-42-04 to 06		2	227.0	26.20	84.3	69.1	138.2
PCHWP-78-01 to 03		3	151.0	20.60	84.3	36.1	108.3
SCHWP-78-01 to 03		2	227.0	39.20	85.8	102	204
Air-side	PAU fan	29	/	/	/	/	513
	AHU fan	152	/	/	/	/	4,600
Design total power load	Chillers			**8,076** kW		**43.38%**	
	Cooling towers			**1,512** kW		**8.12%**	
	Pumps			**3,918.2** kW		**21.04%**	
	AHU and PAU fans			**5,113** kW		**27.46%**	
	Total			**18,619.2** kW		---	

The designed total power load of the main equipment in this air-conditioning system is 18,619.2 kW. Chillers are the largest electricity consumer in this system, which contribute 43.38% of the designed total power load. The second largest electricity consumer is the fans of AHUs and PAUs contributing 27.46% of the designed total power. The designed power loads of the pumps and cooling tower fans

are 3,918.2 kW and 1,512 kW respectively, and they constitute about 21.04% and 8.12% of the total load in the system individually. Based on the data in Table 3.1, it also can be observed that the designed total power load of the central chilling system takes about 72.5% of the designed total power load of the overall air-conditioning system. Therefore, the central chilling system must be controlled properly to achieve reliable and energy efficient operation.

The nomenclatures in Table 3.1 are defined as follows. N is the number of components, M is the flow rate, MCC is the chiller nominal maximum cooling capacity, Q is the heat transfer rate, η is the efficiency, P is the power consumption, and subscripts *w, a, ev, cd* and *rej* represent water, air, evaporator, condenser and rejection respectively.

3.2 Development of the Dynamic Simulation Platform

TRNSYS, a complete and extensible simulation environment for the transient simulation of systems, is selected to develop the complex dynamic simulation platform in this thesis. It is employed by engineers and researchers around the world to validate new energy concepts, from simple domestic hot water systems to the design and simulation of buildings and their equipment, including control strategies, occupant behavior, alternative energy systems (wind, solar, photovoltaic, hydrogen systems), etc.

One of the key factors in TRNSYS' success over the last 25 years is its open, modular structure. The source code of the kernel as well as the component models is delivered to the end users. This simplifies extending existing models to make them fit the user's specific needs.

The DLL-based architecture allows users and third-party developers to easily add custom component models, using all common programming languages (C, C++, PASCAL, FORTRAN, etc.). In addition, TRNSYS can be easily connected to many other applications, for pre- or post-processing or through interactive calls during the simulation (e.g. Microsoft Excel, Matlab, COMIS, etc.). TRNSYS applications include:

- Solar systems (solar thermal and PV)
- Low energy buildings and HVAC systems with advanced design features (natural ventilation, slab heating/cooling, double façade, etc.)
- Renewable energy systems
- Cogeneration, fuel cells
- Anything that requires dynamic simulation

Since the developed optimal control strategies mainly focus on optimizing the control of multiple-chiller systems to determine the suitable number of operating chiller for supplying sufficient cooling, the thermal balance is of major concern and the pressure flow balance in the water and air distribution loops have not been

considered. Therefore, the following simplifications have been made in construction of the dynamic platform.

(a) A simplified typical zone was built instead of construction of multi-zones based on the practical situation in ICC.

(b) A global AHU was used instead of multiple different AHUs for different zones in practice.

(c) One proportional-integral-derivative (PID) controller was used to maintain the supply air temperature at its pre-defined set-point by adjusting the flow rate of chilled water circulating in the global AHU.

(d) Another PID controller was used to maintain the indoor room temperature at its set-point through modulating the flow rate of the supply air.

The constructed central chilling system is shown as Fig. 3.3. The six water cooled centrifugal chillers were interlocked with a constant speed chilled water distribution pump and a constant speed cooling water distribution pump. The rated volumetric flow rates of these pumps were 345L/s and 410L/s respectively. The chilled supply water was circulating in a global AHU, providing cooling for the building by cooling down the supply air temperature to a predefined set-point. The return chilled water was distributed evenly to the operating chillers. Eleven identical cross-flow cooling towers with designed water flow rate of 250kg/s were used to cool down the condensers in the chillers. The cooling return water was distributed evenly to the

operating cooling towers after it has exchanged heat with the condensers. The schematic diagram of the central chiller plant is shown as Fig.3.3.

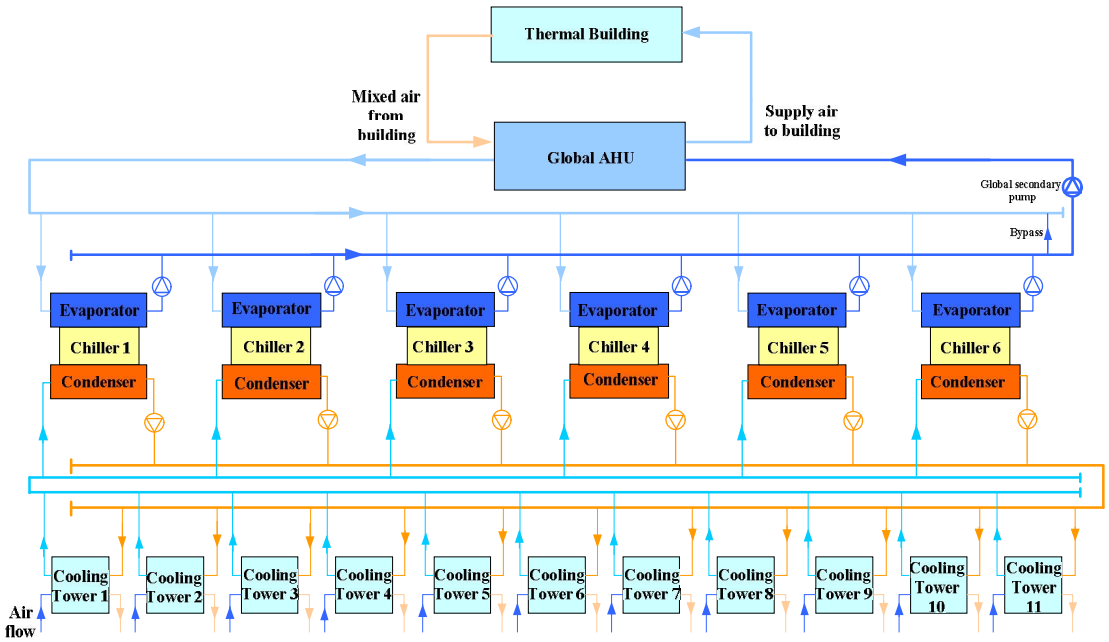

Figure 3.3. Schematic diagram of the chiller plant

The multi-zone building model, Type 56 in the TRNSYS 16, was employed to simulate ICC building [TRNSYS. 2004] for computations of the building cooling load and room temperature. For simplification, the layout of each floor (98 floors in total) in the building was square and the floor area was 3200 m^2. The wall had three layers and its height was 2.5 m. The outside and the inside layers were 5 mm thick concrete layer. The middle layer is a massive brick layer with thickness of 240mm. The ratio of window to each wall is 0.5. In addition, the typical local weather data including temperature, humidity, radiation, cloud level etc., is read from type 89d for the computation of solar load.

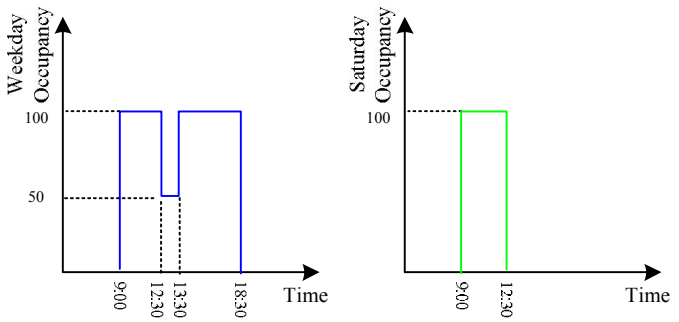

Figure 3.4. Building occupancy schedule

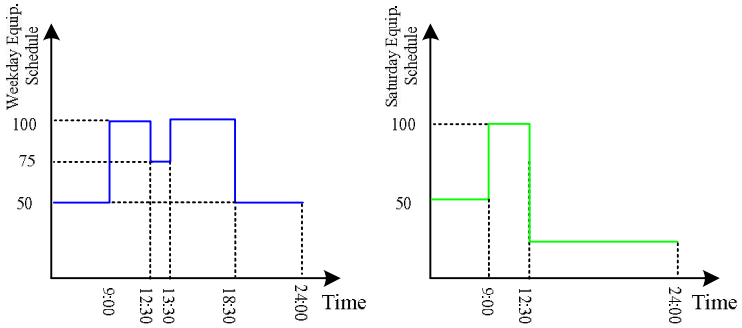

Figure 3.5. Building equipment operation schedule

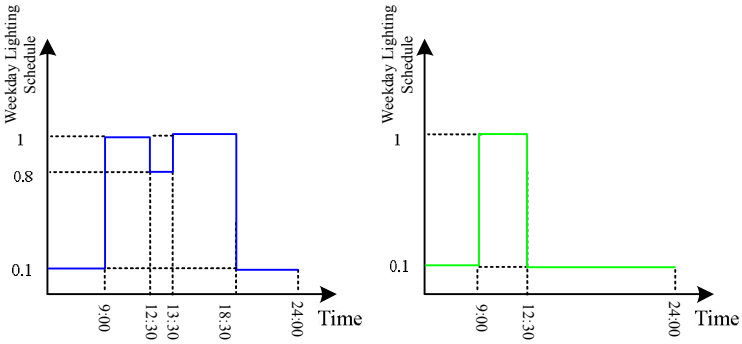

Figure 3.6. Building lighting schedule

The heat loads from the occupants, equipment and lighting system were as well considered in the simulation. The schedule of the occupancy was weekly similar. In the normal weekdays, the occupancy started at 9 a.m. and ended at 18:30 p.m., and half of the occupants were assumed to go outside for lunch from 12:30 p.m. to 13:30

p.m. The profile of the occupancy in the normal weekdays is illustrated in Figure 3.4 (the left plot). In Saturday, the occupants were supposed to work for half day which is usually observed in most of commercial buildings in Hong Kong. The profile of the occupancy in Saturday is illustrated in Figure 3.4 (the right plot). Sunday was a completely off-duty day and therefore no occupancy occurred.

Fig. 3.5 illustrates the operating schedule of building equipment, including computers, printers, copiers, et al., in each floor for the weekdays and Saturday, and Fig. 3.6 describes the operating schedule of lighting system for the weekdays and Saturday. Both Figures show that the lighting and equipment were operating in line with the occupancy schedule although slight differences existed because part of the lighting systems and equipments were left running overnight. The associated parameters for the two PID controllers were well tuned prior to the validation of the proposed strategies.

3.3 Summary

This chapter introduces a super high-rise building and its complex central chilling system concerned in this research. Based on this complex central chilling system, a dynamic simulation platform was constructed with necessary simplifications. The performances of following developed optimal control strategies will be tested and evaluated in terms of robustness and energy efficiency based on this platform.

CHAPTER 4 BUILDING COOLING LOAD MEASUREMENT USING DATA FUSION TECHNIQUE

Accurate and reliable building load measurement is essential for robust chiller automatic control, building air-conditioning system performance monitoring and optimization. This chapter presents a scheme adopting the data fusion technique to improve the quality of building cooling load measurement of building automation systems. Section 4.1 introduces the general framework of building load fused measurement. Realization of the fusion engine as a robust virtual sensor is presented in section 4.2. Two different available cooling load measurements as well as their own advantages and disadvantages are discussed in section 4.3. Capitalizing the characteristics of these two cooling load measurements, a data fusion algorithm is developed in section 4.4. In section 4.5, the identifications of the used parameters as well as periodical update algorithm for them are presented. The application case studies are performed in section 4.6. The final section 4.7 is the summary of this chapter.

4.1 Framework of Building Cooling Load Fused Measurement

The general framework of using data fusion to calculate building instantaneous cooling load of a typical central chilling plant is shown in Figure 4.1. Assume that the central chilling plant has *n* chillers. The direct way calculates the building cooling

load simply by measuring the differential temperature of chilled water return temperature $T_{w,rtn}$ and supply temperature $T_{w,\sup}$, and the total water flow rate M_w. The measurement provided by the direct way is denoted as Q_{dm}. The indirect way uses simplified chiller inverse models, which relates the building cooling load to the instantaneous chiller electrical power input $P_{com,i}$ and the chiller operating condition variables, including the evaporating temperature $T_{ev,i}$ and the condensing temperature $T_{cd,i}$. The measurement provided by the indirect way is denoted as Q_{im}. Data fusion are completed in the data fusion engine, which generates the fused measurement, denoted as Q_f, and the confidence degree, denoted as γ_f. The confidence degree indicates the quality of the fused measurements. Both of them are used by the building automation system (BAS) for the chiller sequencing control strategy.

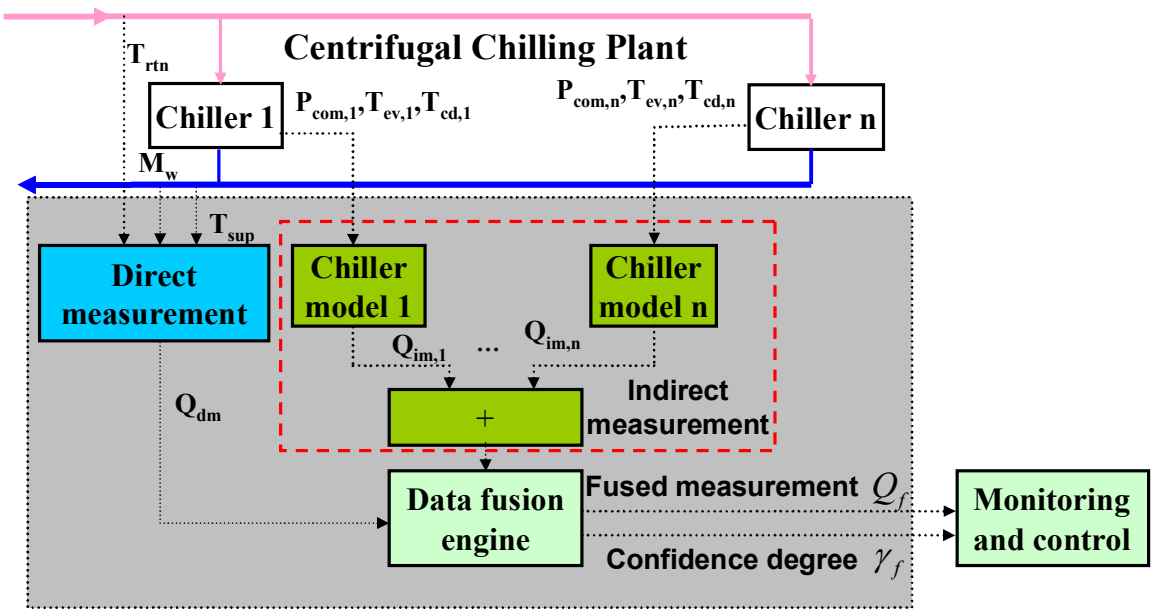

Figure 4.1. General framework of using data fusion to calculate building instantaneous cooling load

4.2 Realization of Fusion Engine as a Robust Virtual Sensor

The data fusion engine can be realized in practice as a robust virtual sensor which connects the building automation system with the physical sensors (data collection) used in the central chilling plant, as shown in Figure 4.2. The robust virtual sensor accepts the measurements of $T_{w,rtn}$, $T_{w,\sup}$, M_w, P_{com}, T_{cd} and T_{ev} as the inputs. It outputs the fused measurement of the building cooling load and the associated confidence degree. All the parameters of the fusion algorithm (described in section4.4) are the parameters of the robust virtual sensor. Other necessary parameters may also be needed, for example an on/off status to decide whether the fusion engine works or not. When the fusion algorithm is considered as a robust virtual sensor, it can be realized independently in programming. This makes it easy to imbed the fusion algorithm into the existent building automation system without resulting in significant changes in the building automation system.

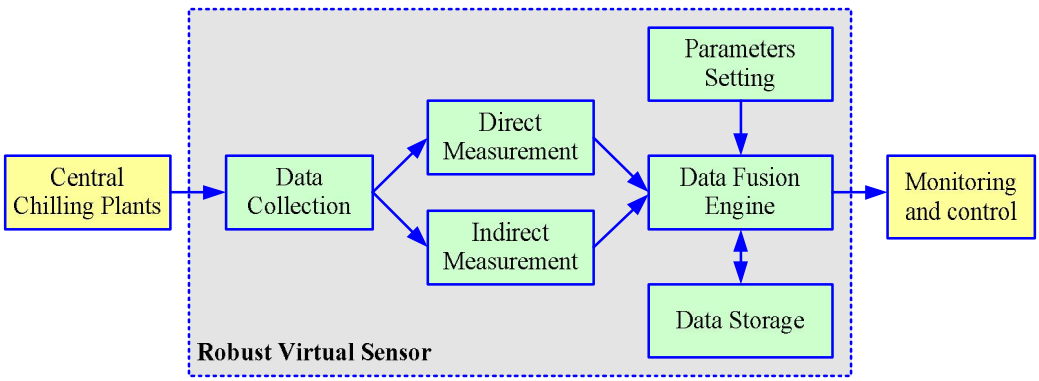

Figure 4.2. Realization of data fusion as a robust virtual sensor in BAS

4.3 Direct and Indirect Measurement of Building Cooling Load

4.3.1 Direct Measurement and the Disadvantages

The commonly-used building cooling load measurement based on the differential temperature and flow rate of chilled water is titled as "direct measurement" (Q_{dm}) in this thesis, which is shown in equation (4.1).

$$Q_{dm,k} = c_{pw}\rho_{w,k}M_{w,k}\left(T_{w,rtn,k} - T_{w,\mathrm{sup},k}\right) \tag{4.1}$$

where k denotes the time instant. c_{pw} is the water specific thermal capacity (kW/kg·K), ρ_w is the water density (kg/L). $M_{w,k}$ is the water flow rate (L/s). $T_{w,rtn}$ and $T_{w,\mathrm{sup}}$ are the temperature of the return and supply chilled water (℃). In practice, M_w is usually measured by water flow meters, $T_{w,rtn}$ and $T_{w,\mathrm{sup}}$ are measured by temperature sensors.

In practical chilling systems in buildings, temperature sensors mostly cannot measure the water temperature directly due to high water pressure that results in higher potential of temperature measurement noise, outlier, systematic error or/and uncertainty [Wang et al., 1999]. The measurements suffer easily from noises and outliers or systematic errors. Figure 4.3 shows an example of temperature measurements of the entering chilled water in a working day. The measurement noises were obvious during 00:00am to 00:70 am in the morning when the water temperature is relatively constant. Outliers are observed when the chilling system starts to work (after 08:00am). These outliers are the spikes in the measurements and clearly

inconsistent with other measurements.

Taking measurement noises and outliers or systematic errors into account, the temperature of the entering chilled water and the leaving chilled water are described by

$$T_{w,rtn,k} = T^r_{w,rtn,k} + e_{rtn,k} + b_{rtn,k}$$

$$T_{w,\mathrm{sup},k} = T^r_{s,\mathrm{sup},k} + e_{\mathrm{sup},k} + b_{\mathrm{sup},k}$$

where $T^r_{w,rtn,k}$ and $T^r_{s,\mathrm{sup},k}$ are the true values of $T_{w,rtn,k}$ and $T_{w,\mathrm{sup},k}$. $e_{rtn,k}$ and $e_{\mathrm{sup},k}$ are considered as white noise, following the normal distribution $e_{rtn} \sim N\left(0, \sigma^2_{rtn}\right)$ and $e_{\mathrm{sup},k} \sim N\left(0, \sigma^2_{\mathrm{sup}}\right)$. $b_{rtn,k}$ and $b_{\mathrm{sup},k}$ denote the possible outliers or systematic errors. Then, direct measurements have the form of

$$Q_{dm,k} = Q^r_k + c_{pw}\rho_w M_{w,k} e_{n,k} + c_{pw}\rho_w M_{w,k} b_{dm,k} \tag{4.2}$$

where Q^r_k is true value of the cooling load, $e_{n,k}$ and $b_{dm,k}$ are defined as

$$e_{n,k} = e_{rtn,k} - e_{\mathrm{sup},k}, \quad b_{dm,k} = b_{rtn,k} - b_{\mathrm{sup},k}.$$

$e_{n,k}$ is also white noise, following the normal distribution $e \sim N\left(0, \sigma^2\right)$, where σ is given by $\sigma = \sqrt{\left(\sigma_{rtn}\right)^2 + \left(\sigma_{\mathrm{sup}}\right)^2}$.

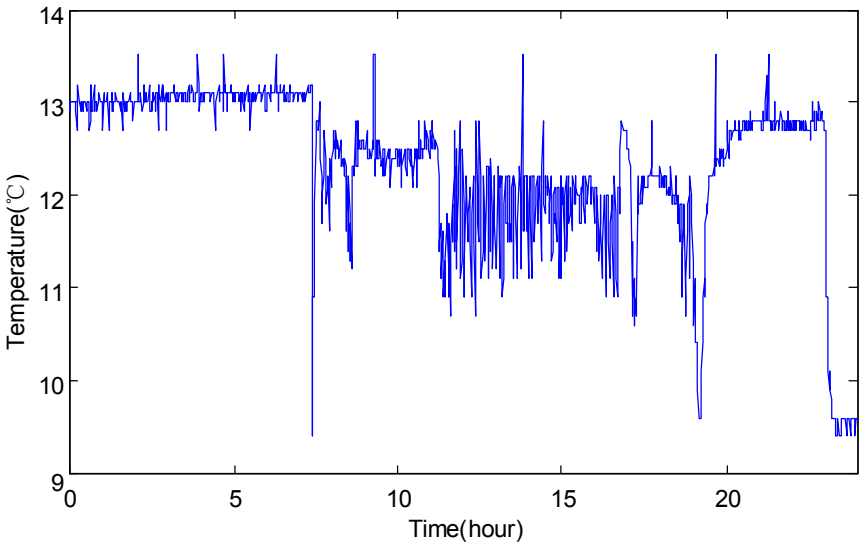

Figure 4.3. Temperature of the return chilled water in a working summer day

The measurement noises and outliers or systematic errors have a significant influence on the values of $Q_{dm,k}$. For example, if $T_{w,rtn,k}$ diverges from its true value by 0.2℃ and $T_{w,\sup,k}$ by -0.2℃, the cooling load will diverge from its true value by 335kw if $M_w = 200$ L/s. Since the temperature difference between the leaving and the entering chilled water is normally 4℃ to 6℃, this divergence is nearly 10% of the cooling load when the chiller works normally. However, since $e_{n,k}$ is assumed to be white noise, its effect on the sum of the direct measurements is reduced because $\sum_{i=1}^{N} e_{n,k} \approx 0$ if N is large enough. When $b_{dm,k} = 0$ and $M_{w,k}$ is fixed,

$$\sum_{i=1}^{N} Q_{dm,k-i} = \sum_{i=1}^{N} Q_{k-i}^{r} + c_{pw}\rho_w M_{w,k} \sum_{i=1}^{N} e_{n,k-i} \approx \sum_{i=1}^{N} Q_{k-i}^{r} \tag{4.3}$$

4.3.2 Indirect Measurement of Building Cooling Load

"Indirect measurement" of building cooling load (Q_{im}) in this thesis is based on the instantaneous chiller electrical power input and the evaporating/condensing temperature. The calculation of indirect measurement for system of multiple chillers is described in equation (4.4).

$$Q_{im} = f\left(\mathbf{P}_{com}, T_{cd}, T_{ev}\right) \tag{4.4}$$

where P_{com} is the power consumption of a chiller (kw), T_{ev} is the evaporating temperature (℃) and T_{cd} is the condensing temperature (℃). i donates one of chillers in a chilling system. P_{com} is the major variable to reflect the size of the cooling load.

The function $f(\cdot)$ can be identified from the ideal refrigerating circle in a chiller. It is assumed that heat loss from the condenser is neglected, and steady state and uniform flow conditions exist in all elements in this circle as well as in the changes in kinetic potential energies [Wang et al., 2000]. A simplified inverse chiller model is developed and used in this study as shown in equation (4.5). The first fraction part is used to calculate the refrigerant mass flow rate based on the power consumption. With the refrigerant mass flow known, the total heat absorbed in the evaporator is computed by multiplying the mass flow with the specific enthalpy difference of gaseous refrigerant between evaporator inlet and outlet. Note, many models in other forms are available for such application.

$$Q_{im} = \frac{P_{com} - \beta}{\alpha \times c_{pg} \times (T_{ev} - T_{cd})} (c_{pl} \times T_{cd} - h_{fg} - c_{pg} \times T_{ev}) \quad (4.5)$$

where α is the loss factor of variable part of electromechanical losses and β is constant part of the electromechanical losses (kw). h_{fg} is the latent heat at reference state pressure (kJ/kg). c_{pg} is the gaseous refrigerant specific heat at a constant pressure (kJ/K·kg). c_{pl} is the liquid refrigerant specific heat at constant pressure (kJ/K·kg). h_{fg}, c_{pg} and c_{pl} are constants. P_{com} is measured electrical power input to a chiller. T_{cd} and T_{ev} can be derived according to the condensing pressure p_{cd} and evaporating pressure p_{ev}. For a chiller, the relationships between the temperatures and the pressures are determined by the refrigerant used in the chiller.

The identification of α and β is described in [Wang et al., 2000]. In application, α and β can be identified using experimental data during commissioning. Good-quality data of temperature, fluid and pressure measurements should be collected. This is not difficult because during commissioning, the cooling load and its variations can be manually controlled to expected points. Then, regular model identification method, such as the least square method, can be used to compute α and β. Three variables, P_{com}, p_{cd} and p_{ev}, are needed to be measured. The measurements of the three variables are generally reliable and usually suffer only from measurement noises. Because the differential temperature (or pressure) has a much larger size, usually over 20℃, the measurement noises have no significant influence on the indirect measurements as much as that of the measurement noises on

the direct measurements. A first-order low-pass filter is therefore used to filter the associated measurement noises with the three measurements.

4.3.3 Characteristics of Indirect Measurement

Model error is the main uncertainties associated with the indirect measurement $Q_{im,k}$. Model error occurs when the model parameters, α and β, deviate from their true values, and when a model bias exists. The existence of the model bias is due to the assumption of the ideal refrigeration circle, which is used in the model identification. Hence, $Q_{im,k}$ has the form

$$Q_{im,k} = Q_k^r + \hat{\Gamma}_k + \Omega_k \tag{4.6}$$

where $\hat{\Gamma}_k$ denotes the error due to the parameter deviation and Ω_k denotes the model bias. It is assumed that the model bias Ω_k is relatively constant.

The indirect measurement can provide relatively accurate measurement of the variations in cooling load. In order to show this, rewritten (4.5) as

$$Q_{im,k} = \frac{1}{\alpha}\left(\theta_{1,k} - \beta\theta_{2,k}\right) \tag{4.7}$$

where $\theta_{1,k}$ and $\theta_{2,k}$ are

$$\theta_{1,k} = \frac{P_{com,k}\left(c_{pl} \times T_{cd,k} - h_{fg} - c_{pg} \times T_{ev,k}\right)}{c_{pg} \times (T_{ev,k} - T_{cd,k})}$$

$$\theta_{2,k} = \frac{c_{pl} \times T_{cd,k} - h_{fg} - c_{pg} \times T_{ev,k}}{\alpha \times c_{pg} \times (T_{ev,k} - T_{cd,k})}$$

The increment in the $Q_{im,k}$ is given by

$$\Delta Q_{im,k} = \frac{1}{\alpha}\left(\Delta\theta_{1,k} - \beta\Delta\theta_{2,k}\right) \tag{4.8}$$

According to equation (4.6), the model bias is removed from the increment in the indirect measurement. Therefore $\Delta Q_{im,k}$ is mainly corrupted by the parameter uncertainties in α and β. However, $\Delta\theta_{1,k}$ and $\Delta\theta_{2,k}$ are generally much smaller than $\theta_{1,k}$ and $\theta_{2,k}$ in application. Figure 4.4 compares $\Delta\theta_{1,k}$ and $\Delta\theta_{2,k}$ with $\theta_{1,k}$ and $\theta_{2,k}$ using the experimental data in a typical summer day. The absolute errors introduced by the model error in $\Delta Q_{im,k}$ are therefore greatly smaller than the errors in $Q_{im,k}$. For example, when $\alpha = 1.1488$ and $\beta = 697.8341$, the errors in $\Delta Q_{im,k}$ are mostly less than 8kW when there are 10% mismatch in α and β. It is, however, 210 kW in $Q_{im,k}$ without taking the model bias into account.

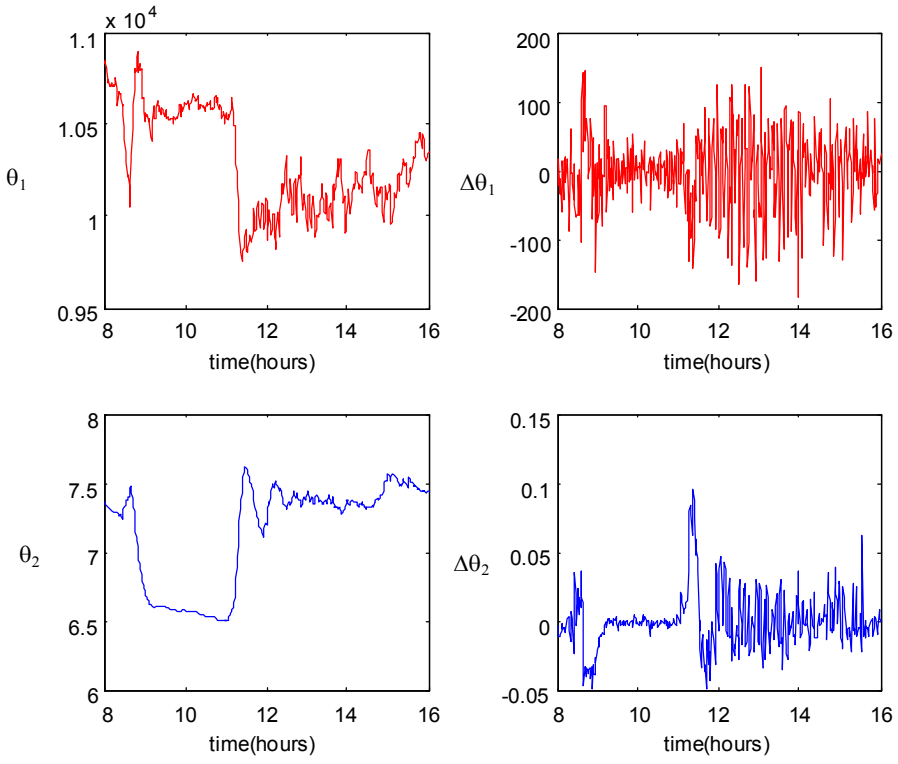

Figure 4.4. Comparison of $\theta_{1,k}$ with $\Delta\theta_{1,k}$ and $\theta_{2,k}$ with $\theta_{2,k}$

In summary, it was observed that measurement noises, outliers and system errors have a significant influence on the accuracy and reliability of the direct measurement of building cooling load. The indirect measurement can provide relatively accurate variations of the building cooling load although model error is the major error associated with indirect measurement.

4.4 Using Data Fusion to Improve Measurement of Cooling Load

The basic approach of the fusion strategy is illustrated in Figure 4.5. The main steps (or tasks) include: 1) to detect and remove outliers from the measurements; 2) to calibrate the direct measurement to reduce the influence of measurement noises; 3) to calibrate the indirect measurement to remove the influence of systematic errors; 4) to evaluate quantitatively the confidence degree of the merged measurement.

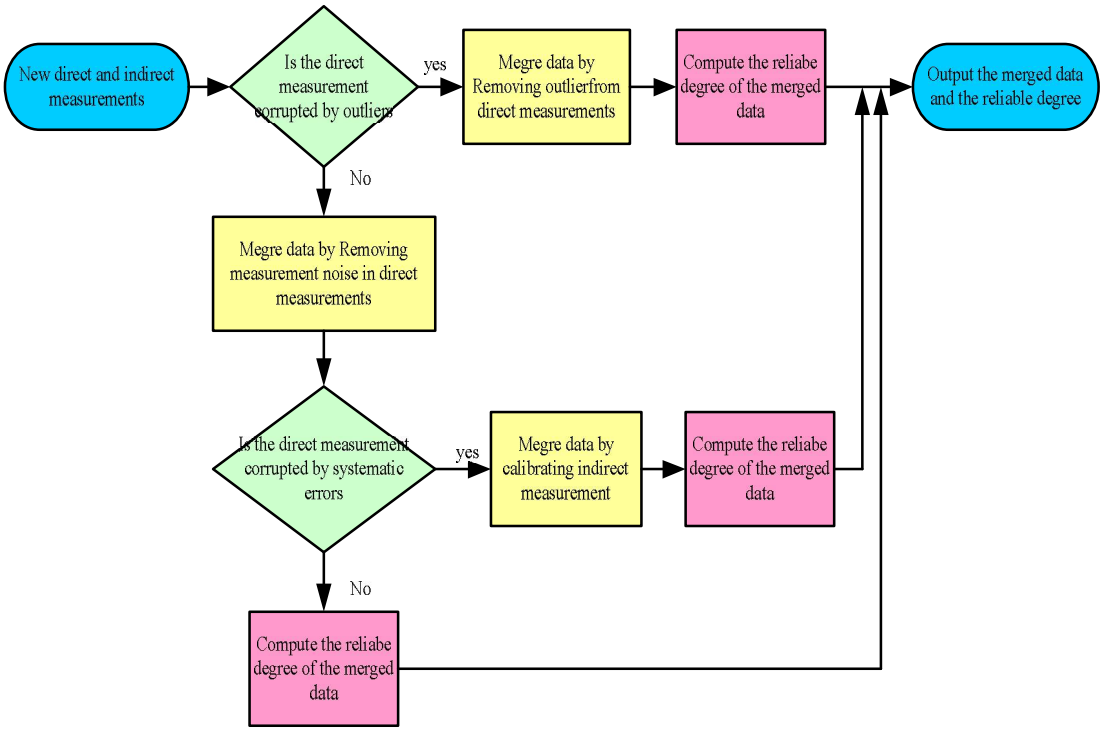

Figure 4.5. Basic approach of the fusion strategy

4.4.1 Removing Outliers in Direct Measurements

The first step in the data fusion strategy is to remove outliers. In order to detect outliers, d_k is used to denote the difference between the increments in the direct measurements and in the indirect measurements

$$d_k = \left|\Delta Q_{im,k} - \Delta Q_{dm,k}\right| \tag{4.9}$$

$Q_{dm,k}$ will be judged as an outlier when it satisfies

$$d_k > E_{m,k} \tag{4.10}$$

where $E_{m,k}$ is the threshold to distinguish the outliers. In this case, $Q_{dm,k}$ is discarded and replaced by

$$Q_{f,k} = Q_{f,k-1} + \Delta Q_{im,k} \tag{4.11}$$

where Q_f denotes the data after fusion.

$E_{m,k}$ is a user-defined parameter and it can be derived according to the characteristics of the noises in the direct measurements

$$E_{m,k} = 2c_{pw}\rho_w M_{w,k}\sigma_\Delta \tag{4.12}$$

The application of equation (4.10) to detect the outliers with E_m computed by (4.12) will cause less than 5% misjudgment when $\Delta b_{dm,k} = 0$. To show this, write the increment $\Delta Q_{dm,k}$ as (when $M_{w,k-1} \simeq M_{w,k}$)

$$\Delta Q_{dm,k} = Q_{dm,k} - Q_{dm,k-1} = \Delta Q_k^r + c_{pw}\rho_w M_{w,k} e_{n,k} + c_{pw}\rho_w M_{w,k} b_{dm,k} \tag{4.13}$$

where $\Delta b_{dm,k}$ and $\Delta e_{n,k}$ are

$$\Delta b_{dm,k} = b_{dm,k} - b_{dm,k-1},\ \Delta e_{n,k} = e_{n,k} - e_{n,k-1}$$

$\Delta e_{n,k}$ follows the normal distribution as well, $\Delta e_{n,k} \sim N\left(0, \sigma_\Delta^2\right)$ and $\sigma_\Delta = \sqrt{2}\sigma$.

Then, rewrite d_k as

$$d_k = \left| d_{1,k} + d_{2,k} \right| \tag{4.14}$$

where $d_{1,k}$ and $d_{2,k}$ are defined as

$$d_{1,k} = \Delta Q_{im,k} - \Delta Q_k^r \,,\; d_{2,k} = c_{pw}\rho_w M_{w,k}\Delta e_{n,k} + c_{pw}\rho_w \Delta b_{dm,k}$$

Compared with $d_{2,k}$, $d_{1,k}$ is negligible (see Section 4.3). Since $\Delta e_{n,k}$ follows a normal distribution, i.e. $\Delta e_n \sim N\left(0, \sigma_\Delta^2\right)$, the possibility of Δe_n lying in the range $\left(-2\sigma_\Delta, 2\sigma_\Delta\right)$ will be over 95%. It implies that when $\Delta b_{dm,k} = 0$ the possibility of d_k inside the range $\left(-2c_{pw}\rho_w M_{w,k}\sigma_\Delta, 2c_{pw}\rho_w M_{w,k}\sigma_\Delta\right)$ is over 95%.

4.4.2 Calibrating Direct Measurements Using Indirect Measurements

$\Delta e_{n,k}$ is assumed to be a white noise, and then the impact of the measurement noise can be reduced by smoothly averaging continuous measurements. It is impractical to use all the previous direct measurements. Hence, a moving window is defined with a horizon of N_w samples. Two groups of data are stored in the window. The first group consists of direct measurements which suffer only from measurement noises (outliers are discarded), denoted as $Q_{dm,1}^{\kappa},\cdots,Q_{dm,N_w-1}^{\kappa},Q_{dm,k}$ and another group is the corresponding indirect measurements, denoted as $Q_{im,1}^{\kappa},\cdots,Q_{im,N_w-1}^{\kappa},Q_{im,k}$. The superscript κ indicates the current moving window and the subscript k indicates the data at current time instant. The fusion equation developed for this case is

$$Q_{f,k} = \left(S_{dm,k} + A^t \times \vec{Q}_k\right) / N_w \tag{4.15}$$

where

$$A^t = \left[N_w\text{-}1,\cdots,1\right],\quad \vec{Q}_k^t = \left[\Delta Q_{im,k}, \Delta Q_{im,N_w-1}^{\kappa},\cdots \Delta Q_{im,2}^{\kappa}\right]$$

$\vec{Q}_k$ is a vector consisting of the increment sequence in the indirect measurements in the moving window. $\Delta Q^{\kappa}_{im,i+1}$, $i = 1,\cdots, N_w - 1$, are given by

$$\Delta Q^{\kappa}_{im,i+1} = Q^{\kappa}_{im,i+1} - Q^{\kappa}_{im,i} \tag{4.16}$$

with $Q^{\kappa}_{im,N_w} = Q_{im,k}$. $\mathrm{S}_{dm,k}$ is the sum of the direct measurements in the moving window

$$\mathrm{S}_{dm,k} = \sum_{i=1}^{N-1} Q^{\kappa}_{dm,i} + \mathrm{Q}_{dm,k} \tag{4.17}$$

Since the increments $\Delta Q^{\kappa}_{im,2},\cdots,\Delta Q^{\kappa}_{im,N_w-1},\Delta Q_{im,k}$ of indirect measurement are more accurate than the increments in the direct measurements, they are used to reconstruct the measurements in the moving window. Thus,

$$\begin{aligned}
\hat{Q}_{dm,k} &= Q_{f,k} \\
\hat{Q}^{\kappa}_{dm,N_w-1} &= Q_{f,k} - \Delta Q_{im,k} \\
\hat{Q}^{\kappa}_{dm,N_w-2} &= Q_{f,k} - \Delta Q_{im,k} - \Delta Q^{\kappa}_{im,N_w-1} \\
&\vdots \\
\hat{Q}^{\kappa}_{dm,1} &= Q_{f,k} - \Delta Q_{im,k} - \Delta Q^{\kappa}_{im,N_w-1} - \cdots - \Delta Q^{\kappa}_{im,2}
\end{aligned}$$

According to the assumption that the measurement noise is white noise, the sum of the noise in equation (4.15) will be closed to zero when N_w is large enough. Therefore, the sum of the reconstructed measurements is assumed to equal to $\mathrm{S}_{dm,k}$. Then it follows that

$$\mathrm{S}_{dm,k} = \sum_{i=1}^{N_w-1} \hat{Q}^{\kappa}_{dm,i} + \hat{Q}_{dm,k} = N_w Q_{f,k} - (N_w - 1)\Delta Q_{im,k} - \left(N_w - 2\right)\Delta Q^{\kappa}_{im,N_w-1} - \cdots - \Delta Q^{\kappa}_{im,2}$$

which finally produces equation (4.15).

The fusion formulation, i.e. equation (4.15), can be explained as a calibration of the direct measurements using the increments in the indirect measurements. To see this, rewrite equation (4.15) as

$$Q_{f,k} = \mathrm{S}_{dm,k} / N_w + A^t \times \vec{Q}_k / N_w$$

The first item in the right-hand side is the mean value of the direct measurements in the moving window, and the second item can be considered as a calibration, which depends on the weighted mean value of the increments in the indirect measurements. The measurement noises in $Q_{f,k}$ are reduced by averaging the data in the moving window. The uncertainty in $Q_{f,k}$ due to the model error are also relatively reduce, especially when S_{dm} is much larger than $A^t \times \vec{Q}_k$. For example, if there is 10% deviation in $\vec{Q}_k$ from its true value, i.e., $\vec{Q}_k^r = 1.1\vec{Q}_k$, the relative error in $Q_{f,k}$ is

$$\frac{Q_k^r - Q_{f,k}}{Q_k^r} = \frac{A^t \times \vec{Q}_k \times 0.1}{\mathrm{S}_{dm} + A^t \times \vec{Q}_k \times 1.1}$$

which will be much smaller than 10% when $A^t \times \vec{Q}_k \ll \mathrm{S}_{dm}$.

4.4.3 Calibrating Indirect Measurements to Avoid Systematic Errors

In practice, system errors may occur in the direct measurements. Different from outliers, system errors might last for a long time, due to misalignments in measurement tools, etc. Generally, system errors are relatively constant or changing gradually with operating conditions so they cannot be detected as outliers using formulation (4.12) since their influence will disappear in the increments $\Delta Q_{dm,k}$ in the direct measurements. Therefore, the merging formulation, equation (4.15), cannot

remove it. The merging formulation, equation (4.11), can be used to produce the merged measurement. However, any error in the previous fusion measurements will accumulate since equation (4.13) works as an integrator. Here an alterative approach is developed.

The differences between the direct measurements and the merged measurements are used to detect the existence of a systematic error

$$E_{f,k} = Q_{im,k} - Q_{f,k} \tag{4.18}$$

A systematic error is detected when $E_{f,k}$ is outside the range $\left[\underline{E}_f, \overline{E}_f\right]$. In this case, $Q_{f,k}$ is recomputed

$$Q_{f,k} = Q_{im,k} + \tilde{E}_f \tag{4.19}$$

where $\tilde{E}_f$ is used to calibrate $Q_{im,k}$. A transient interval, i.e., $E_{f,k} \in \left[\underline{E}_f, \underline{E}_f + \delta\right]$ or $E_{f,k} \in \left[\overline{E}_f - \delta, \overline{E}_f\right]$ is defined in order to avoid sharp changes in $Q_{f,k}$ when it is computed using equation (4.19) instead of (4.15). During the transient interval, $Q_{f,k}$ is recomputed by

$$Q_{f,k} = \lambda\left(\mathrm{S}_{dm} + A^t \times \vec{Q}\right)/N_w + (1-\lambda)\left(Q_{im,k} + \tilde{E}_f\right) \tag{4.20}$$

where λ is defined as

$$\lambda = \begin{cases} \dfrac{E_{f,k} - \underline{E}_f}{\delta}, \text{when } E_{f,k} \in \left(\underline{E}_f, \underline{E}_f + \delta\right) \\ \dfrac{\overline{E}_f - E_{f,k}}{\delta}, \text{when } E_{f,k} \in \left(\overline{E}_f - \delta, \overline{E}_f\right) \end{cases} \tag{4.21}$$

Figure 4.6 illustrates the variation of λ, in which the value of λ are shown by the darken line.

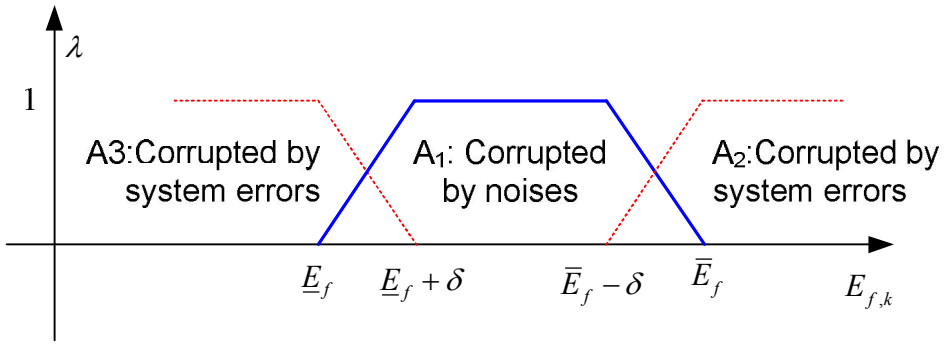

Figure 4.6. Transient intervals defined for $E_{f,k}$

It should be pointed out that the reason for using the difference defined in equation (4.18) is that $E_{f,k}$ is found to be within a range, $E_{f,k} \in \left[\underline{E}_f, \overline{E}_f\right]$, rather constantly when the direct measurements are not corrupted by systematic errors. It can be obtained experimentally when commissioning the chiller model, equation (4.5), and/or can be updated online. This range is considered as the uncertainty range in the indirect measurements introduced by the model error in the simplified inverse chiller model. The more accurate the model is, the smaller the errors are. $\tilde{E}_f$ can be computed according to $\underline{E}_f$ and $\overline{E}_f$, for example, $\tilde{E}_f = \left(\underline{E}_f + \overline{E}_f\right)/2$. δ, which defines the length of the transient interval, is also an application-dependent parameter. It is found that $\delta = \left(\overline{E}_f - \underline{E}_f\right)/4$ can always produce acceptable results.

It should also be noted that the efficiency of detecting systematic error using the model uncertainty range depends on the size of the uncertainty range. If the size is too large, small systematic errors cannot be detected; on the other hand, if it is too small,

the possibility of misjudgment will increase. In applications, if the uncertainty range cannot be obtained from the chiller model commissioning, it should be given relatively conservative values of $\underline{E}_f$ and $\overline{E}_f$ at the beginning, and update these values when more and more information about the model uncertainty are collected.

4.4.4 Confidence Degree of the Fused Measurements

Confidence degree indicates the quality of the merged measurement and who much the users can trust them. It provides useful information to facilitate BAS to make good use of the merged measurement or inform BAS to take actions if the direct measurements are of poor quality. Confidence degree lies in the range [0, 1]. The higher the confidence degree is, the better the quality of the merged measurement. Since the direct measurements suffer from noises, outliers and system errors, thresholds μ_1 and μ_2 are defined to distinguish the confidence degree among the three cases, $\mu_1 > \mu_2$. Based on this, the reliable degree is defined as

$$\gamma_k = \begin{cases} 1-(1-\mu_1)\varsigma_{\mathrm{k}}, \text{ when equation (4.15) is used} \\ \mu_1\gamma_{k-1}, \text{ when equation (4.11) is used} \\ \mu_2\gamma_{k-1}, \text{ when equation (4.19) is used} \\ \lambda\left[1-(1-\mu_1)\varsigma_{\mathrm{k}}\right]+(1-\lambda)\mu_2\gamma_{k-1}, \text{ when equation (4.20) is used} \end{cases} \tag{4.22}$$

where ς_{k} is

$$\varsigma_{\mathrm{k}} = \frac{\left|\Delta S_{im,k} - \Delta S_{dm,k}\right|}{(N_w - 1)\times E_m}$$

$\Delta S_{im,k}$ is the sum of the increments of the indirect measured cooling load and

$\Delta S_{dm,k}$ is the sum of the increments of the direct measured cooling load, defined as

$$\Delta S_{im,k} = \left|\Delta Q^{k}_{im,2}\right| + \cdots + \left|\Delta Q^{k}_{im,N_w-1}\right| + \left|\Delta Q_{im,k}\right|$$

$$\Delta S_{dm,k} = \left|\Delta Q^{k}_{dm,2}\right| + \cdots + \left|\Delta Q^{k}_{dm,N_w-1}\right| + \left|\Delta Q_{dm,k}\right|$$

The definition of confidence degree, equation (4.22), implies that when $\Delta S_{dm,k}$ is closed to $\Delta S_{im,k}$, the merged measurement has a higher degree since the direct measurements suffer little from noises in this case. The confidence degree will decrease with a rate of μ_1 when the measurements are continuously outliers or with a rate of μ_2 if a system error is detected.

In practical application, a warning might be given if the confidence is $\gamma_k < \varepsilon$, where ε is a user-defined positive constant. Then some necessary actions should be taken to check whether there are some faults in the operating system or in the measurement tools.

4.4.5 Computation Algorithm of Data Fusion Strategy

The corresponding computation algorithm is summarized as follows.

Computation Algorithm

(Offline initialization)

Step 1: Set the values of $\underline{E}_f, \bar{E}_f, \tilde{E}_f, \delta, \varepsilon, \mu_1, \mu_2$; choose the horizon N of the moving window;

(Online data fusion)

Step 2: read the new direct and indirect measurement $Q_{dm,k}$ and $Q_{im,k}$;

Step 3: Compute d_k using equation (4.9) and $E_{m,k}$ using equation (4.12); if $d_k > E_{m,k}$ go to step 4 otherwise go to step 8;

Step 4: Compute $Q_{f,k}$ using equation (4.11); go to step 8;

Step 5: Update the moving window by adding the new data $Q_{dm,k}$ and $Q_{im,k}$;

Step 6: In the moving window

Step 6.1: Compute $\mathrm{S}_{dm,k}$ using equation (4.17);

Step 6.2: Compute $Q_{f,k}$ using equation (4.15);

Step 6.3: Compute $E_{f,k}$ using equation (4.18);

Step 6.4: If $E_{f,k} \in \left[\underline{E}_f, \underline{E}_f - \delta\right]$ or $E_{f,k} \in \left[\overline{E}_f - \delta, \overline{E}_f\right]$, repeat $Q_{f,k}$ computation using equation (4.20); if $E_{f,k} \le \underline{E}_f$ or $E_{f,k} \ge \overline{E}_f$, repeat $Q_{f,k}$ computation using equation (4.19);

Step 7: Compute the confidence degree γ_k using equation (4.22); give a warning if $\gamma_k < \varepsilon$;

Step 8: Output the merged measurement $Q_{f,k}$ and the confidence degree γ_k. Then, go back to step 2 at the next time instant.

4.5 Determining Data Fusion Parameters

4.5.1 Parameter Setup

The parameters of the fusion algorithm are listed in Table 4.1. The last three parameters in Table 4.1 are used in computing the confidence degree. The other six parameters have a significant effect on the quality of the fused measurement. Specially, the influences of N_w, E_m and $\underline{E}_f, \overline{E}_f$ are stated as follows.

- A larger N_w will improve the fused measurement robustness to measurement noises; but a larger N_w will increase the amount of data storage and enlarge the time delay in the detection of systematic errors;
- A smaller E_m will improve the capability of the algorithm to detect outliers; but a smaller E_m will increase the possibility of misjudgment of outliers (to be detected as outliers but it is not);
- A narrower range ($\underline{E}_f, \overline{E}_f$) will improve the capability of the algorithm to detect systematic errors; but a narrower range ($\underline{E}_f, \overline{E}_f$) will increase the possibility of misjudgment of systematic errors.

Among these six parameters, N_w is a user-defined parameter and will be tuned online if necessary. The others will be determined during on-site commissioning, which is important to find appropriate values for these parameters. After collected m direct and indirect measurements during commissioning, E_m can be determined by the common used 95% confidence rule [Duta and Henry, 2005], i.e. E_m is

determined such that 95% of the direct measurements should not be taken as outliers when there are no systematic errors. An alternative way of determining E_m is according to the stochastic characteristics of the temperature sensors. Assume that the measurement noises in the temperature sensor are white noises and follow the normal distribution $N\left(0,\sigma_1^2\right)$ and $N\left(0,\sigma_2^2\right)$. Provide that σ_1^2 and σ_2^2 are obtained after analyzing the obtained temperature measurements, then E_m is given by

$$E_{m,k} = 2c_{pw}\rho_w M_{w,k}\sigma_\Delta \quad \text{with} \quad \sigma_\Delta^2 = 2\left(\sigma_1^2 + \sigma_2^2\right) \tag{4.23}$$

$\underline{E}_f$, $\overline{E}_f$ denotes the uncertainty range in the indirect measurement introduced by the model errors in the simplified inverse chiller model [Wang et al. 2000]. The values of them can be determined by analyzing the difference between the fused measurement and the indirect measurement when all the indirect and fused measurements are of high quality. Assume that m groups of measurements are obtained during commissioning, each group consisting of one fused measurement and the corresponding indirect measurement. The differences are computed by

$$E_{f,i} = Q_{im,i} - Q_{f,i}, i = 1,\cdots,m \tag{4.24}$$

Then $\tilde{E}_f$ is chosen as the mean value of $E_{f,i}, i = 1\cdots m$

$$\tilde{E}_f = \frac{1}{m}\sum_{s=1}^{m} E_{f,i} \tag{4.25}$$

δ can also be calculated using the 95% confidence rule: δ is chosen such that 95% of $E_{f,i}, i = 1, \cdots, n$ lies inside the range $[\tilde{E}_f - \delta, \tilde{E}_f + \delta]$. When $\tilde{E}_f$ and δ are known, $\underline{E}_f$ and $\overline{E}_f$ are computed by

$$\underline{E}_f = \tilde{E}_f - 2\delta, \overline{E}_f = \tilde{E}_f + 2\delta \tag{4.26}$$

In application, if $\underline{E}_f, \overline{E}_f$ cannot be obtained appropriately, conservative values should be given at the beginning. These values will be updated when more and more information about the model uncertainty are collected.

Table 4.1 Parameters of the data fusion algorithm

Parameter	Description
E_m	The threshold for determining the outliers
N_w	The length of the moving window
$\underline{E}_f, \overline{E}_f$	The lower and upper threshold for determining systematic errors
$\tilde{E}_f$	The calibration value used in the case of systematic errors
δ	The length of the transient interval
μ_1	The declining rate of the confidence degree in the case of outliers
μ_2	Te declining rate of the confidence degree in the case of systematic errors
ε	The threshold of the confidence degree for warning

4.5.2 Periodical Update of Fusion Algorithm Parameters

When the chiller plant is used for significantly long time, the performance of chillers might change noticeably and the inverse chiller models may not be accurate any longer. The model error changes and hence the normal differences between the

fused measurements and the indirect measurements changes as well. The current fusion parameters $\underline{E}_f, \overline{E}_f, \tilde{E}_f$ and δ, which are used for detecting systematic errors and calibrating the indirect measurement in the case of systematic errors, are therefore required to be updated since all of them are determined according the differences. Periodic update of the fusion parameters can make them suitable for the new chilling plant condition or compensate for deteriorations in the efficiency of the chillers.

Figure 4.7 shows the strategy of periodic updating the fusion algorithm parameters. The fused measurement and the confidence degree are used in chiller sequencing control and generating alarms to operators. The historical data stored in BAS can be used to update the parameters of the data fusion algorithm periodically.

Since the confidence degree indicates the quality of the fused measurement and the direct and indirect measurements as well, it is used to choose which data sets are used in updating the parameter. Only the data sets, which have a high confidence degree and are obtained recently, are used to compute the lower and upper threshold $\underline{E}_f, \overline{E}_f$ for determining systematic errors and the calibration value $\tilde{E}_f$. The new data of $\tilde{E}_f$, δ and $\underline{E}_f, \overline{E}_f$ are then computed using these selected data sets respectively by equation (4.25), the 95% confidence rule and equation (4.26).

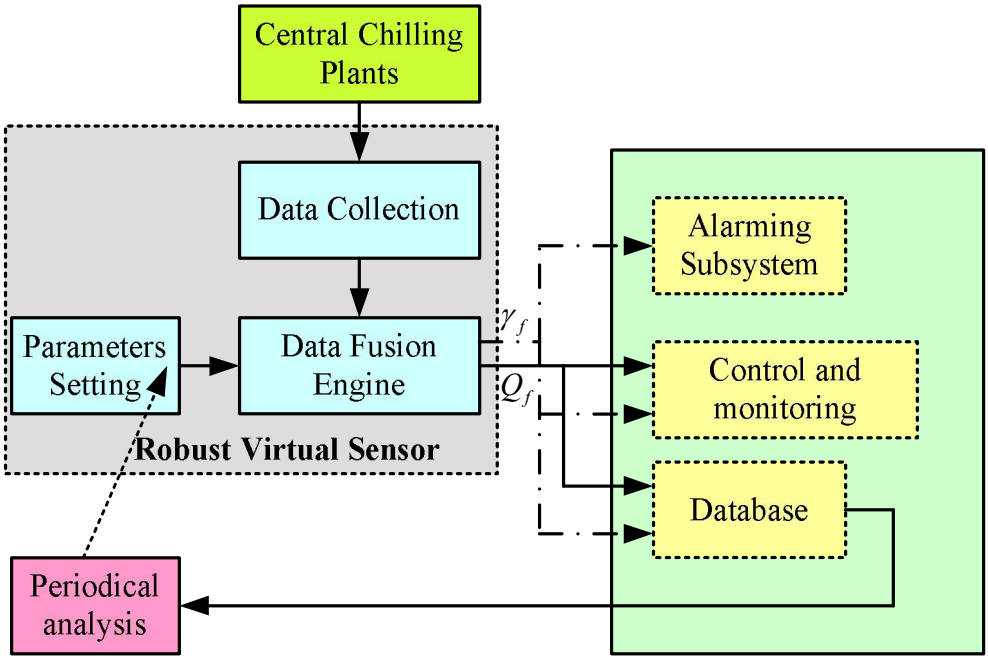

Figure 4.7. Application of building fused cooling load in building automation system

4.6 Validation Case Study

The fusion algorithm was applied to a chiller plant of a building in Hong Kong. The data used in the study were collected from 1st July to 31st July with the sampling interval being 1 minute. There are three identical 1540-ton centrifugal chillers for day mode and two identical 500-ton centrifugal chillers for night/holiday mode. Temperatures were measured using resistance thermometers and water flow rate was measured by the electromagnetic flow meter. Electric powers of individual chiller were measured using three-phase power transducers and evaporating and condensing pressures were measured by pressure transducers.

The normal distributions of the noises, e_{rnt} and $e_{\sup}$, in the temperature measurements were estimated when the temperature sensors were used to measure the water temperature which was relatively constant. $\sigma_{in} = 8.1 \times 10^{-3}$ and

$\sigma_{out} = 5.1 \times 10^{-3}$ were obtained by this way, which yielded $\sigma_{\Delta} = 0.135$. Since the water flow rate M_w was relatively constant and averagely 194 L/s, $E_{m,k} = 219$kW was used to distinguish outliers. The inverse chiller model was identified using the data ($\mathbf{P}_{com}, T_{cd}, T_{ev}$) in the first week, which yielded $\alpha = 1.1488, \beta = 697.8341$. The length of moving window was chosen to be $N_w = 20$.

4.6.1 Case without Systematic Errors

Figure 4.8 compares the fused measurements with the direct measurements from 08:00am to 16:00pm in the 15th July. The direct measurements are presented using the dotted line. It can be seen that the direct measurements are very noisy and suffers obviously from outliers. The maximal direct measurement was close to 6000kw while the minimum was close to 3000kw. Figure 4.9 shows the measured values of the chilled water entering temperature, leaving temperature as well as the flow rate, which can explain the noisy variation in the direct measurements. The fused measurements are illustrated in Figure 4.8 by the solid line. It shows that the influence of the measurement noises on the building cooling load measurements was obviously decreased. The strikes or the outliers in the direct measurements were efficiently removed. After fusion, the cooling load varied nearly between 3800kw and 5200kw, a range much smaller than those achieve in the direct measurement. Therefore, using the fused measurement in the chiller sequence control can avoid frequent switching on/off of chillers if there are no other approaches to limit the switch.

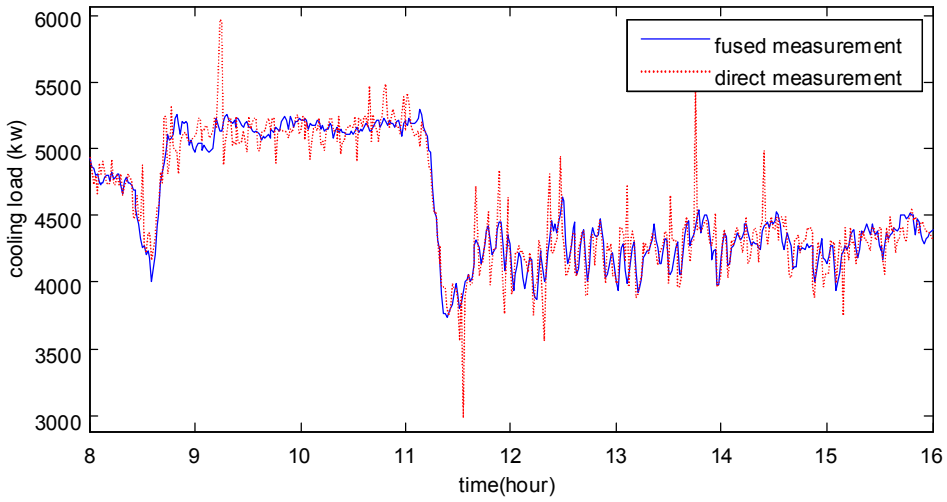

Figure 4.8. Comparison of the fused measurement with the direct measurement

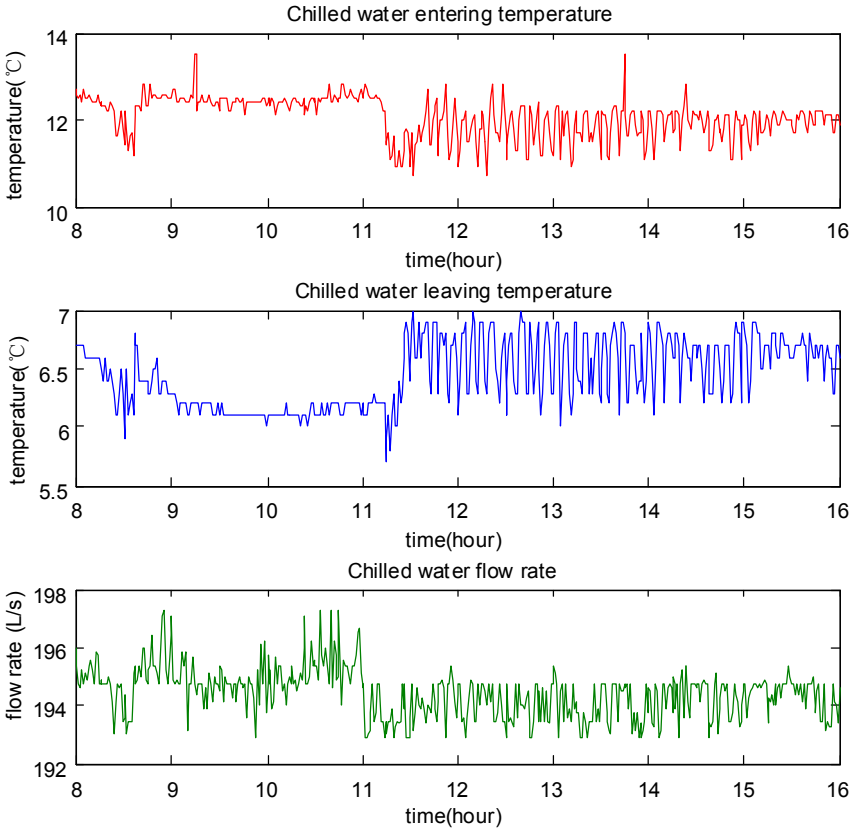

Figure 4.9. The measurement of chilled water entering temperature, leaving temperature and flow rate

Figure 4.10 compares the variations in the number of the operating chillers when the direct measurements were used with the case when the fused measurements were used. The simple chiller sequencing control logic used in the comparison was

- When the building cooling load increases: if it is larger than 2650kW then 2 chillers are switch on; if it is larger than 5300kW; then 3 chillers are stitched on;
- When the building cooling load decreases: if it is smaller than 4900kW then 2 chillers are switch on; if it is smaller than 2450kW; then 1 chillers are stitched on

It can be seen from Figure 4.7 that the number of the operating chillers varied frequently between 2 and 3 when the direct measurements were used. However, the switch frequency was significantly reduced when the fused measurements were adopted.

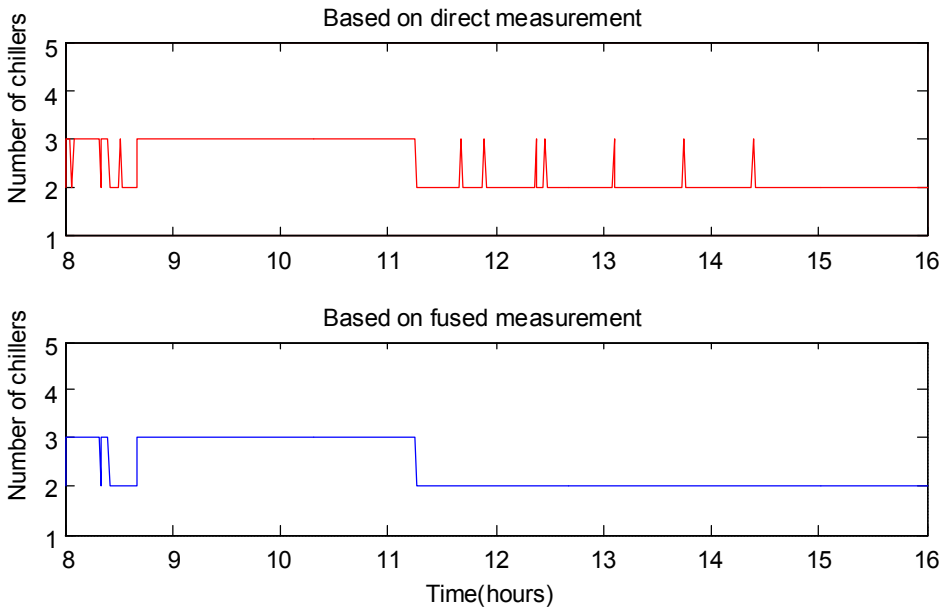

Figure 4.10. Variations in the number of the operating chillers determined when the fused measurements and the direct measurements were used

Figure 4.11 (upper) compares the fused measurements and the indirect measurements. As expected, the two kinds of measurements have similar variations. The differences between the fused measurements and the indirect measurements are shown in Figure 4.10 (bottom). The maximum difference was 5kW and the minimum was -129kW. The average value was -62kW. When there are no systematic errors in the direct measurement, this average value can be considered as the model errors.

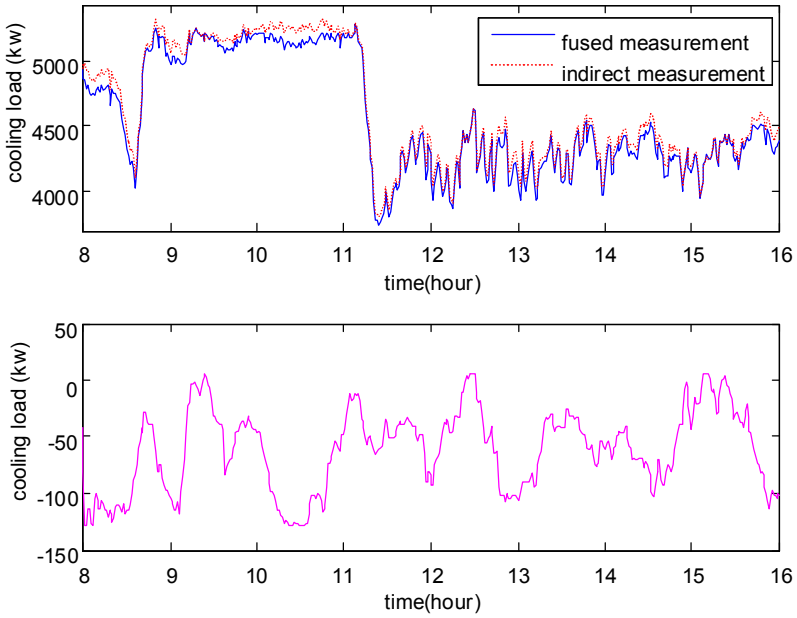

Figure 4.11. Comparison of the fused measurement with the direct measurement (upper); differences between the fused measurement and the indirect measurement (bottom)

Figure 4.12 (upper) compares the indirect measurements when the inverse chiller model used different values of α, β. The solid line represents the cooling load when α, β was identified using the data from the first week (the original values); while the dotted line was obtained when α, β were only 90% of their original values. This

difference produced a large change in the indirect measurements of the cooling load. However, the difference has an insignificant influence on the fused measurement, as shown in Figure 4.12 (bottom).

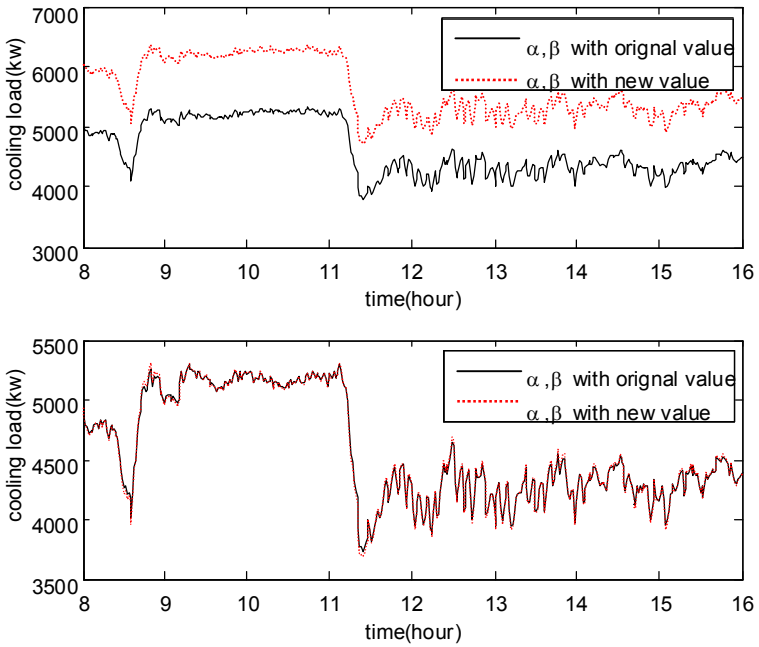

Figure 4.12. Compare the indirect measurements when the inverse chiller model has different values of α, β (upper) and the corresponding fused measurements (bottom)

4.6.2 Case with Systematic Errors

According to the differences shown in Figure 4.10 (bottom), $\tilde{E}_f$ was computed using (4.22) and δ was derived using the 95% confidence rule, producing $\tilde{E}_f = -62$ kW and $\delta = 67$ kW. Then $\underline{E}_f$ and $\overline{E}_f$ were $\underline{E}_f = -196$ kW and $\overline{E}_f = 72$ kW computed by (4.23). These values were used to detect systematic errors and calibrate the indirect measurements when systematic errors were detected. Figure 4.13 (upper) shows an artificial systematic error added to the direct measurements,

starting from 1100 to 1400 with the size of 250kW. The systematic error was nearly 5% of the total building cooling load. Figure 4.13 (bottom) shows the confidence degree associated with the fused measurements. It can be seen that after 11:00, the confidence degree decreases quickly and the confidence degree becomes smaller than 0.1 around 25 minutes. A warning will be given at this time if $\varepsilon = 0.1$. The systematic error was removed at 14:00. However, the confidence degree took nearly 18 minutes to return to its normal value ($\gamma_k > \beta_1$) due to the time delay.

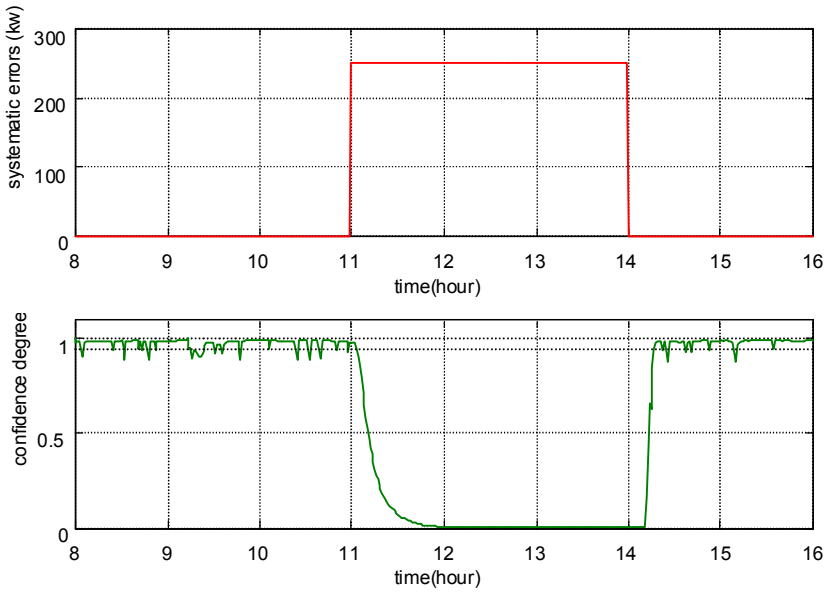

Figure 4.13. An artificial systematic error occurring in the direct measurement (upper); the corresponding confidence degree (bottom)

Figure 4.14 shows the variations in the number of the operating chillers when a systematic error was detected, where the same sequencing logic was used as in the above subsection. When the direct measurement was used, the systematic error had obviously a significant effect on the chiller sequence control since more switches were observed when compared with Figure 4.10. However, this influence disappeared

when the fused measurement was adopted. The reason can be seen from Figure 4.15, which compares the fused measurement obtained when no systematic error occurred in the direct measurement with the case when a systematic error occurred. The differences are mostly smaller than 70kW, which is not over 2% of the total building cooling load.

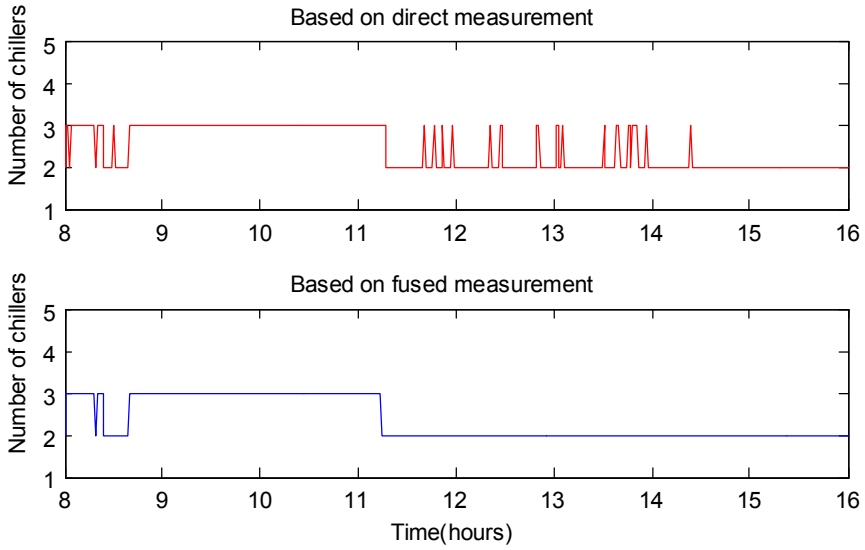

Figure 4.14. Variations in the number of the operating chillers in the case of system error

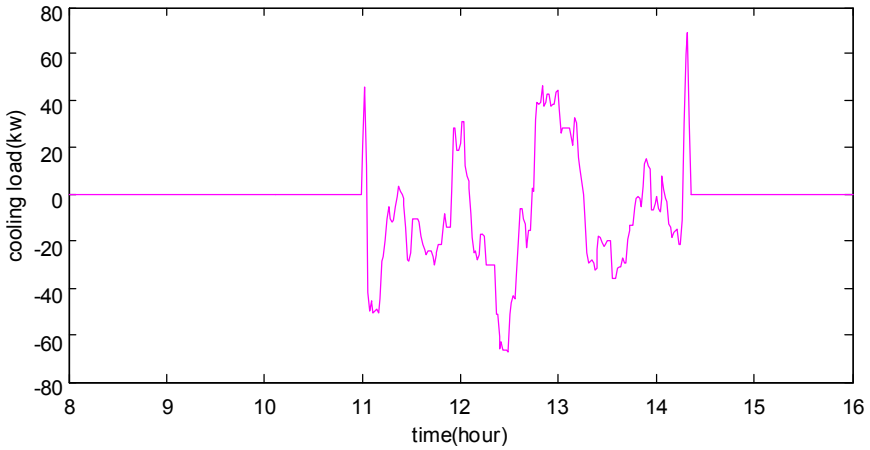

Figure 4.15. Differences between the fused measurements when no systematic error occurred and when a systematic error occurred

4.7 Summary

A method of utilizing fused measurement of building cooling load to improve the reliability of chiller system control and monitoring in building automation systems has been proposed. It has been shown that the fused measurement inherited the complementary advantages of the direct and indirect measurement of building cooling load. Application case study demonstrated that the fused measurements can effectively remove measurement noises, outliers and systematic errors in the direct measurement and the model errors in the indirect measurement. The periodical update of the fusion parameters allows the data fusion technique adaptable to the changes of the system characteristics. A general framework of using data fusion to obtain more accurate and reliable instantaneous building cooling load measurement has therefore been established and it can be used in practice large chiller plant to enhance the reliability of chiller system control and monitoring.

CHAPTER 5 CHILLER SEQUENCING CONTROL WITH ENCHANCED ROBUSTNESS

In order to enhance the robustness of chiller sequencing control, a new strategy is proposed using cooling load fused measurement and calibrated chiller maximum cooling capacity in this chapter. The fused measurement of load is obtained from the data fusion method introduced in previous chapter. A simplified model is developed to calculate the chiller maximum cooling capacity of individual chillers online. The calculated result will be calibrated to deal with the systematic errors occurring in the cooling load direct measurement.

In Section 5.1, the robust chiller sequencing control strategy is outlined as well as the introduction of chiller MCC model. The validations of the MCC model and the proposed sequencing control strategy are carried out in Section 5.2 and 5.3. A summary of this chapter is given in Section 5.4.

5.1 Robust Chiller Sequencing Control Strategy

5.1.1 Outline of the Chiller Sequencing Control Strategy

The basic idea of robust chiller sequencing control is illustrated in Figure 5.1. The fused measurement is used to replace the direct measurement used in the conventional chiller sequencing control. The maximum cooling capacity MCC_0 of individual

chillers is firstly computed online according to the chiller operating conditions using a simplified model. Then, it is calibrated according to the quality of the cooling load fused measurement indicated by the value of the confidence degree in order to deal with the impact of systematic errors on chiller sequencing control. Next, chiller sequencing control determines the chiller operating number based on the calibrated maximum cooling load MCC and the fused measurement Q_f.

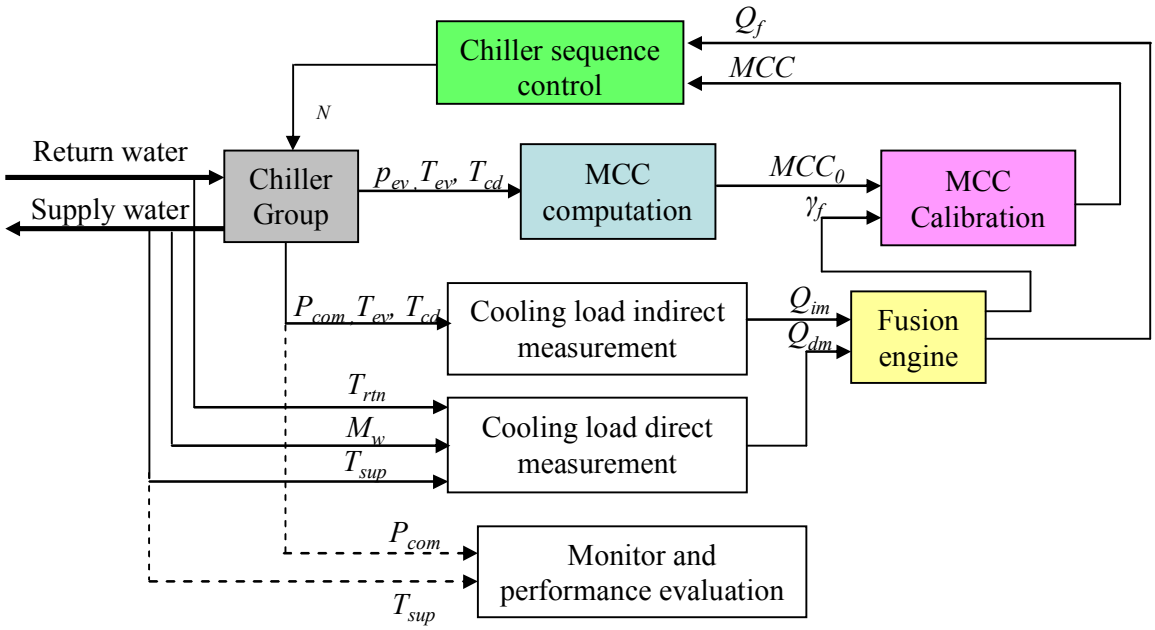

Figure 5.1. Schematics of robust chiller sequencing control

5.1.2 A Simplified Chiller Maximum Cooling Capacity Model

As the chiller cooling capacity is mainly controlled by modulating the chiller inlet vane, the simplified model for online calculating the maximum cooling capacity of a single stage centrifugal chiller with constant speed driver can be formulated as

$$MCC_0 = \frac{q_v \times P_{ev}}{R \times Z \times (273.15 + T_{ev})} \left(h_{fg} + c_{pg} \times T_{ev} - c_{pl} \times T_{cd} \right) \qquad (5.1)$$

The simplified model for calculating the maximum cooling capacity is derived based on the following simplifications:

1). The inlet flow vector triangle of the impeller is a right-angle one and the gas relative velocity direction is in line with the vane angle [Brown 2005];

2). Various kinds of losses including the incidence and friction loss are neglected;

3). The gaseous refrigerant at the inlet of the impeller is assumed to be saturated, and the pressure drop between the inlets of the compressor and the impeller is neglected;

4). The liquid refrigerant is assumed to be saturated before it flows through the expansion device.

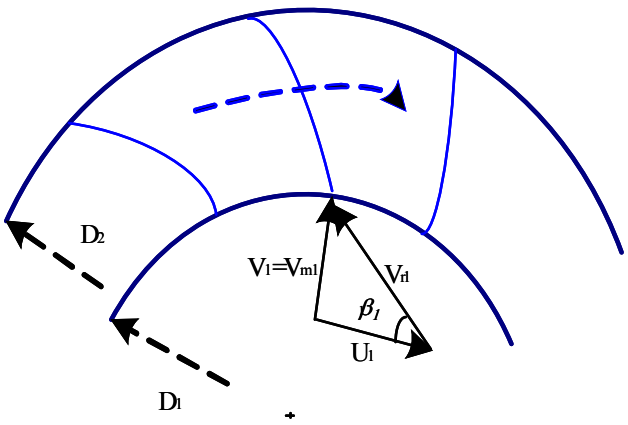

Figure 5.2. Impeller inlet flow vector triangle

The equation (5.1) is derived as follows. Firstly, when the centrifugal chiller operates at its maximum capacity, the inlet guide vane is fully open to allow maximum mass flow rate of the gaseous refrigerant [Stanford 2003]. The computation

of the maximum mass flow rate is illustrated by Figure 5.2.

According to the simplification 1), the gas relative velocity can be computed by

$$V_{r1} = U_1 / \cos\beta_1 \tag{5.2}$$

Therefore, the volumetric flow rate q_v of the gaseous refrigerant at the entry of impeller can be calculated using the following equation

$$q_v = A_1 \times U_1 / \cos\beta_1 \tag{5.3}$$

In Equation (5.3), A_1 is a constant for a particular centrifugal compressor. Since the vane leading edge velocity is invariant due to the use of a constant speed driver and the vane inlet angle is also fixed, the maximum volumetric flow rate of gaseous refrigerant is a constant, which can be specified if the values of vane angle and the rotating speed are known.

Secondly, according to the simplification 2) to 4), the maximum cooling capacity Q_{max} supplied by the chiller in a basic refrigeration circle can be computed by

$$MCC_0 = q_m \times (h_1 - h_2) = \frac{q_v}{v_1}\left(h_{fg} + c_{pg} \times T_{ev} - c_{pl} \times T_{cd}\right) \tag{5.4}$$

When the perfect gas formula is used, the specific volume of gaseous refrigerant is

$$\frac{1}{v_1} = \frac{P_{ev}}{R \times Z \times (273.15 + T_{ev})} \tag{5.5}$$

Substituting Equation (5.3) and (5.5) to Equation (5.4), the equation (5.1) computing the maximum cooling capacity is obtained. It should be noted that q_v cannot be computed directly in practice since A_1 and β_1 cannot be measured directly. An indirect

way is used to identify its value, which will be introduced in Section 5.2.

5.1.3 Calibration of the Chiller Maximum Cooling Capacity

When the confidence degree is low, the fused measurement is of poor quality since systematic errors may occur in the cooling load direct measurements. In this case, the fused measurement might be much larger or smaller than the actual building cooling load. Concerning about the energy efficiency, an approach is adopted to calibrate the maximum cooling capacity in order to maintain the number of the operating chiller as small as possible. The strategy of online calibrating the maximum cooling capacity is described by

$$MCC = \begin{cases} MCC_0, \text{ when } \gamma_{\mathrm{f}} > \varepsilon \\ \zeta \times MCC_0, \text{ otherwise} \end{cases} \tag{5.6}$$

where the calibrating factor $\zeta > 1$.

The calibrating factor ζ is a user-defined parameter, and its value will affect the control performance of the robust chiller sequencing control, as shown in the case studies in Section 5.3. A systematic way of choosing an appropriate value for the calibrating factor is difficult to develop. However, it should be reminded that the larger its value is, the larger the switch-on and the switch-off thresholds become. This enlargement aims to keep the number of the operating chillers as small as possible and hence ensure the energy performance. The strategy can provide enough cooling when the fused measurement of the building cooling load is larger than the actual one. However, if the fused measurement is less than the actual cooling load, the strategy may not be able to provide sufficient cooling. An additional scheme is therefore

needed, which monitors the supply chilled water temperature and switches on one more chiller if the temperature is significantly above its set-point for certain time period. It should be noted that the online calibration of the maximal cooling capacity is not an optimal solution since it might result in low control performance and likely low energy efficiency, especially the actual building cooling load is much smaller than the measurements. Therefore, the operators are suggested to check the measurement instruments (e.g. chilled water return and supply temperature sensors) in the case of low confidence degree and remove the measurement errors.

5.1.4 Application Issues

In chiller sequencing control, the following operation constraints are widely cosidered in practice [Chang 2005].

i) Switch-on/off threshold constraint: the threshold for switching on one more chillers is slightly larger than the threshold for switching off one more chillers (see Figure 2.2). Assume the current operating chiller number is N_0 and the switch-on and off threshold, ST_{on} and ST_{off} are separately defined by

$$\begin{aligned} ST_{on} &= N_0(MCC + db) \\ ST_{off} &= (N_0 - 1)(MCC - db) \end{aligned} \tag{5.7}$$

ii) Minimum up time constraint T_{mu}: a chiller should not be switched off immediately after it is switched on;

iii) Minimum down time constraint T_{md}: the chiller should not be switched on immediately after it is switched off.

These constraints are mainly used to prevent chillers from frequently switching

on/off in order to avoid mechanic damages. With the application of the calibrated maximum cooling capacity and the fused cooling load measurement, the optimal number of operating chillers is

$$N_c = \begin{cases} N_0 + 1, \text{if } Q_{f,k} > ST_{on} \\ N_0 - 1, \text{if } Q_{f,k} < ST_{off} \end{cases} \tag{5.8}$$

Taken account of the minimum up/down time constraints, the improved chiller sequencing control strategy is summarized as follows.

Robust chiller sequencing control algorithm

Step 1: Compute the fused measurement of the building cooling load and the confidence degree using the algorithm referred to Chapter 4;

Step 2: Compute the maximum cooling capacity by Equation (5.1);

Step 3: Calibrate the maximum cooling capacity by Equation (5.6);

Step 4: Compute the switch on/off thresholds by Equation (5.7);

Step 5: Compute the number of chillers to be put into operation by Equation (5.8);

Step 6: Check the satisfaction of the minimum up/down time constraints. If the constraints are satisfied, switch on/off one more chillers; otherwise, no action is taken;

Step 7: Go back to step 1 at the next time instant.

5.2 Case Study 1: Validation of the Maximum Cooling Capacity Model

The unknown parameter q_v in the simplified model (5.1) was identified by an associated preprocessor using chiller performance data under full load [Wang 1999].

Several groups of site data, which were obtained by manually adjusting the chiller to its full load and collected from a chilling system in Hong Kong, were used here to validate the maximum cooling capacity model. These data are listed in Table 5.1. The refrigerant used in the chiller is *R134a*. The constants used in the model are *R*Z*: 73.41kJ/(kg·K); h_{fg}: 197.9kJ/kg; c_{pg}: 0.89kJ/(kg·K), c_{pl}: 1.27kJ/(kg·K). The first four groups of data in Table 5.1 were used to calculate the parameter q_v using least square method, which yielded q_v = 1488.71m^3/s. Using this value and the measurements of p_{ev}, T_{ev}, T_{cd}, the maximum cooling capacity was computed by Equation (5.1). The computed values of the maximum cooling capacity were compared with these measurements. Figure 5.3(a) shows that the computed maximum cooling capacity matched the measurements well because the maximum relative error was less than 0.5%.

Table 5.1. Site data obtained from a middle-sized office building in Hong Kong

Variable Data no.	p_{ev} (kPa)	T_{ev} (℃)	T_{cd} (℃)	Measured MCC (kW)
1	245.6	4.83	41.79	2676
2	257.7	5.82	42.18	2806
3	270.1	6.81	42.54	2936
4	282.8	7.8	42.89	3066
5	257.2	5.78	34.45	2968
6	257.2	5.78	36.41	2936
7	257.4	5.8	38.27	2898

The simplified formulation (5.1) was also compared with another sophisticated chiller model developed in [Wang 1999], which can also be used to compute the

chiller maximum cooling capacity but need more than 15 coefficients as well as iteration operations. A detailed simulation of a centrifugal chiller was used to generate validation data. The inlet vane angle of the chiller was fully open. The supply chilled water temperature varied from 4℃ to 7.5℃ with a step increment 0.25℃ and the supply cooling water temperature varied from 30℃ to 37℃ with a step increment 0.25℃ in order to obtain the maximum cooling capacity under various operating conditions.

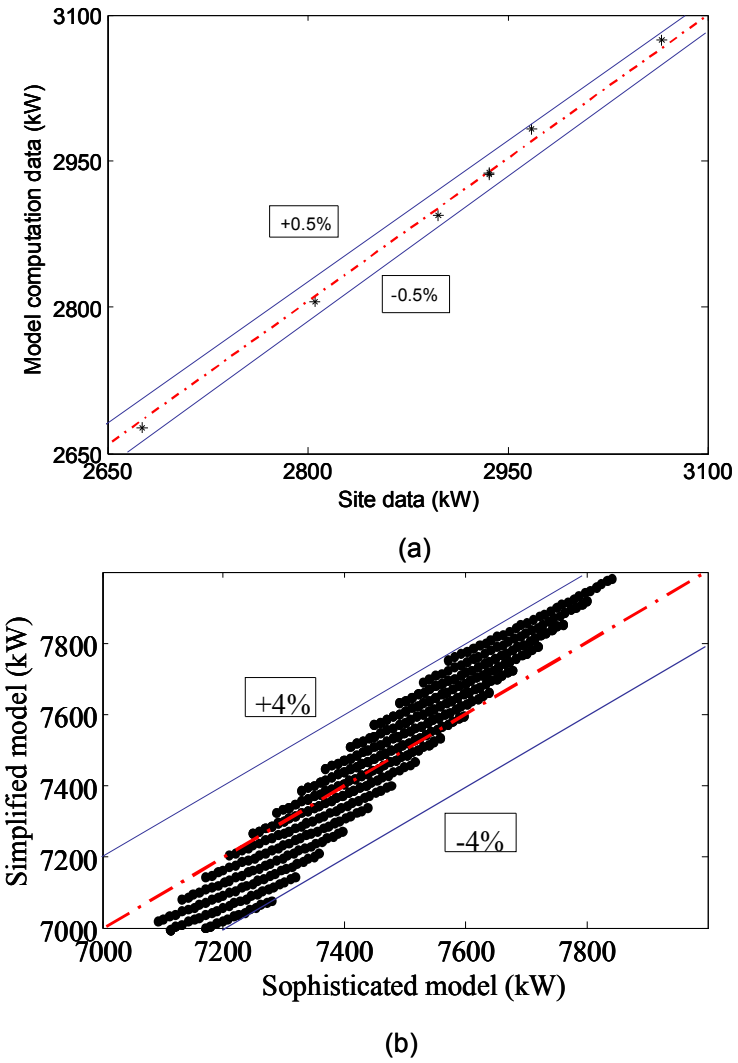

Figure 5.3. Comparison (a) between the computed and measured maximum cooling capacity; (b) between the simplified model and another sophisticated model

The comparison between the sophisticated model and the simplified model is illustrated in Figure 5.3(b), which shows that the difference between them was less than 4%. Note that there are no iteration operations in the model (5.1) and the computational burden is much lower than the sophisticated chiller model. Therefore, the simplified mode is more suitable for online application in practice.

5.3 Case Study 2: Validation of the Robust Chiller Sequencing Control Strategy

The improved chiller sequencing control strategy, illustrated in Figure 5.1, was validated using the dynamic simulation platform introduced in Section 3.2. The sequencing control strategy was programmed in MATLAB and embedded in TRNSYS 16 using the interface provided by TRNSYS 16. The proposed chiller sequencing control algorithm was used in the case study with the following parameters

- The calibrating factor $\zeta = 1.02$ (in Equation 5.6);
- The calibrating threshold $\varepsilon = 0.08$ (in Equation 5.6);
- The minimum up time constant $\tau_{mu} = 30$ minutes;
- The minimum down time constant $\tau_{md} = 30$ minutes.
- The simulation period is 120 hours.

The performance of the chiller sequencing control was evaluated using the total energy consumption EC_{total}, the total switching number Num and the total integrated time τ_{over} of the thermal building's average temperature being 0.4℃ over its set point.

Such a deviation may probably result in thermal discomfort and occupants' complaints. The total energy consumption EC_{total} consists of the energy consumed by the chillers EC_{chi}, the pumps EC_{pum} and the cooling towers EC_{ct}. In this study, comparison was mainly made between the conventional chiller sequencing control scheme with the improved one.

5.3.1 without Systematic Errors in the Direct Measurement

Figure 5.4(a) illustrates the performance of the improved chiller sequencing control strategy, including the number of the operating chillers (upper) and the variations in the average temperature of the thermal building (bottom). Correspondingly, Figures 5.4(b) shows the performance of the conventional chiller sequencing control scheme. It can be seen that the frequency of the chiller switch was greatly reduced by the improved strategy.

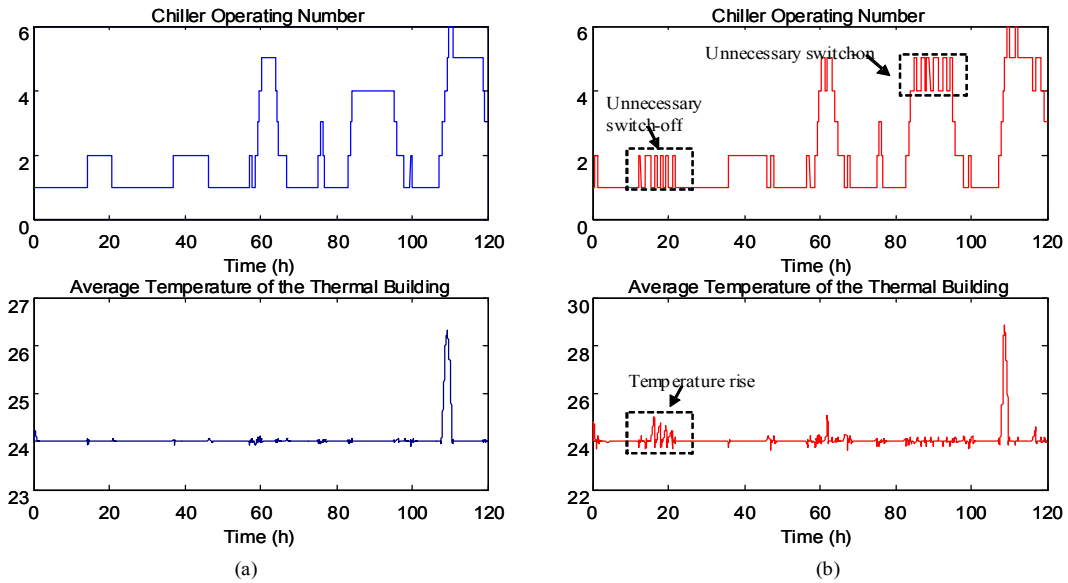

Figure 5.4. Control performance of the improved method (plots on the left) and the conventional method (plots on the right)

As listed in Table 5.2, the total switch number of the improved strategy was 34, half of the conventional one (68). Unnecessary switch-on/off actions were observed in the conventional strategy. For example, one chiller was unnecessarily switched off during the period from t = 12:00 to t = 20:00. Obviously, the switch-off action resulted in temperature rise in the average temperature of the thermal building (compare Figure 5.4(a) and 5.4(b)). An unnecessary switch-on action occurred during the period from t = 85:00 to t = 95:00, which certainly wasted energy. This can explain why both EC_{tot} and τover of the conventional chiller sequencing control scheme were larger than the improved strategy. As shown in Table 5.2,

τover of the conventional chiller sequencing control was 8.4 hours and it was reduced to 3.9 hours by the improved strategy, decreased by 53.57%. Total energy reduction consumed in the improved strategy was 4.73×105 kWh, reduced by 0.8% when compared with the consumption in the conventional strategy (4.77×10^5 kWh).

Table 5.2. Control performance comparison between the robust and conventional strategies

Variables / Strategy	τ_{over} (h)	EC_{chi} (kWh)	EC_{pum} (kWh)	EC_{ct} (kWh)	EC_{tot} (kWh)	N_{um}
Conventional Control	8.4	3.26×10^5	7.45×10^4	7.66×10^4	4.77×10^5	68
Robust Control	3.9	3.26×10^5	7.26×10^4	7.47×10^4	4.73×10^5	34

Use $E_{fr,k}$ to denote the errors between the actual cooling load and the fused measurement

$$E_{fr,k} = \left| Q_{f,k} - Q_{r,k} \right| \tag{5.9}$$

The values of $E_{fr,k}$ are plotted in Figure 5.5 (middle). The average error was 317 kW and 95% of $E_{fr,k}$ were in the range [-1.1×10^3 kW, 1.1×10^3 kW]. The values over this range mainly occurred in the transients when a chilled was turned on or off, see Figure 5.5 (middle) the dotted boxes for example. During these transients, the indirect measurement was unstable and therefore the fused measurement was set to equal to the direct measurement. Due to the use of the minimum up/down time constraints, the fused measurement in the transients did not affect the reliability of chiller sequencing control. Since there were no systematic errors, the confidence degree was always high. Small values were observed occasionally due to the presence of outliers.

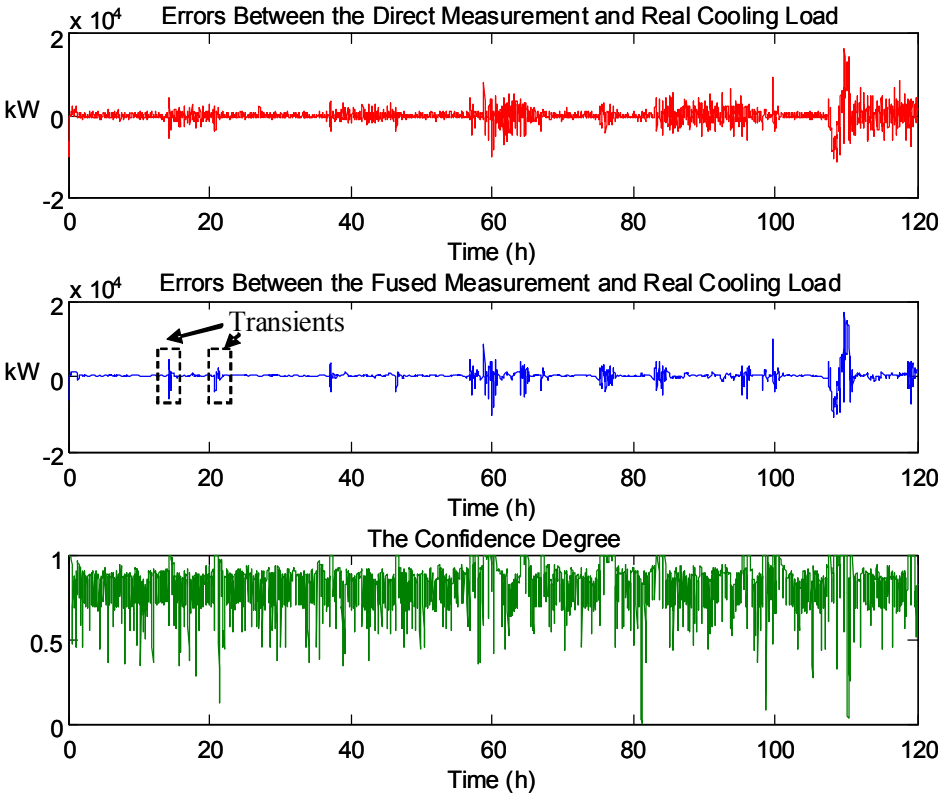

Figure 5.5. Comparison the direct measurement (upper) and the fused measurement (middle) with the real cooling load; and the confidence degree (bottom).

However, the difference between the direct measurements and the real values were much larger. Define $E_{dr,k}$ as the error between the direct measurement and the actual cooling load

$$E_{dr,k} = \left| Q_{d,k} - Q_{r,k} \right| \tag{5.10}$$

Figure 5.5 (upper) shows the values of $E_{dr,k}$,. The average value was 702 kW, twice larger than the average value of $E_{fr,k}$. 95% of $E_{dr,k}$ was in the range [-2.6×10^3 kW, 2.6×10^3 kW]. It was also found that the more the operating chillers were, the larger the differences were. Even when the chillers worked stably, the differences were sometimes over 5.0×10^3kW.

The improvements were achieved by the use of the fused measurement of the building cooling load and the online computation of the maximum cooling capacity. Figure 5.6(a) illustrates the variations in the chiller maximum cooling capacity. The maximum value was 8.91×10^3kW while the minimum was 7.09×10^3kW. The maximum cooling capacity was set to 7230kw in the conventional chiller sequencing control scheme. In this case, the largest deviation was over 1650kw. That is another reason why the conventional scheme led to misbehaviours in chiller sequencing control sometimes.

Figure 5.6(b) demonstrates the performance of the chiller sequencing control with the fused measurement but without online computation of the maximum cooling capacity. Delayed switch-on and off actions were observed when compared with Figure 5.4(a). The delayed switch-on actions yielded a rise in the average temperature of the thermal building and caused certain thermal discomfort accordingly when a

larger maximum cooling capacity than the real one was used. The switch-off actions were delayed probably because of the use of a smaller maximum cooling capacity than the real one. In this case, extra energy was consumed.

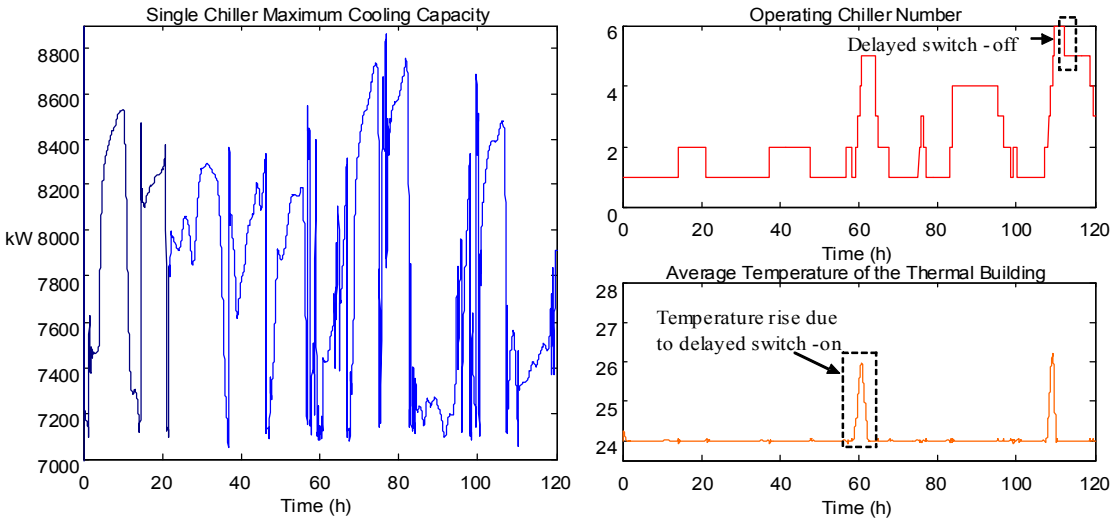

Figure 5.6. (a) Variations of the chiller maximum cooling capacity; (b) Control performance of the method which uses the fused measurement but do not use the calibrated maximum cooling capacity)

5.3.2 with Systematic Errors in the Direct Measurement

The performance of the improved chiller sequencing control strategy was also validated when systematic errors occurred. It is known that systematic errors affect significantly the accuracy of the cooling load measurement and therefore reduce the reliability of chiller sequencing control. Pseudo systematic errors with different magnitude were added in the measurements of the chilled water supply and return temperature. It can be seen from Figure 5.7 (upper) that those systematic errors influenced the direct measurements greatly. The largest error was close to 2.0×104kW when the systematic error was -0.9℃ (0.9℃) in the chilled water supply (return)

temperature. As a consequence, misbehaviors in the chiller sequencing control increased. Examples of misbehaviors in the chiller sequence were given in Figure 5.8(a). As listed in Table 5.3, τ_{over} (the total time of the chiller water supply temperature over its set point by 0.4℃) was 41.2 hours, much larger than that the case without systematic errors (3.9 hours).

Table 5.3. Control performance comparison between the improved strategy and the conventional strategy

Variables / Strategy	τ_{over} (h)	EC_{chi} (kWh)	EC_{pum} (kWh)	EC_{ct} (kWh)	EC_{tot} (kWh)	N_{um}
Conventional CSC	41.2	3.32×10^5	7.55×10^4	7.71×10^4	4.85×10^5	70
Robust CSC	3.9	3.26×10^5	7.28×10^4	7.50×10^4	4.74×10^5	36

In the improved chiller sequencing control strategy, those systematic errors were detected by the confidence degree. As shown in Figure 5.7 (bottom), the confidence degree decreased quickly to zero when the systematic errors were detected. In this case, the fused algorithm calibrated the indirect measurement to avoid the influence of these systematic errors [Huang et al. 2009]. Hence, the systematic error did not influence the fused measurement seriously, shown as Figure 5.7 (middle). For example, the average temperature of the thermal building over its set-point by 0.4℃, listed in Table 5.3, was also round 4 hours. However, there was a considerably large energy saving (2.31%) when the improved chiller sequencing control strategy was adopted in this case. The major reason was that many unnecessary switch-on

operations, which were caused by systematic errors and wasted extra part of energy, were avoided (compare Figure 5.8(a) and (b)).

Once again, significant deviations of the fused measurement were observed during chiller switching-on transients, especially when systematic errors happened during this time (see Figure 5.7 (middle), the dotted box).

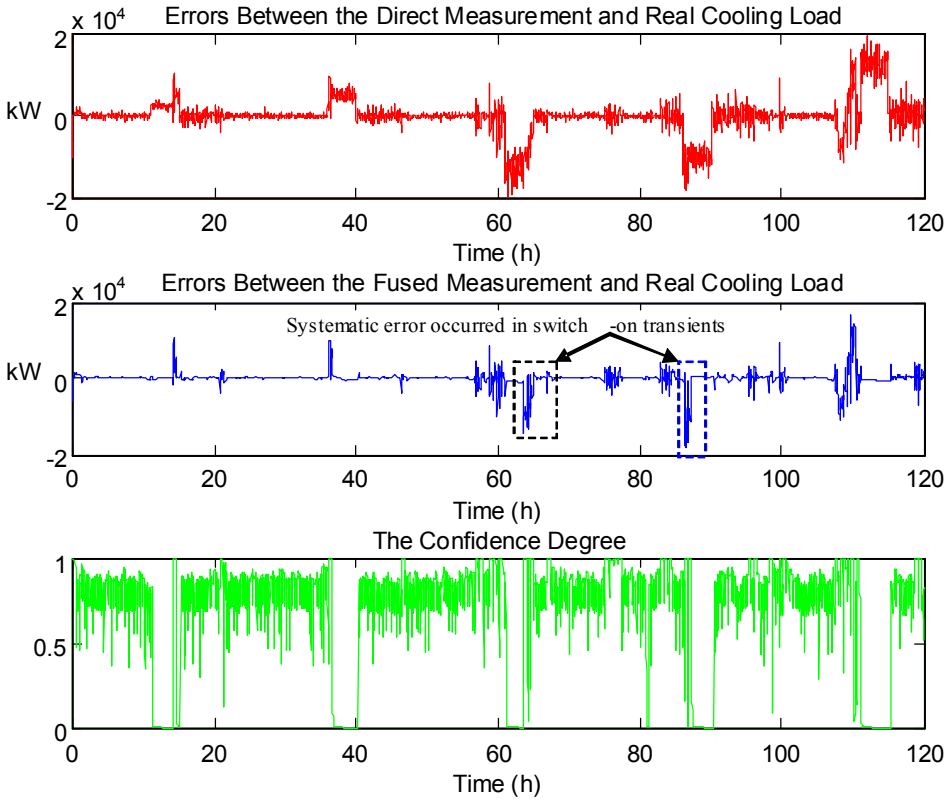

Figure 5.7. Comparison the direct measurement (upper) and the fused measurement (middle) with the real cooling load; and the confidence degree (bottom) when systematic errors occurred

However, it did not affect the chiller sequence because of the minimum up/down time constraints. It should be noted that systematic errors may slightly cause the

chiller sequence misbehaving (see Figure 5.8(b), the dotted box) since the indirect measurement was calibrated using a constant value [Huang et al. 2009].

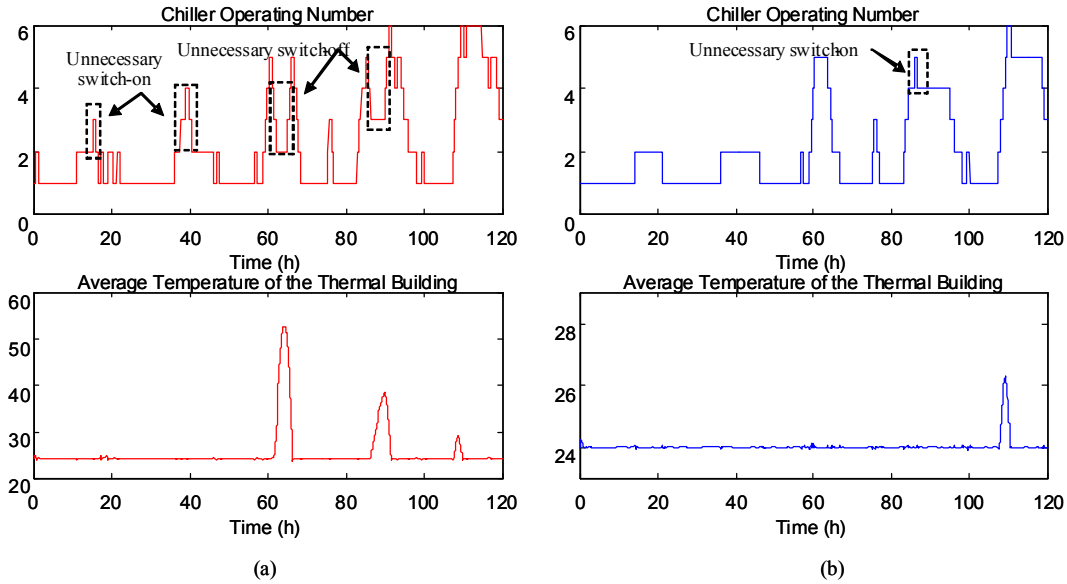

Figure 5.8. Control performance of the conventional method (plots on the left) and the improved method (plots on the right) when systematic error occurred

The calibrating factor ζ in the online calibration of the maximum cooling capacity is designed for energy efficiency in the case of systematic errors. Its choice will affect the control performance of the improved chiller sequencing control. As an example, Figure 5.9 shows the control performance when $\zeta = 1.2$ was used. When a systematic error occurred, the switch-off/on threshold was enlarged. Hence, it was observed that chillers were switched off sometime earlier than necessary (see Figure 5.9, the dotted boxes). Although there is always a backup strategy to switch on one more chillers when insufficient cooling is supplied, it is still suggested that the chiller operator should check the measurement equipments to check and fix the possible faults and

maintain the chiller sequencing control work in its normal state (i.e. without systematic errors).

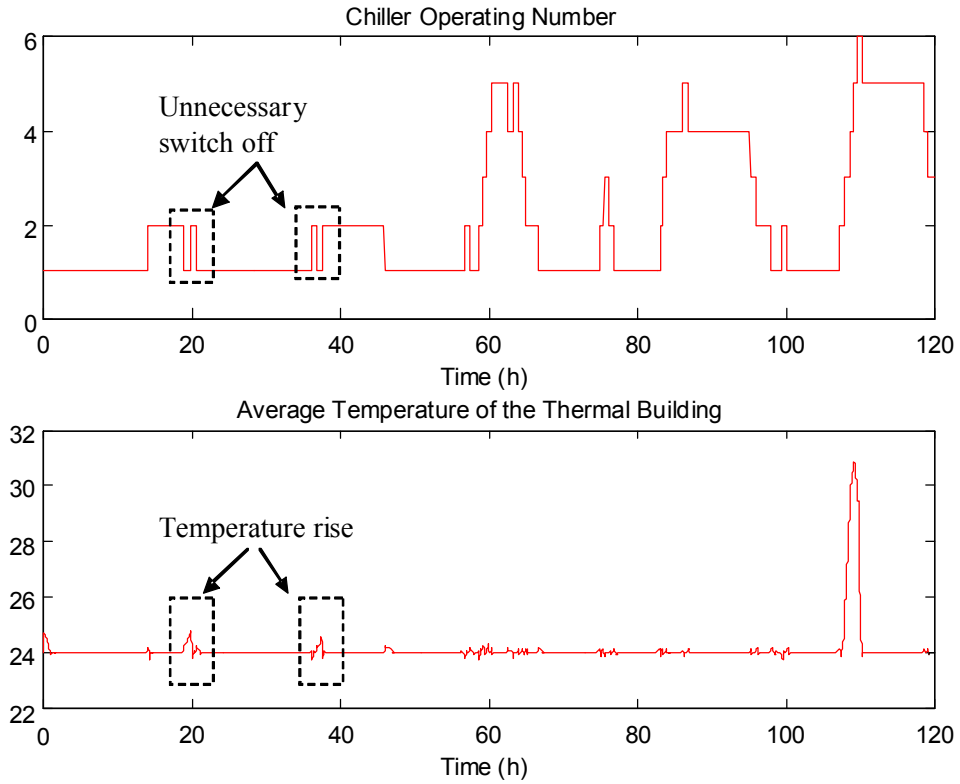

Figure 5.9. Control performance of the improved method when $\zeta = 1.2$

5.4 Summary

This chapter has investigated the improvement of the reliability and energy efficiency of chiller sequencing control. The improved chiller sequencing control uses the fused measurement of building cooling load to replace the direct measurement, computes online the chiller maximum cooling capacity by a simplified model, and calibrates it according to the quality of the fused measurement. Case studies have shown that

- The improved strategy can greatly reduce unnecessary switches of chillers, which happens in the conventional chiller sequencing control scheme due to inaccuracy of the building cooling load measurement and the derivation of the chiller maximum cooling capacity from its actual value. The reduction can avoid potential damage to chillers due to chiller frequent switch-on and off actions and therefore reduce the maintenance cost.
- The improved strategy is more robust to measurement systematic errors since these errors can be detected using the quality of the fused measurement and be dealt with directly.
- Energy saving can be achieved while the average temperature of the thermal building can be maintained more stable at its set-point temperature

Therefore, the improved chiller sequencing control strategy should be more applicable than the conventional chiller sequencing control scheme in building automation systems. It should be note that the proposed method improves the chilling plant performance by enhancing the measurement reliability and robustness. It can also cooperate with optimal chiller sequencing control to further improve the energy efficiency of chilling plants.

CHAPTER 6 ONLINE SENSOR FAULT DIAGNOSIS FOR ROBUST CHILLER AUTOMATIC CONTROL

Site experience indicates that the measurements used for direct cooling load measurement (i.e. measurements of chilled water flow rate, supply and return temperatures) are easily corrupted by systematic errors or other measurement faults. These faults result in poor quality of cooling load fused measurement and consequently poor chiller automatic control. Thus, an online sensor fault detection and diagnosis (FDD) strategy based on the confidence degree generated from cooling load fusion engine is developed to promptly identify the faults.

Section 6.1 presents the basic idea of the sensor fault diagnosis strategy for enhancing the chiller automatic control. The specific criteria for diagnosing the faults occurring in different sensors are proposed in section 6.2. Four different cases have been studied in section 6.3 to validate the developed diagnosis strategy in diagnosing the different types of faults added to the sensor measurements. A brief summary is presented in the final section 6.4.

6.1. Sensor Fault Diagnosis for Enhanced Chiller Automatic Control

The basic idea of the chiller robust automatic control strategy is shown in Figure 6.1, where there are two methods to measure building instantaneous cooling load. The first one is the building cooling load direct measurement. The other one is the

building cooling load indirect measurement. The direct and indirect measurements are taken as the inputs of the data fusion process, which generates a more accurate and reliable cooling load fused measurements. Chiller maximum cooling capacity calculated from a simplified model is calibrated according to the confidence degree. The fused cooling load together with the calibrated maximum cooling capacity is sent to chiller automatic control for determining the chillers operating number.

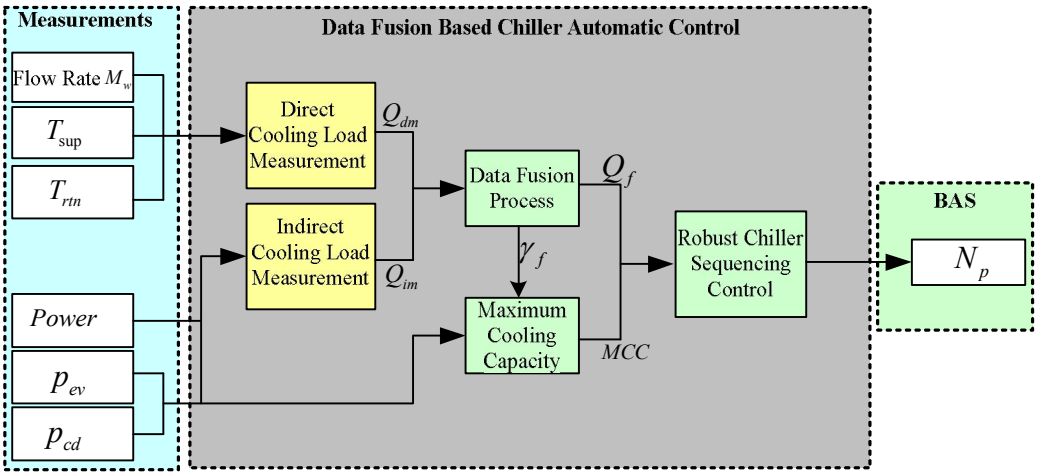

Figure 6.1. Data fusion based chiller automatic control

The fusion algorithm is also developed to detect systematic errors in the direct measurements by comparing the fused measurements with the indirect measurements. When the fused measurements fall outside of the acceptable region, defined as $\left[Q_{im}-\underline{E}, Q_{im}+\overline{E}\right]$ (see Figure 6.2), a systematic error is believed to occur in the direct measurements. Note that the acceptable region is used to account for the model error in the chiller inverse model of computing the building cooling load and its parameters $\underline{E}, \overline{E}$ are set up experimentally during commissioning, see Chapter 4.

The existence of the systematic errors in the direct measurement is indicated by the confidence degree, which will decrease quickly to a threshold in this case.

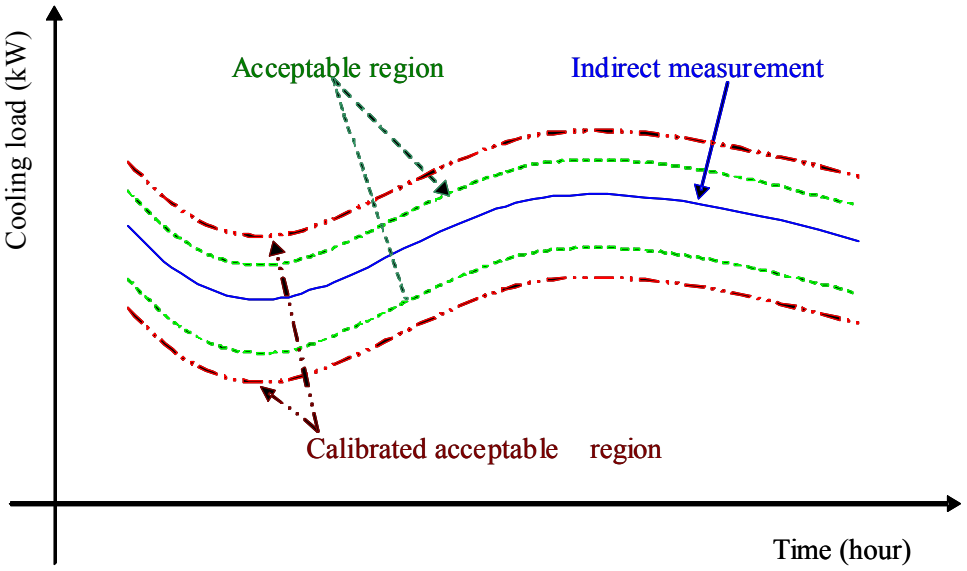

Figure 6.2. Definition of the acceptable region for the fused measurement

When the confidence degree is below the threshold, the chiller maximum cooling capacity is calibrated in order to deal with the impact of sensor measurement faults (e.g. systematic errors) on chiller automatic control. Although the robust chiller automatic control can guarantee enough supplied cooling even when a systematic error in the direct measurements is detected, the automatic control performance and the energy efficiency may deteriorate, especially when the actual building cooling load is much smaller than the measurements used for the automatic control. Therefore, prompt diagnosis of sensor faults is essential to improve the performance of chiller automatic control. The confidence degree is used as a trigger in the fault diagnosis strategy.

Sensor fault diagnosis aims at improving the performance of chiller automatic control by helping BAS operators to remove sensor faults quickly. Since the confidence degree becomes low when there is a considerable discrepancy between the fused and indirect cooling load measurements, faults might occur in either the direct or indirect measurements. It is known that a number of sensor fault diagnosis methods has been developed for dealing with the sensor measurements concerning individual chiller (e.g. volts, currents, evaporating and condensing pressure), for example by Wang and Chen [2004]. Therefore, this paper will focus on developing sensor fault diagnosis approach for isolating the faults occurring in the cooling load direct measurement, i.e., in the chilled water flow, supply and return temperature measurements.

6.2. Online Sensor Fault Diagnosis Algorithm

6.2.1 Outline of the Fault Diagnosis Algorithm

The online sensor fault diagnosis algorithm is illustrated in Figure 6.3. The fault diagnosis algorithm follows a procedure of two steps. The first step is to check whether there is any fault in the chiller water flow and supply temperature measurements, both of which have expected values. The expected value of the chiller water flow rate in the header pipe is calculated based on mass balance between the header pipe and the interlocked pumps of chillers. The expected value of the chilled water supply temperature is its set point, which can be tracked by the chiller control system when the operating chillers can provide sufficient cooling. The Moffat

consistency test is conducted to diagnose fault by checking the Moffat distance between the measurements and their expected values [Moffat R.J., 1982]. The second step is to diagnose faults in the chilled water return temperature measurements. If no fault is found in the first step, a fault is believed to exist in the chilled water return temperature measurements and the diagnosis algorithm ends with a fault report to BAS. Otherwise, the diagnosis algorithm will continue to check whether there is any further fault. Since the chilled water return temperature varies with the building cooling load and the building cooling load is difficult to compute, the Moffat consistency test is not used in this case. The fault is diagnosed by reconstructing the confidence degree using the chilled water flow measurements (when a fault is detected) or its expected value (when no fault is detected) and the supply temperature measurements (when a fault is detected) of its expected value (when no fault is detected). Fault report is also sent to BAS.

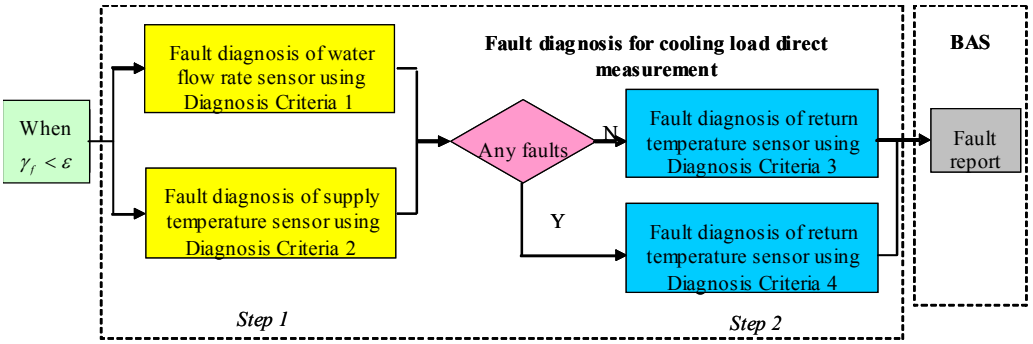

Figure 6.3. Framework of the fault diagnosis algorithm

6.2.2 Fault Diagnosis of Chilled Water Flow Rate and Supply Temperature Measurements

In the fault diagnosis for the header pipe chilled water flow measurements, the available redundant information in BAS include:

- Header pipe chilled water flow measurements M_{hp};
- Operating pump water flow direct measurements $M_{pum,j}$, $j = 1,\ldots,N_{pum}$;
- Operating pump water pressure drop (or pump head loss) measurements $H_{pum,j}$.

The pump water pressure drop is related to the pump water flow rate by the pump performance curve, which can be described as

$$H_{pum,j} = a_0 + a_1 \times M^*_{pum,j} + a_2 \times \left(M^*_{pum,j}\right)^2 \tag{6.1}$$

The pump water flow rate $M^*_{pum,j}$, calculated from Eqn. 6.1, is titled as pump water flow indirect measurement. The diagnosis criterion for the header pipe water flow measurement is developed based on the mass balance between the header pipe water flow and the water flow in these operating pumps, i.e., the water mass flow through the header pipe is equivalent to the sum of the water mass flow through the operating pumps. The diagnosis criterion is descried as follows:

Diagnosis criterion 1: In a moving window with N_w continuous measurements of the chilled water flow rate in the header pipe, if 80% of the Moffat distances between *the header pipe chilled water flow measurements* and *the sum of the flow measurements*

in these operating pumps are larger than unity, then there is a fault in the header pipe water flow measurement; otherwise, the header pipe water flow measurement is free of faults.

The Moffat distance in Diagnosis Criterion 1 is defined by Eqn. 6.2, where the sum of the flow measurements in the operating pumps M^i_{sum} is calculated by Eqn. 6.3 and the uncertainty Δ_{wm} associated with $M^i_{hp} - M^i_{sum}$ is computed by Eqn. 6.4. In Eqn. 6.3, M^i_{sum} consists of two parts: the direct measurements $M^i_{pum,j}$ from the operating pump flow meters which work healthily and the indirect measurements $M^{*,i}_{pum,j}$ from the operating pump flow meters which work unhealthily, i.e., with systematic errors.

$$md^i_{hs,k} = \frac{\left| M^i_{hp} - M^i_{sum} \right|}{\Delta_{wm}}, \quad i = 1, \cdots, N_w \tag{6.2}$$

$$M^i_{sum} = \sum_{j=1}^{L_{pum}} M^i_{pum,j} + \sum_{j=L_{pum}+1}^{N_{pum}} M^{*,i}_{pum,j} \tag{6.3}$$

The uncertainty Δ_{wm} is derived as follows.

$$\Delta_{wm} = \sqrt{(\Delta_{hp})^2 + \sum_{j=1}^{L_{pum}} (\Delta_{pum,j})^2} + \sum_{j=L_{pum}+1}^{N_{pum}} \Delta^*_{pum.j} \tag{6.4}$$

When the header pipe water flow meter in primary loop is free of fault, the measurement M^i_{hp} can be written as

$$M^i_{hp} = M^i_{hp,act} + e^i_{hp}, \quad e_{hp} \sim N\left(0, \sigma_{hp}{}^2\right) \tag{6.5}$$

According to the study reported in [Duta M., Henry M., 2005], the uncertainty associated with M^i_{hp} can be defined as

$$\Delta_{hp} = 1.96\sigma_{hp} \tag{6.6}$$

Similarly, when the pump flow meters work healthily, the direct measurements $M^i_{pum,j}$ have the form of

$$M^i_{pum,j} = M^i_{pum,act,j} + e^i_{pum,j}, \quad e_{pum,j} \sim N\left(0, {\sigma_{pum,j}}^2\right) \tag{6.7}$$

and the associated uncertainty is

$$\Delta_{pum,j} = 1.96\sigma_{pum,j} \tag{6.8}$$

When the pump flow meters work unhealthily, the indirect measurement $M^{*,i}_{pum,j}$ is used to replace the direct measurements $M^i_{pum,j}$. Considering about model mismatches introduced in the pump performance curve (see Eqn. 6.1), the indirect measurement $M^{*,i}_{pum,j}$ can be expressed as

$$M^{*,i}_{pum,j} = M^i_{pum,act,j} + \hat{\delta}^i_{pum,j}, \quad \left|\hat{\delta}^i_{pum,j}\right| \le \Delta^*_{pum,j} \tag{6.9}$$

Assume there are L_{pum} pump flow meters work healthily and $N_{pum} - L_{pum}$ pump flow meters work unhealthily. The sum of the operating pump flow measurements M^i_{sum} in Eqn. (6.3) is rewritten as

$$M^i_{sum} = \sum_{j=1}^{N_{pum}} M^i_{pum,act,j} + e^i_{sum} + \hat{\delta}^i_{sum}; \quad e^i_{sum} = \sum_{j=1}^{L_{pum}} e^i_{pum,j}; \quad \hat{\delta}^i_{sum} = \sum_{j=L_{pum}+1}^{N_{pum}} \hat{\delta}^i_{pum,j} \tag{6.10}$$

The mass balance between the header pipe water flow and the operating pump water flow gives

$$M^i_{hp,act} = \sum_{j=1}^{N_{pum}} M^i_{pum,act,j} \tag{6.11}$$

which yields

$$M^i_{hp} - M^i_{sum} = e^i_{hp} - e^i_{sum} - \hat{\delta}^i_{sum} \tag{6.12}$$

Since the operating pump flow meters works independently with each other and

also with the header pipe flow meter, $\left(e_{hp}^{i}-e_{sum}^{i}\right)$ follows a normal distribution

$$\left(e_{hp}^{i}-e_{sum}^{i}\right)\sim N\left(0,\sigma_{hp}{}^{2}+\sum_{j=1}^{L_{pum}}\sigma_{pum,j}{}^{2}\right) \tag{6.13}$$

The total calculation uncertainty δ_{sum}^{i} lies in the range

$$\left|\hat{\delta}_{sum}^{i}\right|\le\sum_{j=L_{pum}+1}^{N_{pum}}\Delta_{pum,j}^{*} \tag{6.14}$$

Hence, the uncertainty associated with $M_{hp}^{i}-M_{sum}^{i}$ is

$$\Delta_{wm}=1.96\sqrt{(\sigma_{hp})^{2}+\sum_{i=1}^{L_{pum}}(\sigma_{pum,j})^{2}}+\sum_{j=L_{pum}+1}^{N_{pum}}\Delta_{pum,j}^{*} \tag{6.15}$$

Then, Eqn. 6.4 is obtained according to Eqn. 6.6, 6.8 and 6.15.

Diagnosis Criterion 1 indicates that if the header pipe water flow measurements are not consistent with the sum of the pump flow measurements, then there is a fault in the header pipe flow measurements. It should be noted that when the measurement uncertainties Δ_{hp} and $\Delta_{pum,j}$, $j=1,\ldots,L_{pum}$, are appropriately set, a single Moffat consistency test still fails with 5% probability due to the normal distribution of the measurement noises [Duta M., Henry M., 2005]. Therefore, a moving window is adopted in Diagnosis Criterion 1, which is used to reduce the possibility of such misdiagnosis. The index 80% is set experimentally here because this value can produce an acceptable result in the case study in Section 4.

The healthy operation of the pump flow meter is judged by examining the consistency between the pump water flow direct measurements and the corresponding indirect measurements. As in Diagnosis Criterion1, Moffat distances are used and defined as

$$md^{*,i}_{pum,j} = \frac{\left| M^{i}_{pum,j} - M^{*,i}_{pum,j} \right|}{\Delta_{pum,j} + \Delta^{*}_{pum,j}} \tag{6.16}$$

Once again, if $md^{*,i}_{pum,j}$ is larger than unity, then a fault is found in the corresponding flow meter; otherwise, the flow meter works healthily. Note that this judgment is based on the fact that the pressure measurement is reliable.

Diagnosis Criterion 2: In a moving window with N_w continuous measurements of the supply temperatures, if 80% of the Moffat distances between *chilled water supply temperature measurements* and *its set point* are larger than unity, then there is a fault in the chilled water leaving temperature measurement.

The Moffat distances in Diagnosis Criterion 2 are defined by

$$md^{i}_{\text{sup},k} = \frac{\left| T^{i}_{\text{sup},mes} - T_{\text{sup},set} \right|}{\Delta_{\text{sup},mes} + \Delta_{\text{sup},set}}, i = 1, \cdots, N_w \tag{6.17}$$

The development of Diagnosis Criterion 2 is similar to Diagnosis Criterion 1. When the chiller automatic control guarantees sufficient cooling supplied and the operating chillers are free of faults, the actual chilled water supply temperature can be manipulated to track its set point with small disturbances by the chiller closed-loop control. Hence, the chilled water actual supply temperature can be described by

$$T_{\text{sup},act} = T_{\text{sup},set} + \hat{\delta}_{\text{sup},set} \tag{6.18}$$

The disturbance $\delta_{\text{sup},set}$ occurs due to chiller imperfect closed-loop control as well as its unstable operating environment. Again, the disturbance $\hat{\delta}_{\text{sup},set}$ is assumed

to lie in an uncertainty range, i.e., $\left|\hat{\delta}_{\text{sup},set}\right| \le \Delta_{\text{sup},set}$. Without systematic errors, the temperature measurement $T_{\text{sup},mes}$ is described by

$$T_{\text{sup},mes} = T_{\text{sup},act} + e_{\text{sup},mes}, \quad e_{\text{sup},mes} \sim (0, \sigma^2_{\text{sup},mes}) \tag{6.19}$$

Similar to Eqn. 6.6, the measurement uncertainty $\Delta_{\text{sup},mes}$ is

$$\Delta_{\text{sup},mes} = 1.96\sigma_{\text{sup},mes} \tag{6.20}$$

The moving window is used in Diagnosis Criterion 2 for the same reason as it is used in Diagnosis Criterion 1.

6.2.3 Fault Diagnosis of the Chilled Water Return Temperature Measurement

As illustrated in Figure 6.3, two cases should be considered in the fault diagnosis of the chilled water return temperature measurements. The first case is that there are no faults found in both the chilled water flow and supply temperature measurements. In this case, the diagnosis criterion is described as follows.

Diagnosis Criterion 3: When there is no fault found in the chilled water flow and supply temperature measurements, there is a fault in the chilled water return temperature measurements.

The second case is that a fault is detected in either the chilled water flow measurements or the supply temperature measurements. In this case, the fault diagnosis algorithm will check whether there is a further fault in the return water temperature measurements. Because the chilled water return temperature varies with the building cooling load and the building cooling load is difficult to calculate

accurately, it is difficult to use the consistency test to diagnose fault. A confidence degree reconstruction scheme is developed to diagnose faults in the return water temperature measurements. In this scheme, the cooling load direct measurements are firstly reconstructed by

$$\tilde{Q}_{dm} = c_{pw} \times \tilde{M} \times (T_{rtn,mes} - \tilde{T}_{\sup}) \tag{6.21}$$

where

$$\tilde{M} = \begin{cases} M_{hp}, \text{ if no fault is found} \\ M_{sum}, \text{ if a falut is found} \end{cases}$$

$$\tilde{T}_{\sup} = \begin{cases} T_{\sup,mes}, \text{ if no fault is found} \\ T_{\sup,set}, \text{ if a fault is found} \end{cases}$$

Then, the fusing algorithm developed in Chapter 4 is used to reconstruct the fused measurements and the confidence degree. Compared with the fusion algorithm in Chapter 4, the only difference is that the direct measurements (Q_{dm}) is replaced by the reconstructed fused measurements ($\tilde{Q}_{dm}$). The regenerated confidence degree $\tilde{\gamma}_f$ is used for fault isolation in the return chilled water temperature measurements.

Diagnosis criterion 4: If the reconstructed confidence degree $\tilde{\gamma}_f$ is still smaller than the threshold ε, then there is a fault in the chilled water return temperature measurements.

When M_{sum} and/or $T_{\sup,set}$ are used to replace the corresponding measurements M_{hp} and $T_{\sup,mes}$, the uncertainty $e_{sum} + \hat{\delta}_{sum}$ and/or $\hat{\delta}_{\sup,set}$ will be introduced in the computation of $\tilde{Q}_{dm}$. To see this, rewrite Eqn. (6.21) as Eqn. (6.22) when both M_{sum} and $T_{\sup,set}$ are used

$$\tilde{Q}_{dm} = c_{pw} \times M_{sum} \times \left(T_{rtn,mes} - T_{\sup,set} \right) \tag{6.22}$$

The nominal value of the direct measurements $\tilde{Q}_{dm,nom}$ is the one without any faults in the water flow and chilled water supply temperature measurements

$$\tilde{Q}_{dm,nom} = c_{pw} \times M_{hp} \times \left(T_{rtn,mes} - T_{\sup,mes} \right) \tag{6.23}$$

Assume Δ_{sum} and $\Delta_{\sup,set}$ are

$$\Delta_{sum} = \hat{\alpha}_1 \times M_{sum} \quad \text{and} \; \Delta_{\sup,set} = \hat{\alpha}_2 \times \left(T_{rtn,mes} - T_{\sup,set} \right) \tag{6.24}$$

i.e., $\left| e_{sum} + \hat{\delta}_{sum} \right| \le \hat{\alpha}_1 \times M_{sum}$ and $\left| \hat{\delta}_{\sup,set} \right| \le \hat{\alpha}_2 \times \left(T_{rtn} - T_{\sup,set} \right)$. According to Eqn. 6.12, 6.18 and 6.19, Eqn. 6.23 can be rewritten as

$$\begin{aligned} \tilde{Q}_{dm,nom} = c_{pw} \times & \left(M_{sum} + \hat{\delta}_{sum} + e_{sum} \right) \\ & \times \left[T_{rtn,mes} - T_{\sup,set} - \hat{\delta}_{\sup,set} - e_{\sup,mes} \right] \end{aligned} \tag{6.25}$$

Since the measurement noises e_{sum} and $e_{\sup,mes}$ are independent and with zero expectations, both of them will disappear in the fused measurement because the sum of a continuous sequence of $\tilde{Q}_{dm}$ is used to compute the fused measurement. However, the uncertainties $\hat{\delta}_{sum}$ and $\hat{\delta}_{\sup,set}$ cannot be removed in this way. Therefore, the uncertainty $\hat{\delta}_{sum}$ and $\hat{\delta}_{\sup,set}$ will enter into the reconstructed fused measurement as well as $\hat{\gamma}_f$.

The "worst" increment in the fused measurements is when $\hat{\delta}_{sum} = \pm\hat{\alpha}_1 \times M_{sum}$ and $\hat{\delta}_{\sup,set} = \pm\hat{\alpha}_2 \times \left(T_{rtn,mes} - T_{\sup,set} \right)$

$$\Delta\tilde{Q}_{dm} = \left(\hat{\alpha}_1 + \hat{\alpha}_2 + \hat{\alpha}_1 \times \hat{\alpha}_2 \right) \tilde{Q}_{dm} \tag{6.26}$$

This increment $\Delta\tilde{Q}_{dm}$ should be taken into account in reconstructing $\tilde{\gamma}_f$ in order to avoid the decrease of $\tilde{\gamma}_f$ due to the introduction of $\hat{\delta}_{sum}$ and $\hat{\delta}_{\sup,set}$. A simple way is to calibrate the acceptable region using $\Delta\tilde{Q}_{dm}$. The calibrated acceptable region is also shown in Figure 6.2 by the solid-dotted lines, where the calibration value is $\pm\Delta\tilde{Q}_{dm}$, which is calculated according to Δ_{sum} and $\Delta_{\sup,set}$. For example, when both the chilled water flow rate and supply water temperature measurement are with faults, $\Delta\tilde{Q}_{dm}$ is be computed using Eqn. 6.26.

6.2.4 Parameters Setup

The parameters of the online sensor fault diagnosis algorithm are summarized in Table 6.1. All these parameters are required to be set during on-site commissioning. For example, σ_{hp} and $\sigma_{\sup,mes}$ can be calculated by analyzing the stochastic distribution of a sequence of chilled water flow and supply temperature continuous measurements when the measurands are relatively constant and the measurements are free of faults. Then, Δ_{hp}, $\Delta_{pum,j}$ and $\Delta_{\sup,mes}$ can be calculated using Eqn. 6.6, 6.8 and 6.20 separately. The estimation of $\Delta_{\sup,set}$ requires a number of data when the chillers works at steady state. The common used 95% confidence rule can be used in this case, i.e., 95% of these measurements should fall inside the range specified by $\Delta_{\sup,set}$ [Duta M., Henry M., 2005]. As well, $\Delta^{*}_{pum,j}$ can be also determined using the 95% confidence degree. Other confidence rules can also be used.

Table 6.1. Parameters of the online sensor fault diagnosis algorithm

Parameter	Description
Δ_{hp}	Uncertainty associated with the water flow measurement in header pipe
$\Delta_{pum,j}$	Uncertainty associated with the water flow measurement for j^{th} operating pump
$\Delta^{*}_{pum,j}$	Uncertainty associated with calculated water flow $M^{*}_{p,j}$ for j^{th} operating pump based on pressure drop
$\Delta_{\mathrm{sup},set}$	Uncertainty associated with the tracking control of $T_{\mathrm{sup},set}$
$\Delta_{\mathrm{sup},mes}$	Uncertainty associated with chilled water supply temp measurement
N_w	Length of the moving window used in the diagnosis criteria

However, it should be noted that when these uncertainty-related parameters, including $\Delta_{hp}, \Delta_{pum,j}, \Delta^{*}_{pum,j}, \Delta_{\mathrm{sup},set}, \Delta_{\mathrm{sup},mes}$, have a larger value, the diagnosis criterions become less sensitive to the faults. when the number of operating chillers are different, the uncertainty related to the sum of water flow of operating pumps Δ_{sum} might be different and therefore different values of Δ_{sum} should be used.

The fault report consists of three items $F_w, F_{\mathrm{sup}}, F_{rtn}$ denoting the fault status of the chilled water flow rate, supply and return temperature respectively. The value of these items is zero indicating there are no faults in the corresponding measurement;

while the value is unity indicating a fault is found. The fault report will be sent to BAS to notify system operators to repair the faults promptly.

6.3. Validation Case Studies

The dynamic simulation platform constructed in chapter 3 is used to validate the developed FDD strategy. For simulating the realistic sensor measurements, noises and outliers were deliberately added to the related measurements. The Gaussian noise with the distribution $N(0,0.01)$ was added to the measurements of temperature sensors. The outliers were set to 1℃ or -1℃ randomly. Pseudo systematic errors were added to represent the faults occurred in the chilled water flow and temperature measurements. Four different cases were studied. In the first three cases, faults occurred solely in each of the three measurements; while in the last case, faults occurred in the three measurements simultaneously.

The threshold of the confidence degree for detecting systematic error was set to $\varepsilon = 0.001$. Least square fitting was used to identify the parameters of Eqn. 6.1, which yielded $a_0 = 972.7, a_1 = -3.0, a_2 = 0.0032$. Tests under different operating conditions showed that the relative error introduced by Eqn. 6.1 was less than 2%. Therefore, the uncertainty Δ^*_{pum} was assigned the value $2\% \times M_{pum}$. $\Delta_{pum,j}$ due to measurement noises was set to 20.58kg/s for operating pumps; while Δ_{hp} for the header pipe was set to 35.8kg/s. The length of the moving window Nw was 8. The parameter $\Delta_{\mathrm{sup},set}$, which is used to account for the imperfect close-loop temperature control of chillers as well as disturbances, was set to 0.18℃. It is because simulation study showed that

when the set point for the chilled water was 5.5℃, 95% of the temperature measurements were inside the range [5.5±0.18] ℃. The standard deviation of the noise in the chilled water supply temperature measurement was 0.1℃, and hence $\Delta_{\text{sup},mes} = 0.196℃$.

Two different types of errors were employed in the simulation. One was used to represent the slow drift fault of the sensor measurement and it was entitled *ramp error*. The ramp errors started with different changing rate and were kept at their maximum absolute value after reached them. The second one was used to represent abrupt faults in the sensor measurement and it was called *step error*. Its value was maintained constant in the duration.

6.3.1 Case with Fault Occurring in the Flow Meter

Ramp and step errors were both added to the chilled water flow rate measurements. The durations of the ramp errors were 6 hours. One of the ramp errors reached its maximum absolute value (i.e. 15% of its total water flow rate) at the end of the duration; others changed with a greater rate and achieved the peak absolute value earlier. The step errors also lasted for 6 hours and their absolute values were assigned to 15% of the total water flow, shown in Figure 6.4 (top). The systematic errors were detected by the confidence degree of the fused measurement. It can be seen from Figure 6.4 (middle) that the confidence degree fell rapidly down to smaller than ε until the systematic error disappear. The bottom one is the chiller automatic control performance.

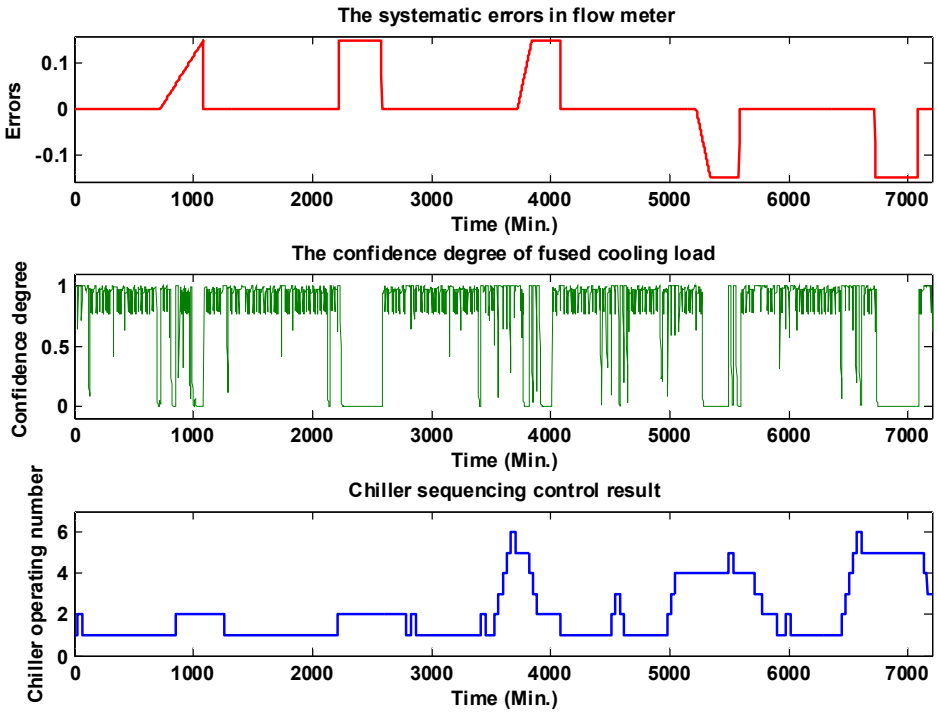

Figure 6.4. Confidence degree and chiller automatic control performance when faults only occurred in flow meter

Figure 6.5 illustrates the results of the sensor fault diagnosis algorithm, which shows that all systematic errors were successfully isolated. It should be noted that there is delay in the fault diagnosis for the ramp errors as well as in the step errors. This is because the data fusion algorithm needs time to detect the systematic errors and the time is smaller than the time span of the moving window, usually less than 20 minutes, see Section 4.6. Also, the moving window used in Diagnosis Criterion 1 will lead to short term time delay. Since the fusion algorithm needs longer time to detect the ramp errors, the delay in diagnosing the ramp errors was larger than in diagnosing the step errors, see Figure 6.5 the top plot.

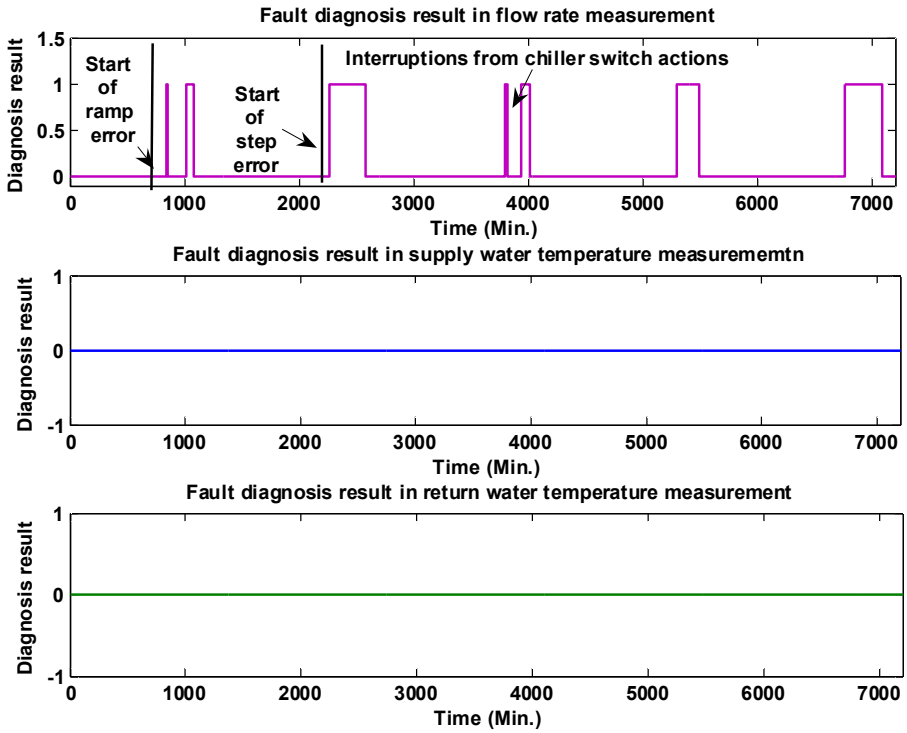

Figure 6.5. Fault diagnosis results of the three measurements

The fusion algorithm stopped working during transients (*i.e.*, a chiller was switched on or off and the chilling system has not reached its stable state), the fault diagnosis algorithm also stopped working. This was the reason why the duration of diagnosed faults was shorter than the duration of the actual fault, which can be observed in Figure 6.5.

6.3.2 Case with Fault Occurring in the Supply Temperature Sensor

The systematic errors added to the supply water temperature measurement included both ramp and step errors. The maximum absolute value of the ramp errors was 0.9℃ and each of them lasted for 6 hours. The varying rates of them were different from each other. The step errors kept their values at either 0.9℃ or -0.9℃

for 6 hours, shown as Figure 6.6 (top). Figure 6.6 (middle) shows that all the faults in the supply temperature measurement were detected by the low confidence degree and they rose up when switch action of chiller occurred, shown in dotted box.

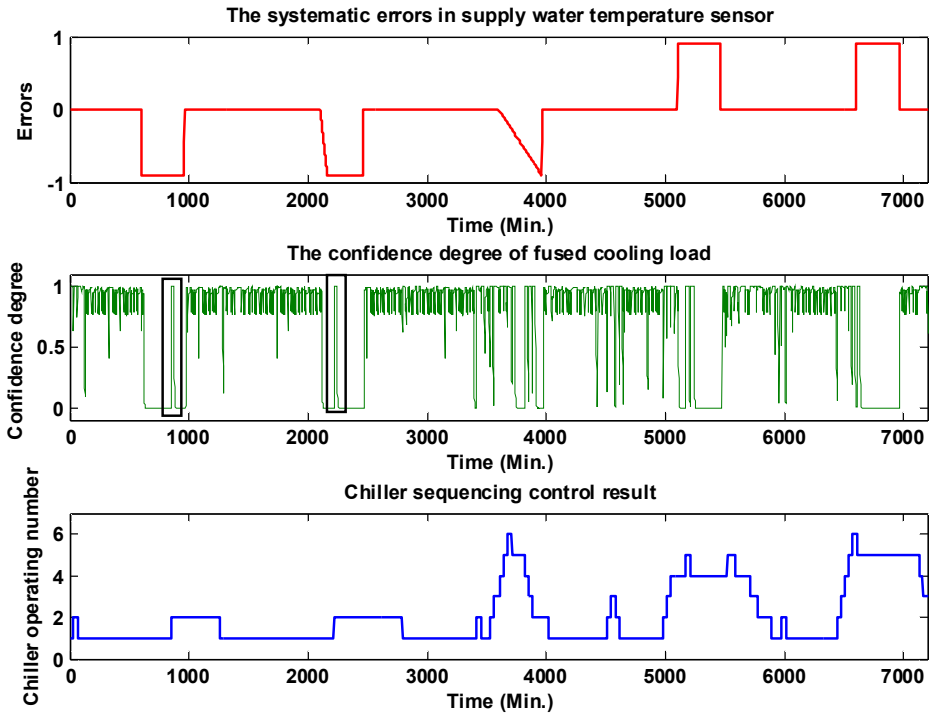

Figure 6.6. Confidence degree and chiller automatic control performance when faults only occurred in supply water temperature sensor

Figure 6.7 presents the diagnosis results. It can be seen that all the faults were successfully diagnosed although delay in the diagnosis and the influence of the transients on the diagnosis results were still observed. Note that the performance of chiller automatic control in this case was slightly different from the one when faults occurred in the supply water flow measurements, which shows the necessity of fault diagnosis.

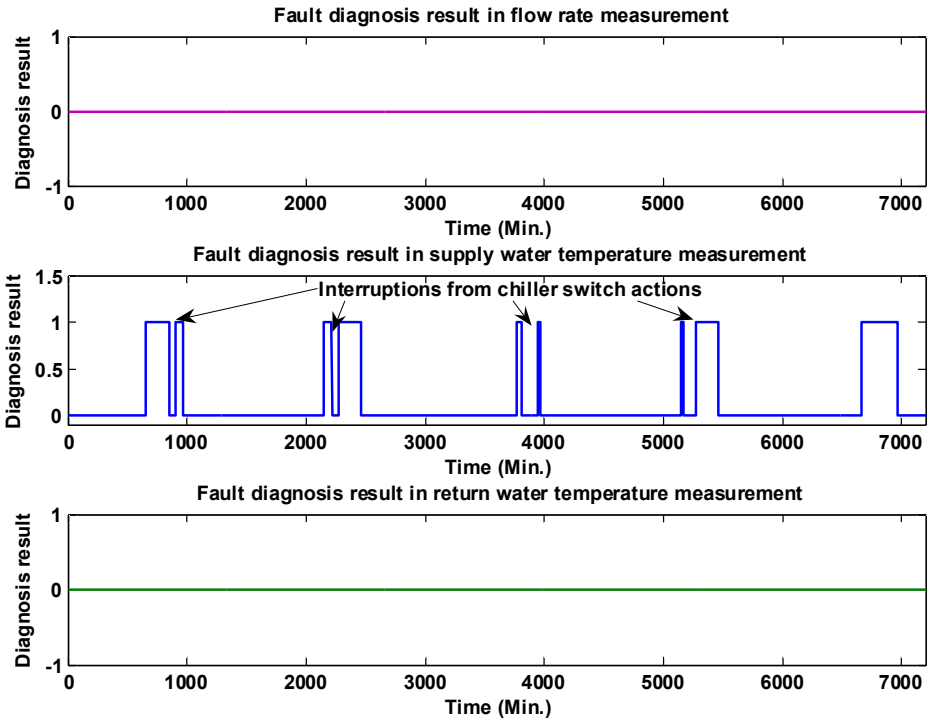

Figure 6.7. The fault diagnosis results of the three measurements

6.3.3 Case with Fault Occurring in the Return Temperature Sensor

The errors added to the return chilled water temperature measurement included two six hour-lasting ramp errors with different increasing rates and the same maximum value 0.9℃ and three step errors with assigned value -0.9℃ lasting for six hours, shown as Figure 6.8.

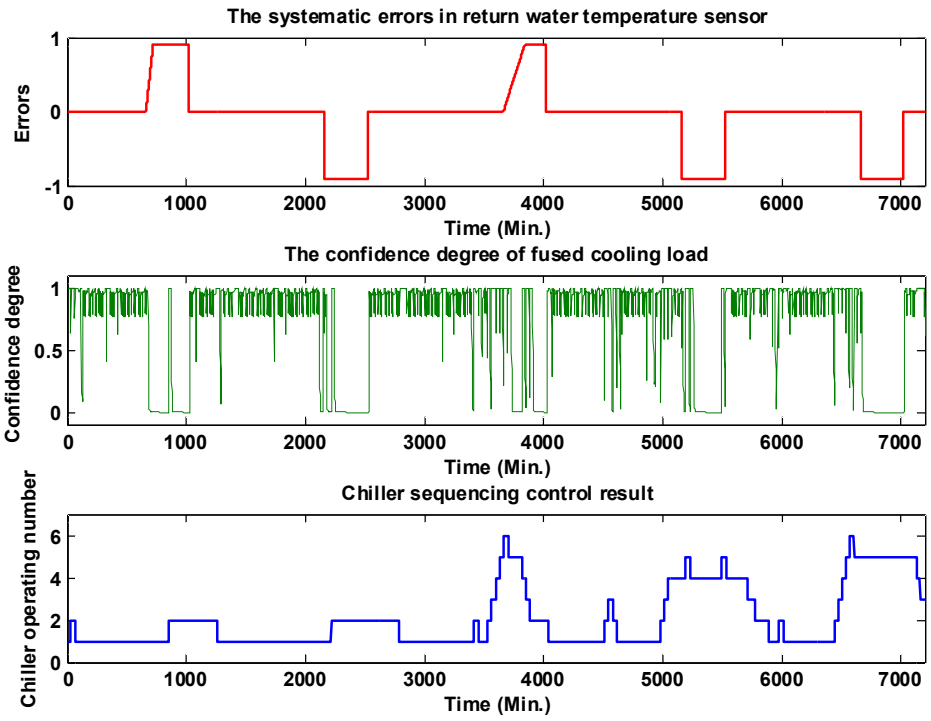

Figure 6.8. The confidence degree and chiller automatic control performance when faults only occurred in return water temperature sensor

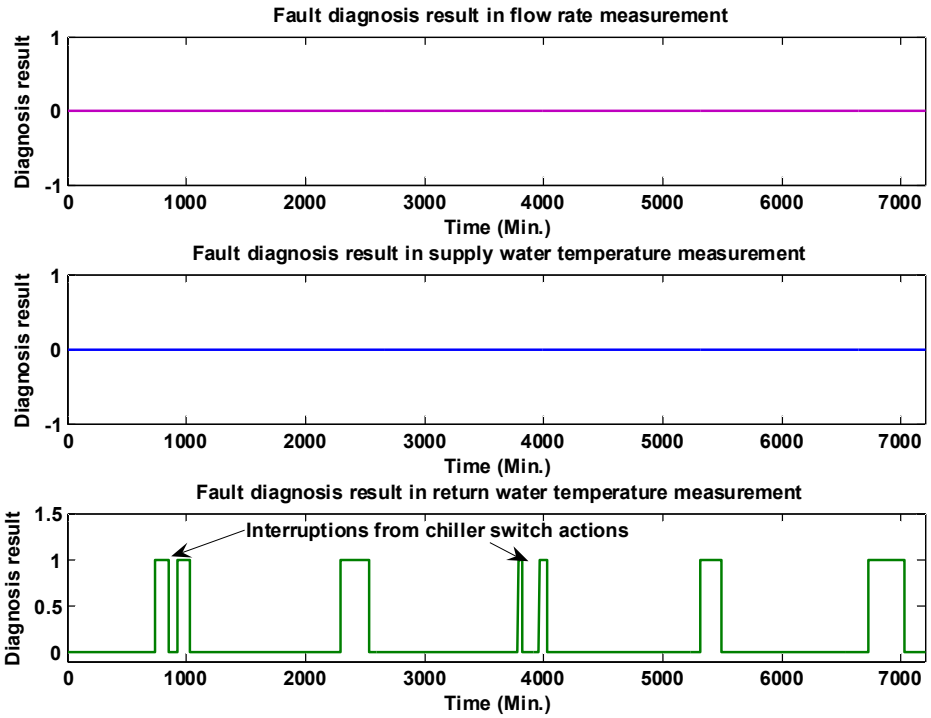

Figure 6.9. The fault diagnosis results of the three measurements

Figure 6.8 (middle) described the confidence degree, which shows that the systematic errors were successfully detected. Figure 6.8 (bottom) illustrates the operating chiller number given by chiller automatic control.

Figure 6.9 shows the diagnosis results. Once again, the faults were isolated but with a slight delay. Note that in this case, Diagnosis Criterion 3 was used because there were no faults in both the chilled water flow measurements and the chilled supply water temperature measurements.

6.3.4 Case with Multiple Faults Occurring in All Three Measurements

For fully testifying the fault diagnosis strategy, all of the measurements were added systematic errors, see Figure 6.10 (the top three plots).

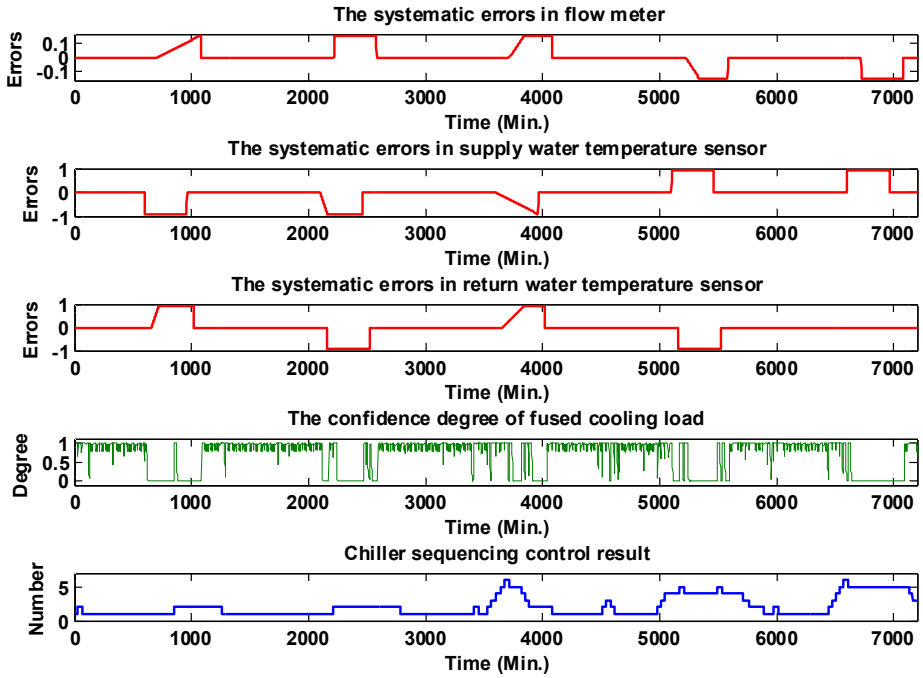

Figure 6.10. The confidence degree and chiller automatic control performance when faults occurred in all three measurements

Due to the simultaneous occurrence of these systematic errors, interruptions of chiller switching actions，the fault detection by the confidence degree became more difficult. However, these faults were detected by the confidence degree as shown in Figure 6.10. Since there are faults in the chilled water flow and supply temperature measurements, Diagnosis Criterion 4 was used to diagnosis faults in the chilled water return temperature measurements. Figure 6.11 presents the diagnosis results, which shows that these faults were also diagnosed correctly.

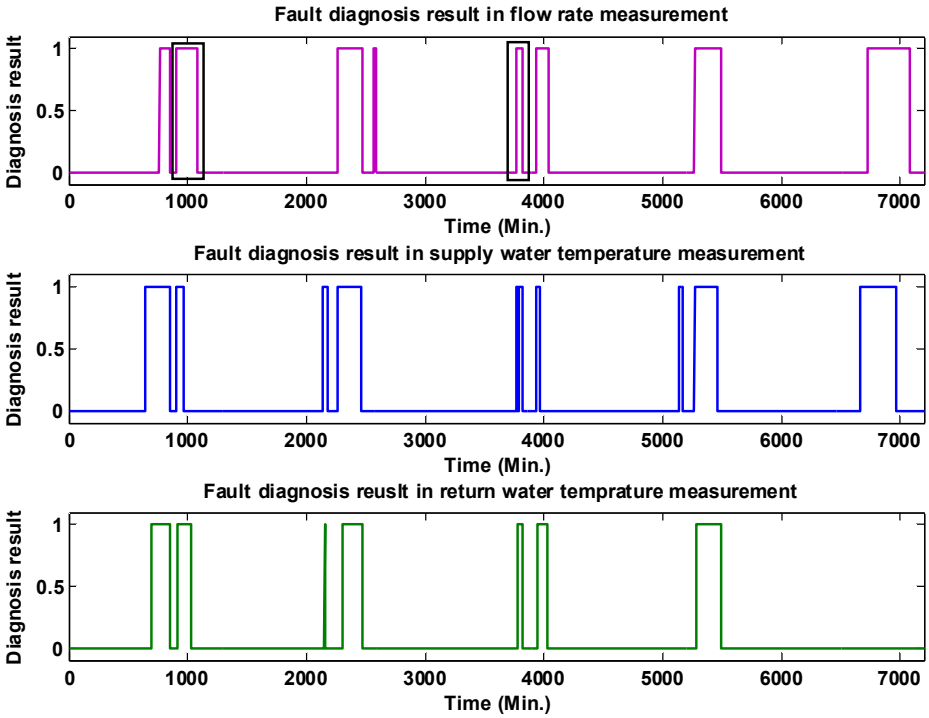

Figure 6.11. The fault diagnosis results of the three measurements

Although the errors in the chilled water flow measurements and in the chilled water supply temperature measurements were the same with those used in previous subsections, the diagnosis results given by Diagnosis Criterion 1 and Diagnosis

Criterion 4 may be different due to the overlapping of these faults. For example, the first and the third fault diagnosed in the chilled water flow measurements in Figure 6.5 were shorter than the corresponding faults shown in dotted box in Figure 6.11. As many other diagnosis strategies, parameter set-up is also significant for appropriate diagnosis in this strategy. Figure 6.12 gives an example when $\Delta\hat{Q}_{dm}$ used a different value, i.e., $\Delta\hat{Q}_{dm} = 60kW$. Misjudgment was observed as shown in the dotted box in the diagnosis result in the chilled water return temperature. Therefore, in practical application, the parameters in these diagnosis criteria should be carefully set during commissioning.

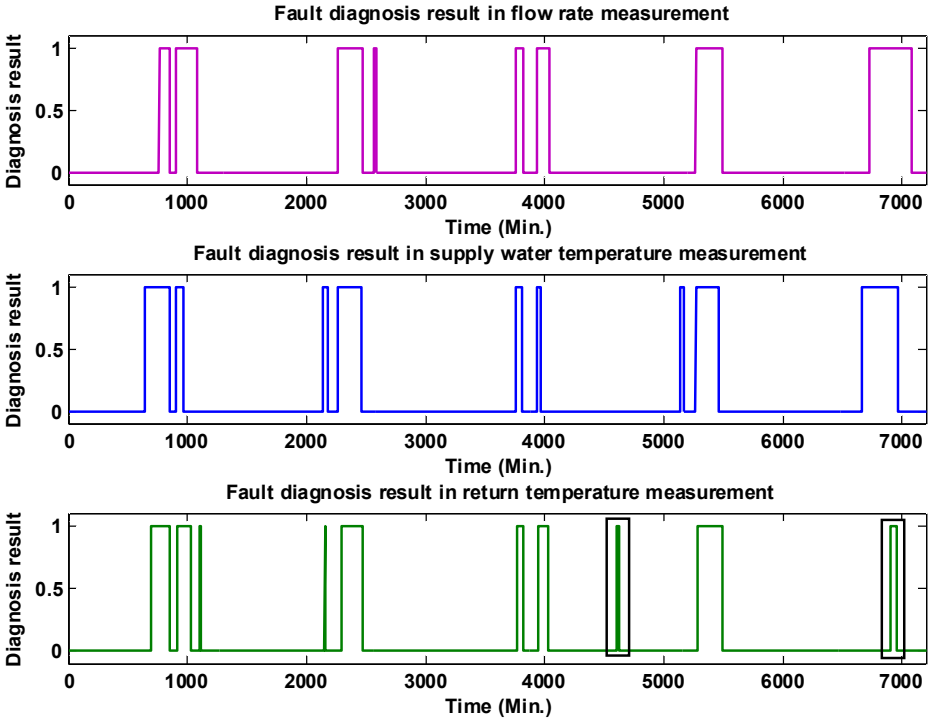

Figure 6.12. The fault diagnosis results of the three measurements when $\Delta\hat{Q}_{dm}$ was inappropriately set

6.4. Summary

An online sensor fault diagnosis strategy based on the data fusion technology has been presented to diagnose sensor faults in building cooling load direct measurement for improving the robustness of chiller performance monitoring and automatic control. It has been shown that faults in the chilled water flow and supply temperature measurement can be efficiently diagnosed using the Moffat consistency test method since both measurements have an expected value while faults in the chilled water return temperature measurement can be diagnosed using the confidence degree reconstruction method.

Tests results showed that whether faults occurred solely or simultaneously in the three measurements, they can be successfully isolated by the proposed strategy. It will be helpful to inform the operator to repair/replace the faulty measuring instruments in time. Hence the healthy sensor measurements are guaranteed which will further enhance the robustness of chiller performance monitoring and the reliability of automatic control for energy efficiency. It should be noted that the properly assigned values for the parameters used in the method are significant for ensuring a satisfactory diagnosis result. Therefore, careful parameters configuration in the commissioning period is required before the method is applied.

CHAPTER 7 MODEL-BASED OPTIMAL START CONTROL STRATEGY

Chiller plant optimal start control aims to recover the indoor room temperature to a desired level before occupancy with as less energy consumption as possible. A model-based optimal start control strategy is proposed in this chapter, which considers both the recovery ability and the pre-cooling lead time as the optimizing variables. In most previous studies, only the pre-cooling lead time is of major concern.

Section 7.1 briefly introduces the basic idea of the developed mode-based optimal start strategy. The essential cooling load prediction, estimation of pre-cooling lead time and calculation of energy consumption are as well addressed in this section. The validation of proposed strategy is performed in section 7.2. The associated application issues are discussed in section 7.3 and a brief summary of this chapter is presented in section 7.4.

7.1 Model-Based Optimal Start Control Strategy

7.1.1 Outline of the control Strategy

Assume there are *Nc* chillers equipped in a commercial building. The two steps in the model-based optimal start control strategy are illustrated in Figure 7.1. In the first step, a feasible set is determined for the operating chiller number.

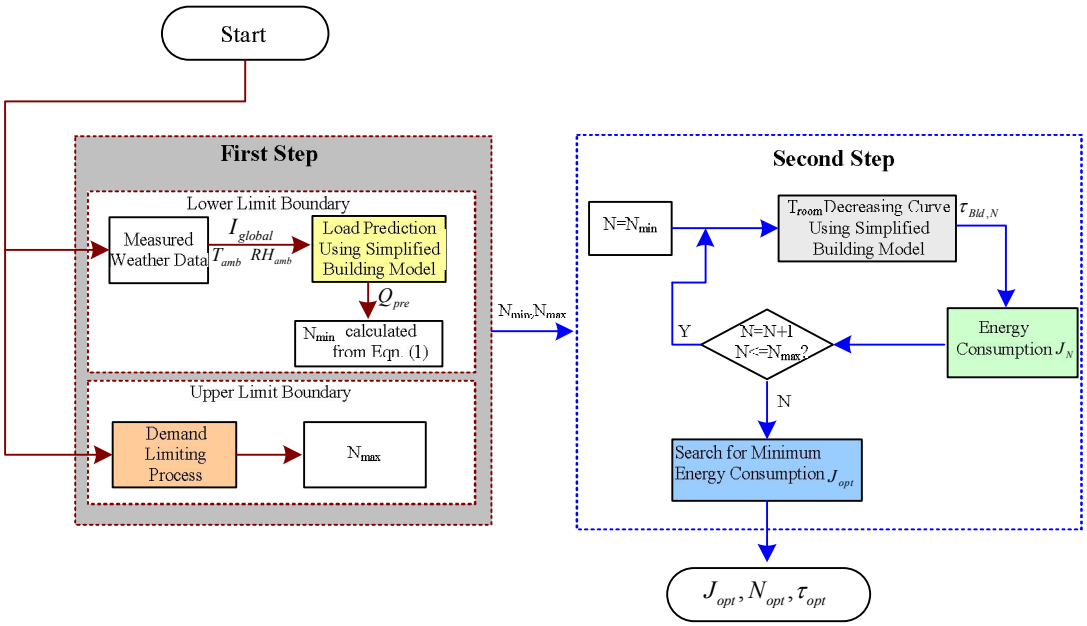

Figure 7.1. The schematic diagram of the proposed optimal start control strategy

The feasible set should satisfy the condition that any number of chillers in the set is able to fulfill the building cooling load requirement, *i.e.* the building internal temperature can be cooled down to its set-point in a limited pre-cooling period. Denote the feasible set as E_c and define it as (7.1), where $N_{\min}$ is the minimum number and $N_{\max}$ is the maximum number. The minimum number is calculated according to the predicted building cooling load Q_{pre} in the pre-cooling period and the chiller rated cooling capacity *MCC*, as shown by (7.2), where *ceil*(x) is a function to round x to the integer toward positive. The prediction of Q_{pre} is performed using the measured weather data including global solar radiation I_{global}, outdoor temperature T_{amb} and the relative humidity RH_{amb} at the time to run the program of generating the chiller optimal start schedule, usually one hour ahead of occupancy in the morning.

$$E_c := \{N : N_{\min} \le N \le N_{\max}\} \tag{7.1}$$

$$N_{\min} = ceil\left(Q_{pre} / MCC\right) \tag{7.2}$$

Theoretically, any number larger than $N_{\min}$ can satisfy the cooling load requirement. However, if the number is large enough, the risk of exceeding the pre-defined electrical demand limit will be high. Therefore, the maximum number in the feasible set should satisfy the building cooling load but not break the pre-defined electrical demand limit. It can be obtained from the related building demand limiting control strategy [J.E. Seem et al., 1989].

In the second step, the pre-cooling lead time is estimated for each number in the feasible set as well as the corresponding energy consumption J_N. Given the operating chiller number N for pre-cooling and the predicted cooling load (obtained in the first step), the simplified building model employed in the first step is used to compute the building pre-cooling lead time $\tau_{Bld,N}$. The model-based pre-cooling lead time calculation is presented in Section 2.3. The energy consumption of the chiller plant is computed by summarizing all the energy consumed by components, which is illustrated in Section 2.4. The optimal schedule is selected by comparing the total energy consumption of different numbers of operating chillers.

7.1.2 Model-based Cooling Load Prediction

Building cooling load is predicted using the measured weather data at the moment running the program of the start control strategy to generate the chiller optimal start schedule (*e.g.* one hour ahead of occupancy) and the simplified building

model developed by Wang and Xu [2006]. The prediction of cooling load for the central chilling system (i.e. building cooling load) is performed as (7.3), where these temperature variables *T*s and resistance parameters *R*s are defined in Figure 7.2; Q_{win} is the heat gain through the window; Q_{conv} is the convection heat gain; Q_{fr} is the heat gain introduced by the fresh air; and $Q_{la,occup}$ are the latent load from the building occupants. These heat loads computation processes are presented in details in [X.H. Xu, 2005.].

$$Q_{pre} = \sum_{i=1}^{n}\left(\frac{T_{ei,4(t)} - T_{in(t)}}{R_{ei,5}}\right) + \frac{T_{rf,4(t)} - T_{in(t)}}{R_{rf,5}} + \frac{T_{im,2(t)} - T_{in(t)}}{R_{im,2}} + Q_{win} + (Q_{conv} + Q_{fr} + Q_{la,occup}) \tag{7.3}$$

The simplified building model is in the electrical analogue pattern with resistance (*R*) and capacitance(*C*), as illustrated in Figure 7.2. For building cooling load prediction Q_{pre}, the simplified model takes the measured weather data (T_{amb}, I_{global}, and RH_{amb}) as its inputs and systematically calculates the various heat gains including heat transfer from walls, roofs and windows, heat charge and discharge through the internal mass and internal air. Heat gain from the fresh air, infiltration, lighting and equipments are also considered. It should be noted the latent load from occupants (shown as the dotted box part) has no impact on the node temperature in the thermal network. However, it is need to be considered if the humidity control is performed. In this calculation process, the internal room temperature is assumed to be its set-point. The simplified building is comprised of two parts. The first one is the building envelopes including walls and roofs represented with 3R2C. The resistance R and capacitance C in this part can be identified by matching frequency response

characteristics of physical walls with that of optimization from genetic algorithm (GA). The second part is the internal mass consisting of partitions, furniture, etc., represented with 2R2C. These four parameters are identified in a different way which is based on the heat balance principle [S.W. Wang, X.H. Xu. 2006] The main reason for the different parameters identification methods is the availability of the theoretical building envelope model and no theoretical internal mass model available.

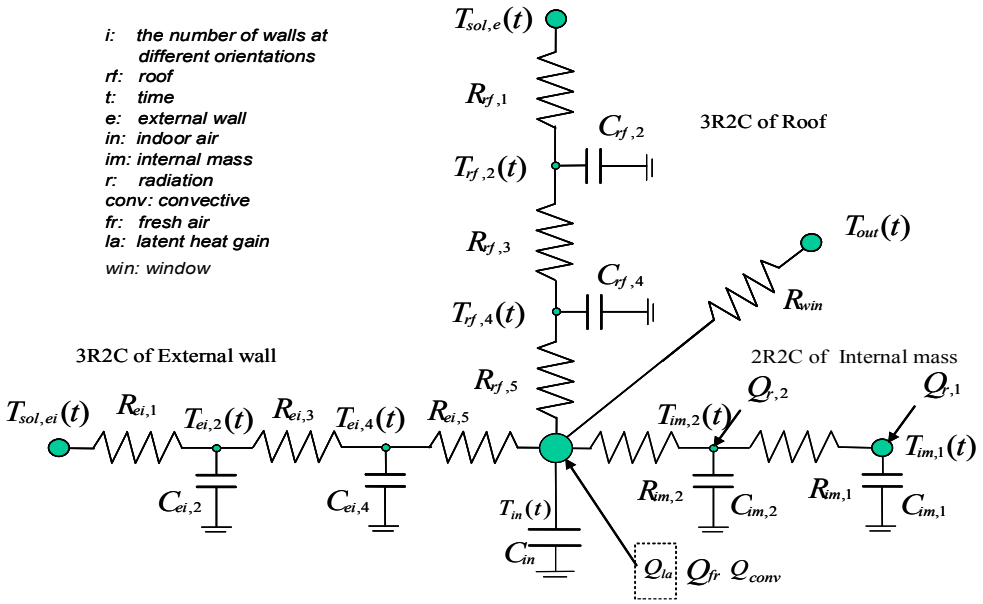

Figure 7.2. Schematic structure of the simplified building thermal network

The procedures for the building cooling load prediction are as follows. Firstly, the outdoor temperature T_{amb} and the wall absorbed radiation W_{Rad} calculated from the global radiation I_{global} (see the Appendix A) are used to calculate the solar air temperature T_{sol} by (7.4), where $\hat{\varepsilon}$ is the wall absorption coefficient; $\hat{\Omega}$ is external wall heat transfer coefficient; and the two coefficients are determined by the wall material. Then, the node temperatures such as $T_{ei,4}$, $T_{rf,4}$, $T_{im,2}$ are computed by solving

the differential equations after the solar air temperature T_{sol}, predicted RH_{amb} and the identified resistance R and capacitance C are known . Details are referred to the reference [S.W. Wang, X.H. Xu. 2006].

$$T_{sol} = T_{amb} + \frac{\hat{\varepsilon} \times W_{Rad}}{\hat{\Omega}} \tag{7.4}$$

7.1.3 Model-based Pre-cooling Lead Time Prediction

The simplified building model is also used to describe the indoor temperature variation, shown as equation (7.5), where Q_{sup} is the cooling supplied from chiller plant. When the variables in the right hand side of (7.5), such as Q_{sup}, Q_{win}, *etc.*, are known, the indoor room temperature variation curve is obtained by solving (7.5). The building pre-cooling lead time $\tau_{Bld,N}$ is the time span from the start moment to the moment as building internal temperature stabilized into the area defined by the indoor room temperature set-point with ±0.2℃ error. As an example, Figure 7.3 illustrates the indoor room temperature variation and the definition of the building pre-cooling lead time $\tau_{Bld,N}$, where N represents the number of operating chillers. The initial indoor and outdoor temperatures are measured at the beginning of start control implementation.

$$\begin{aligned} C_{in}\frac{dT_{in(t)}}{dt} = Q_{\sup} - \sum_{i=1}^{n}\left(\frac{T_{ei,4(t)} - T_{in(t)}}{R_{ei,5}}\right) - \frac{T_{rf,4(t)} - T_{in(t)}}{R_{rf,5}} \\ - \frac{T_{im,2(t)} - T_{in(t)}}{R_{im,2}} - (Q_{win} + Q_{conv} + Q_{fr} + Q_{la,occup}) \end{aligned} \tag{7.5}$$

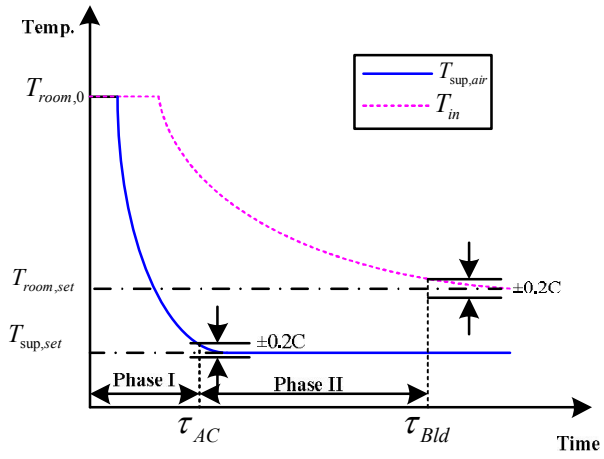

Figure 7.3. The indoor room temperature and supply air temperature variation curve

7.1.4 Energy Consumption Estimation

The total energy consumption is calculated using (7.6), where J_N is the energy consumption of the chiller plant when N chillers operate; EC is the energy consumption of the components and the subscripts 'fan','cp','ct', 'chi' and 'vp' represent supply fan in the air handling unit (AHU), constant speed pumps, cooling towers, centrifugal chillers and variable speed pumps respectively.

$$J_N = EC_{fan} + EC_{cp} + EC_{ct} + EC_{chi} + EC_{vp} \tag{7.6}$$

The energy consumption of the AHU fans, the cooling towers and the constant-speed pumps are calculated by (7.7), (7.8) and (7.9) separately, where P is the rated power consumption, Num is the number of operating component. Here, the power consumptions of these components do not change significantly in the pre-cooling process because they operate at a relatively constant speed (e.g. the supply fan in AHU maintains at its maximum speed prior to the building indoor temperature reaching its set-point).

$$EC_{fan} = Num_{fan} \times P_{fan} \times \tau_{Bld,N} \tag{7.7}$$

$$EC_{CT} = Num_{ct} \times P_{ct} \times \tau_{Bld,N} \tag{7.8}$$

$$EC_{cp} = Num_{cp} \times P_{cp} \times \tau_{Bld,N} \tag{7.9}$$

The calculation of the chiller energy consumption is divided into two parts: Phase I and Phase II. As shown in Figure 7.3, Phase I, denoted as the air-conditioning system pre-cooling lead time $\tau_{AC,N}$, is the time interval from the chiller start moment to the moment when the supply air temperature is stabilized into its set-point area with ±0.2℃ error. Phase II is the time span defined by $\tau_{Bld,N} - \tau_{AC,N}$. The energy consumed in Phase I and Phase II is calculated by (7.10) based on the assumption that the cooling load variation in Phase II is negligible. In Phase I, $P_{chiller}$ takes its rated power because the supplied cooling is insufficient for the supply air temperature reaching its set-point and chillers are controlled to operate at its maximum cooling capacity during this period. In Phase II, the chillers work at part load condition and hence the actual power consumption is calculated based on the predicted building cooling load and the chiller coefficient of performance (*COP*). The *COP* is calculated by (7.11), where *PLR* is the part load ratio between the single chiller actually supplied cooling Q_{sup} and the chiller rated cooling capacity Q_{rated}, *i.e.* $\mathrm{PLR} = \mathrm{Q_{sup}} / Q_{rated} = Q_{pre} / (N \times Q_{rated})$. $c_0,\ldots,c_n$ are the coefficients that can be obtained during commissioning.

$$EC_{chiller} = \underbrace{N \times P_{chiller} \times \tau_{AC,N}}_{Phase\ \mathrm{I}} + \underbrace{Q_{pre} \times (\tau_{Bld,N} - \tau_{AC,N}) / COP}_{Phase\ \mathrm{II}} \tag{7.10}$$

$$COP = c_n \times PLR^n + \ldots + c_1 \times PLR + c_0 \tag{7.11}$$

The energy consumption of the variable speed pumps, which are used to

distribute chilled water into the secondary loop, is calculated in a similar way, as shown in (7.12). The first part is the energy consumed in Phase I, during which the chilled water from the primary loop is assumed to be completely distributed to the AHU. In this part, P_{vp} is the rated power of the pump motor, $M_{pum,sup}$ is the actual water flow rate which is determined by the operating chiller number N, operating variable speed pump number Num_{vp} and the rated chilled water flow rate of single chiller $M_{chi,rated}$, as shown in (7.13). In the second part, the surplus chilled water will be bypassed and the actual distributed water flow rate is approximated by (7.14) with the assumption that the temperature difference ΔT in chilled supply and return water varies not significantly in the period. $M'_{pum,\sup}$ is the actual water flow rate in the secondary phase; $M_{pum,rated}$ represents pump rated water flow rate; and Q_0 represents the cooling amount when rated chilled water flow is distributed.

$$EC_{vp} = \underbrace{Num_{vp} \times \left(\frac{M_{pum,\sup}}{M_{pum,rated}} \right)^3 \times P_{vp} \times \tau_{AC,N}}_{Phase\ \mathrm{I}} + \underbrace{Num_{vp} \times \left(\frac{M'_{pum,\sup}}{M_{pum,rated}} \right)^3 \times P_{vp} \times \left(\tau_{Bld,N} - \tau_{AC,N} \right)}_{Phase\ \mathrm{II}} \tag{7.12}$$

$$M_{pum,\sup} = N \times M_{chi,rated} / Num_{vp} \tag{7.13}$$

$$\frac{M'_{pum,\sup}}{M_{pum,rated}} = \frac{Num_{vp} \times C_p \times M'_{pum,\sup} \times \Delta T}{Num_{vp} \times C_p \times M_{pum,rated} \times \Delta T} = \frac{Q_{pre}}{Q_0} \tag{7.14}$$

The length of $\tau_{AC,N}$ is estimated as follows. Firstly, a first-order plus time-delay transfer function (7.15) is used to represent the supply air temperature descending process, where K, Γ, ς are the process gain, time constant and time delay respectively. Since under different cooling load conditions, the time constant Γ are different. Therefore, Equation (7.16) is derived based on the case study results to approximate

the relationship between Γ and the cooling load Q_{pre}, where $a_{0,N}$ and $a_{1,N}$ are coefficients and can be identified using field data. The time delay ς is calculated as (7.17), where L_{pipe} is the pipe length and Λ is the cross area of the pipe. Then, the length of τ_1 is given by (7.18), where '4' is used because the settling time (±0.2℃ error) for a first-order system is approximately 4 times of the system time constant [K. Ogata. 1996].

$$G(s) = \frac{K}{1+\Gamma_N s} e^{-\varsigma_N s} \tag{7.15}$$

$$\Gamma_N = a_{1,N} \times Q_{pre} + a_{0,N} \tag{7.16}$$

$$\varsigma_N = \frac{L_{pipe} \times \Lambda}{N \times M_{chi,rated}} \tag{7.17}$$

$$\tau_{AC,N} = 4\Gamma_N + \varsigma_N \tag{7.18}$$

7.2. Validation Case Studies

The reliability and accuracy of the strategy depends mainly on the reliability of the simplified building model and on the accuracy of calculating the air-conditioning system pre-cooling lead time $\tau_{AC,N}$ (the length of Phase I), building pre-cooling lead time $\tau_{Bld,N}$ and J_N (the energy consumption). Because the reliability of the simplified building model was studied in the references [Q. Zhou et al., 2009.] and [X.H. Xu. 2005] separately, this paper focuses on validating the calculation accuracy of $\tau_{AC,N}$, $\tau_{Bld,N}$ and J_N. Before these validations, the significance of selecting proper operating chiller number for pre-cooling was investigated.

7.2.1 Energy Consumption When Different Number of Chillers Operating

Figure 7.4 presents the energy consumption in the pre-cooling period when the chiller operating number varies from 2 to 6 in the simulated building system. The case of only one chiller operating is omitted due to its incapability of cooling down the building to the desired condition. The Figure confirms that different number of operating chillers for pre-cooling results in different energy consumption in the pre-cooling period. If an inappropriate number of chillers is selected, a large amount of energy may be wasted. For instance, the energy consumed by two chillers on the 22nd day was about as twice as that consumed by 4 chillers. The difference was mainly due to the significant difference in the length of the pre-cooling lead time. When two chillers were switched on for pre-cooling, the system took around 50 minutes to cool down the building internal temperature to the desired level, while 4 chillers took about 15 minutes.

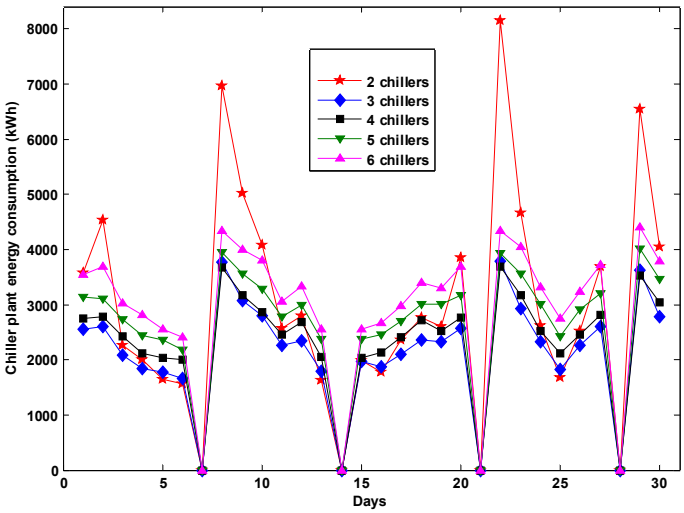

Figure 7.4. Energy consumptions of 30 days in pre-cooling period when different number of chillers operate

7.2.2 Validation of Air Conditioning System Pre-cooling Lead Time

The calculation of $\tau_{AC,N}$ by (7.18) is based on the assumption that the supply air temperature variation can be approximated by a first-order plus time delay model (7.15). The solid line in Figure 7.5 shows the supply air temperature variation when two chillers were used for pre-cooling. It can be observed that the first-order transfer function (i.e. dotted line) can well describe the supply air temperature descending process. This conclusion is also true when other numbers of chillers were used for pre-cooling.

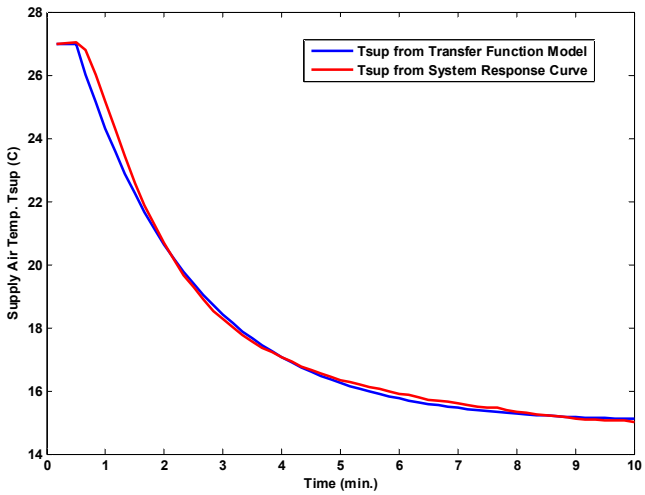

Figure 7.5. The supply air temperature variation procedure: the dotted line obtained from the transfer function model (7.15) and the solid line obtained from the system response curve

The data in the first week (obtained in the case study described in the previous section), including the cooling load and the values of Γ, were use to identify the parameters in (7.18), *i.e.* a_1 and a_2, with the least square method. The identification results are listed in Table 7.1, which shows that the values of a_1 and a_2 were different

for different operating chiller numbers. In addition, the length and the cross area of the pipe for delivering the chilled water are 250m and 0.5m^2 separately; and $M_{chl,rated}$ is set to 0.345m^3/s. The rest data obtained in the case study described in the section 4.1 were used to validate the relationship function (7.18). Figure 7.6 shows the comparison of the values of $\tau_{AC,N}$ computed using (7.18) with those computed from the system response curves. The average relative errors were 13.6%, 7.7%, 5.20%, 4.51% and 4.33% respectively when the number of operating chillers changed from 2 to 6. A big error occurred when only two chillers were used. This is probably because the approximation (7.16) might not be accurate enough when the supply air temperature descending process has a significantly different time constant at different load condition.

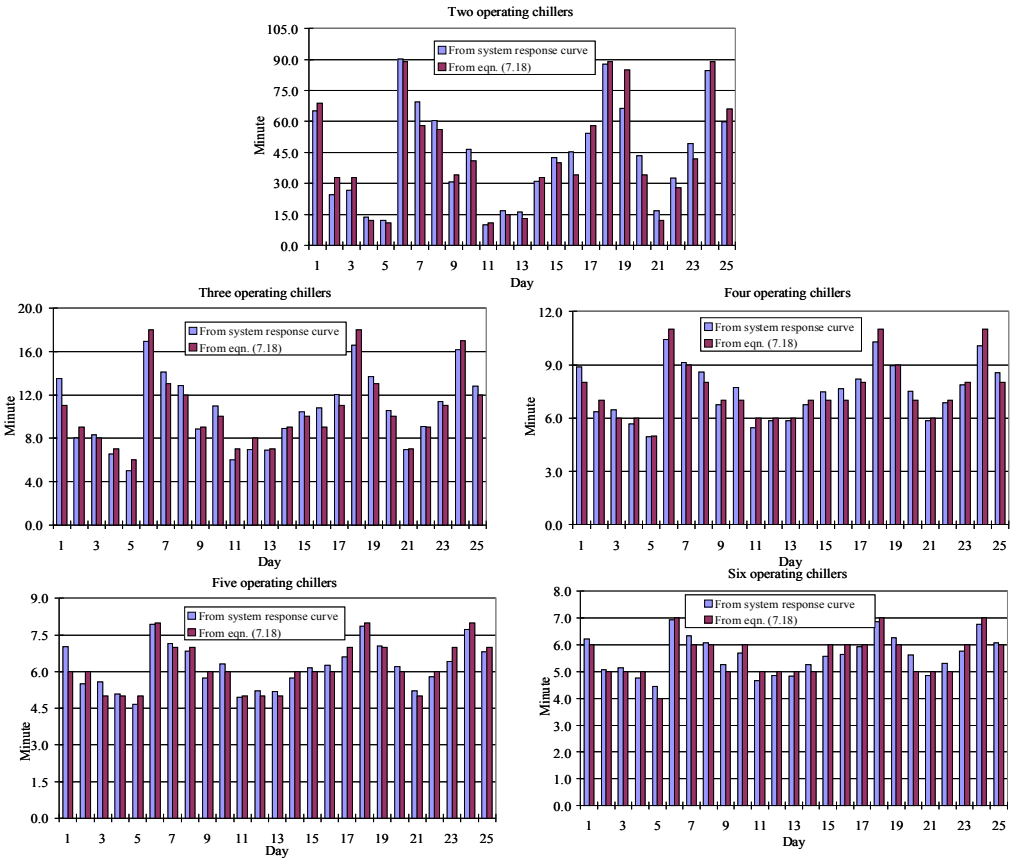

Figure 7.6. Comparison of the length of air-conditioning system pre-cooling lead time

Figure 7.6 also shows that $\tau_{AC,N}$ decreases accordingly with the increase of the operating chiller number. There are drastic reductions in the time length when the operating chiller number was changed from two to three. However, this type of significant reductions was not observed when four or more chillers were used. The reason may be that since the building internal temperature is under feedback control, the more than necessary operating chillers are controlled to operate at low part load condition for solely ensuring the internal room temperature maintain at its set-point in the pre-cooling period.

Table 7.1. The values assigned to the used parameters

N_{chiller}	ς (Min.)	a_1	a_0
1	6	----	----
2	3	1.3×10^{-3}	-15.00
3	2	2.0×10^{-4}	-0.8607
4	1.5	1.0×10^{-4}	0.2781
5	1.2	5.0×10^{-5}	0.5884
6	1	2.5×10^{-5}	0.6682

7.2.3 Validation of Building Pre-cooling Lead Time

Figure 7.7 compares the values of $\tau_{Bld,N}$ when they were computed from the simplified model (7.5) with those computed from the system response curves. The average relative errors were 14.5%, 4.58%, 3.20%, 2.93% and 2.31% respectively when the number of operating chillers changed from 2 to 6. It was also observed that the increase of chiller operating number from two to three was able to greatly reduce the pre-cooling lead time from 50 minutes to less than 25 minutes. However, further

increase of chiller operating number had less significant impact on the reduction in the pre-cooling lead time. This may due to the same reason explained in previous section.

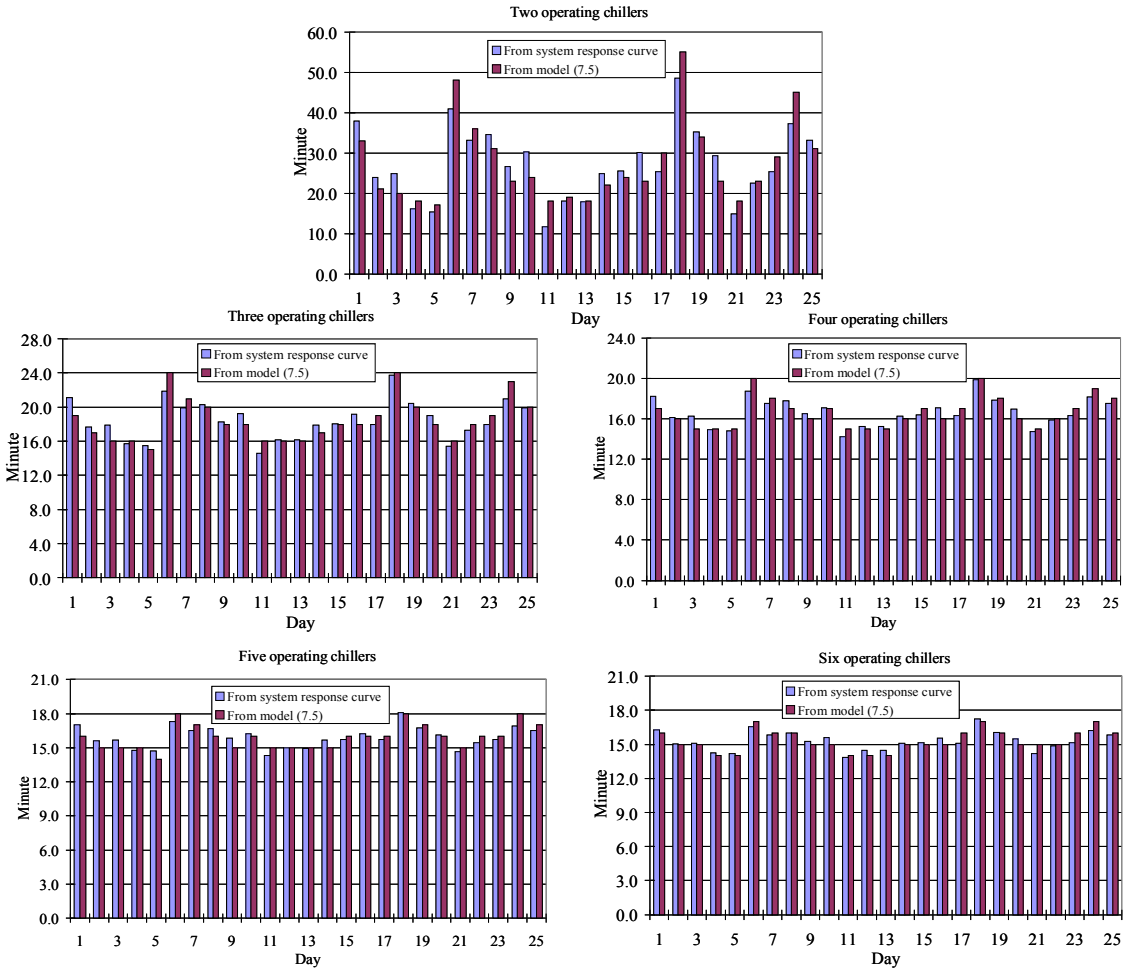

Figure 7.7 Comparison of the length of the building pre-cooling lead time

It should be noted that the building pre-cooling lead time should generally be no smaller than the air-conditioning system pre-cooling lead time. However, it was found in Figure 13 that in some days when there were two chillers used for pre-cooling, the building pre-cooling lead time was shorter than the air-conditioning system pre-cooling lead time. This is probably because the cooling provided by the operating chillers was not sufficiently enough. Therefore, it took a longer time to cool down the supply air to its set point than to cool down the zone indoor temperature to its set point.

7.2.4 Validation of Energy Consumption

Table 7.2 lists the number of the components used in the simulated system and their rated power consumption. For calculating the energy consumption of chillers under partial load, n in (7.10) was selected to 2 which was able to well depict the relationship between COP and the partial load ration. The coefficients used in (7.10) were $c_2 = -4.6; c_1 = 7.32; c_0 = 3.36$.

Table 7.2. The rated power of component and related total number in the chiller plant

Component	Rated Power (kW)	Overall Number
Supply Fan	6000	1
Cooling Tower Fan	152	11
Chiller Motor Size	1346	6
Constant Speed Pump for Chilled Water Distribution	110	6
Constant Speed Pump for Cooling Water Distribution	185	6
Variable Speed Pump Motor Size	7980	1

The energy consumption J_N computed from (7.6) was compared with the actual energy consumption of the system, as shown in Figure 7.8. It can be seen that equation (7.5) can offer a satisfactory accuracy in the energy consumption prediction. The average relative errors were 7.08%, 5.51%, 6.94%, 8.18% and 8.76% respectively when the number of operating chillers changed from 2 to 6. Estimation deviations in the energy consumption were caused by the simplified approach for energy consumption computation as well as the deviation from the pre-cooling lead time estimation by the developed strategy.

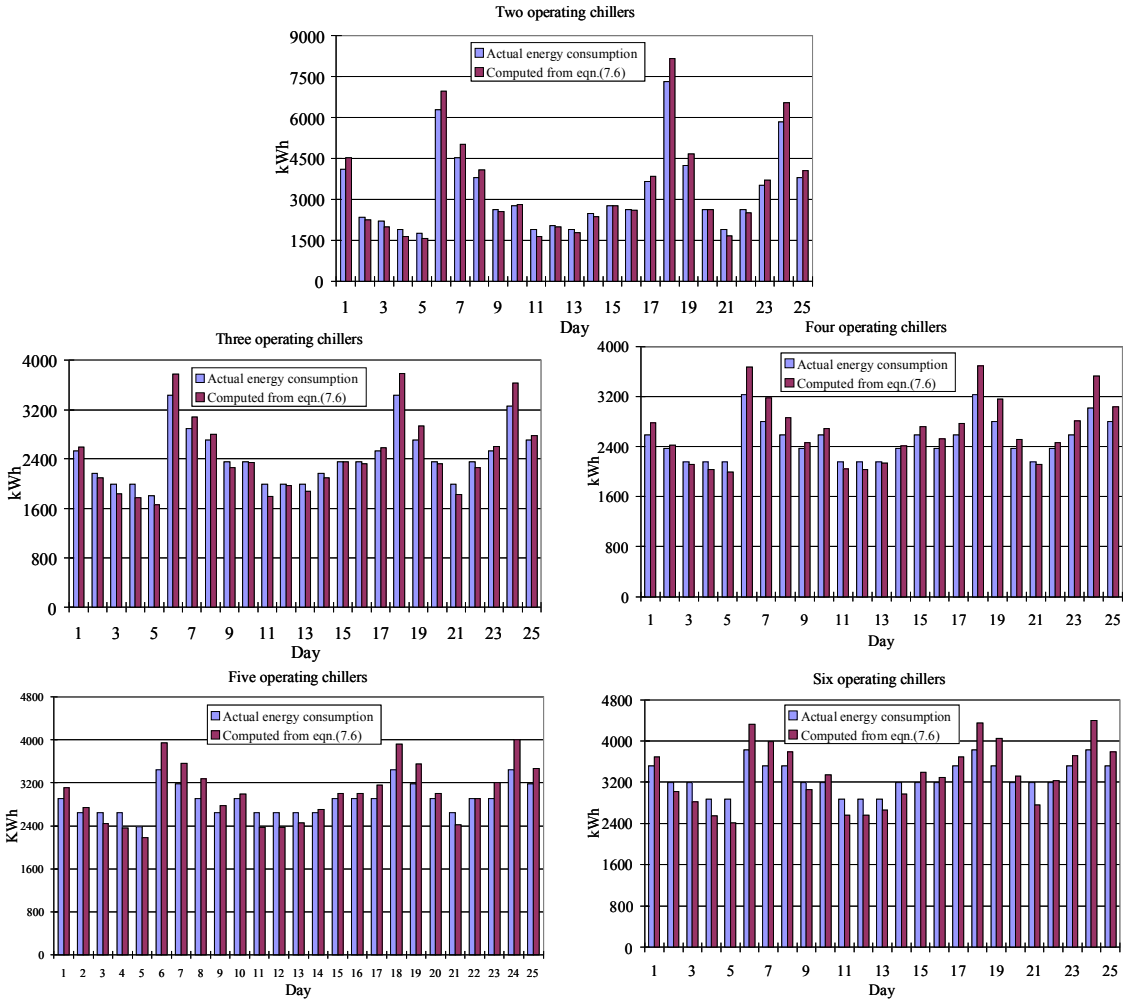

Figure 7.8. Comparison of the energy consumption

7.2.5 Validation of the Developed Optimal Start Control Strategy

The optimal start control aims at finding the optimal operating chiller number and the associated pre-cooling lead time which lead to the least energy consumption in the pre-cooling period. Table 7.3 shows the optimal start schedules in a month (excluding the weekends) computed from the proposed strategy, and compares them with the ideal schedules which were obtained by repeatedly running the simulated system with different number of chillers for pre-cooling under the same weather

conditions. In the Table, N_{opt}, τ_{opt} and J_{opt} are the computed optimal chiller operating number, pre-cooling lead time and chiller plant energy consumption (i.e. the sum of the components energy consumption) from the developed strategy. $N'_{opt}, \tau'_{opt}, J'_{opt}$ are the corresponding ideal results.

From the results shown in Table 7.3, only two days' optimal chiller operating numbers computed from the strategy are different from the simulation result, i.e. 7th and 8th day. The computed pre-cooling lead time and related energy consumption are quite close to their ideal values. About 85% of the relative differences were smaller than 13%, which shows that in most cases, an acceptable accuracy of the developed strategy for choosing optimal start control can be achieved.

Table 7.3. The optimal start control results comparison between the strategy and the simulation

Days	Proposed Strategy			Ideal results			Relative Difference	
	N_{opt}	τ_{opt} (Min.)	J_{opt} (kWh)	N'_{opt}	τ'_{opt} (Min.)	J'_{opt} (kWh)	$\frac{\tau_{opt}-\tau'_{opt}}{\tau'_{opt}}$ (%)	$\frac{J_{opt}-J'_{opt}}{J'_{opt}}$ (%)
1	3	21	2531.6	3	19	2596.5	10.5	-2.5
2	3	17	2169.9	3	17	2091	0	3.7
3	3	17	1989.1	3	16	1838.2	6.3	8.2
4	2	16	1898	2	18	1653.5	-11.1	14.8
5	2	15	1752	2	17	1561.7	-11.7	12.2
6	4	19	3235.5	4	20	3671	-5.0	-11
7	**4**	**18**	**2804**	**3**	**21**	**3078**	**-14.3**	**-8.9**
8	**4**	**18**	**2588.4**	**3**	**20**	**2797.7**	**-10**	**-7.5**
9	3	18	2350.7	3	18	2265.3	0	3.8

10	3	19	3350.7	3	18	3337.8	5.56	0.4
11	2	12	1925	2	18	1636.8	-33.3	17.7
12	3	16	2040.4	3	16	1975.5	0	3.3
13	2	18	1988	2	18	1774	0	12.1
14	3	18	2169.9	3	17	2097.2	5.9	3.4
15	3	18	2350.7	3	18	2358.2	0	-0.3
16	3	19	2364.7	3	18	2324	5.56	1.7
17	3	20	2531.6	3	19	2578	5.26	-1.8
18	4	20	3235.5	4	20	3689.7	0	12.3
19	3	20	2712.4	3	20	2934.7	0	-7.5
20	3	19	2350.7	3	18	2329	5.56	0.9
21	2	15	1922	2	18	1672.5	-16.7	14.9
22	3	17	2364.5	3	18	2263.8	-5.6	4.4
23	3	18	2528.4	3	19	2603.2	-5.3	-2.9
24	4	18	3019.8	4	19	3525.2	-5.3	14.4
25	3	20	2742.4	3	20	2780.8	0	-1.4

7.3. Application Issues

The main steps for application of the model-based optimal start strategy are summarized as follows.

1). Identify the simplified building model (3R2C).

2). Measure the required weather data (i.e. global radiation I_{globle}, ambient temperature T_{amb} and relative humidity RH_{amb}) at the moment one hour ahead of the occupancy. If the lead time is longer than one hour, the weather prediction module developed by Zhou et al [2009] can be used to predict weather condition in order to improve the accuracy of computing the cooling

load and the pre-cooling lead time.

3). Compute the cooling load Q_{pre} using the simplified building model according to the measured global radiation I_{globle}, ambient temperature T_{amb} and relative humidity RH_{amb}.

4). Specify the feasible set for operating chiller number. The minimum number N_{min} is calculated by (7.1); the maximum number N_{max} can be specified from the demand limiting strategy. If no special requirement in demand limiting, N_{max} equals the total number of chillers N_c.

5). Calculate the pre-cooling lead time $\tau_{Bld,N}$ for each operating chiller number in the feasible set and the corresponding energy consumption. Note that in this step, the parameters $a_{0,N}, a_{1,N}$ for computing $\tau_{AC,N}$ should be identified during commissioning.

6). Select the optimal operating chiller number N_{opt} and the related building pre-cooling lead time τ_{opt} according to the energy consumption comparison.

Note that no iterations are required in the proposed strategy, thus the computation burden of the model-based start strategy is not heavy. Due to the uncertainties associated with the simplified building model, the pre-cooling lead time should be little longer than the computed one in order to guarantee the building internal temperature can safely reach its set point before occupying. According to the case study, the uncertainty associated with the pre-cooling lead time is not larger than 10% in most cases. Hence, the suggested pre-cooling lead time should be 10% longer than the computed one.

7.4. Summary

This paper presented a model-based optimal start control strategy for multi-chiller plants in commercial buildings. A simplified building model has been used for predicting building cooling load, based on which the optimal operating chiller number and the related pre-cooling lead time can be identified. Case studies have showed that the operating chiller number plays an important role in energy efficiency during chiller pre-cooling period and the developed strategy considering the effects of both *the recovery ability* and *the weather conditions* can efficiently optimize the energy consumption during pre-cooling periods for multi-chiller plants. Also, the methods of computing the pre-cooling lead time and total energy consumption calculation used in the strategy is accurate and reliable. Therefore, the developed optimal start control strategy can offer advantages in practical application in multi-chiller plants in commercial buildings for energy saving.

CHAPTER 8 DEMAND LIMITING STRATEGY FOR MINIMIZING MONTHLY ELECTRICITY BILL

The monthly peak demand limiting is of great significance in reducing the overall monthly electricity bill of commercial buildings. In this chapter, a new demand limiting strategy aiming to optimize the monthly cost saving is proposed. The new strategy is realized in two steps. The first one is to predict a suitable monthly demand threshold. In the second step, the extended pre-cooling duration will be computed based on the difference between the demand threshold and the predicted daily peak demand. The specific proportional-integral (PI) demand limiting algorithm is executed to restrain the daily peak demand under the given threshold by using the building thermal mass.

In section 8.1, the necessity of suitable monthly peak demand threshold identification is discussed. Section 8.2 outlines of the proposed demand limiting strategy. The essential modules used in the demand limiting strategy are as well presented in this section. Section 8.3 conducts a comprehensive validation of the used modules and the whole demand limiting strategy. A brief summary is given in section 8.4.

8.1 Necessity of a Suitable Monthly Peak Demand Threshold Identification

For optimizing the monthly cost savings, a monthly peak demand threshold is essential to eliminate the unnecessary daily peak demand reduction. Figure 8.1 is used to illustrate the unnecessary daily peak demand reduction when demand limiting strategy aiming to maximize the daily cost saving is performed.

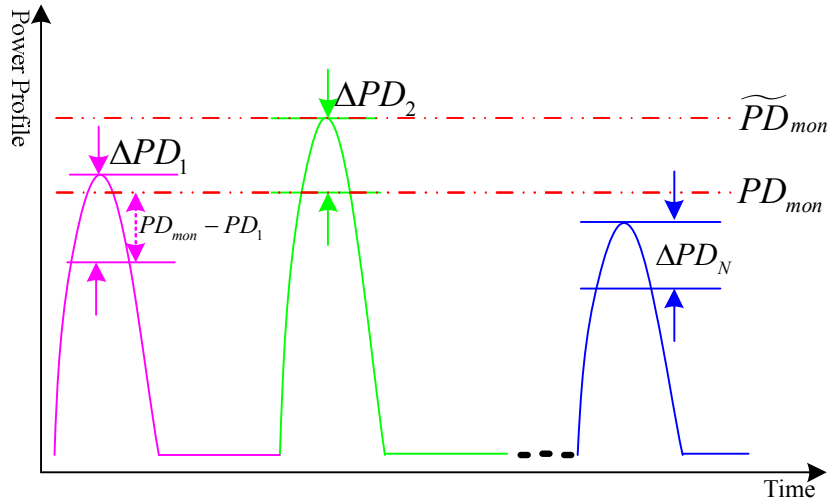

Figure 8.1. Unnecessary daily peak demand reduction

In the Figure, $\widetilde{PD}$ represents the peak demand before the implementation of demand limiting strategy and PD is the value after its implementation. Subscripts $1....N$ indicate day index and PD_{mon} is short for monthly peak demand which is equivalent to the maximum value of daily peak ones, i.e. $PD_{mon} = \max(PD_i)$. Symbol ΔPD means the reduction of peak demand. Shown as Figure 8.1, the demand limiting strategy for maximizing daily cost saving will not reach an optimal result for the monthly electricity cost reduction due to the generated unnecessary daily demand reduction. For example, the demand reduction parts $PD_{mon} - PD_1$ in day one

and ΔPD_N in the N^{th} day are useless in reducing the monthly peak demand simply because they are above the new monthly peak demand PD_{mon}. Much worse, these useless demand reduction parts consume extra energy and cause further rise of related energy cost. Obviously, the elimination of these unnecessary daily peak demand reduction helps optimize the monthly electricity cost saving. It can be accomplished by identifying a monthly peak demand threshold PD_{Thres}. The identified threshold only requires the days with daily peak demand larger than the threshold to implement a demand limiting control for removing the exceeding demand part. For other days with peak demand smaller than the threshold, there is no need of such control action.

The threshold also needs to be assigned a suitable value. Otherwise, only limited/none monthly cost saving can be reached. If an inappropriately high threshold is used, the limited demand cost reduction obtained results in limited overall monthly cost reduction. In contrast, the demand cost reduction may be completely compromised by the related energy rise cost part if an inappropriately low threshold is adopted. It should be mentioned that occupants' thermal comfort could also be severely sacrificed in the low threshold case. The main reason is the low threshold may require switching off several operating chillers which causes insufficient cooling supplied. Figure 8.2 is used to show the monthly peak demand and overall energy costs vary with the threshold. The suitable peak demand threshold $PD_{Thres,opt}$ leads to the minimal total monthly electricity bill which is the sum of peak demand cost and energy cost.

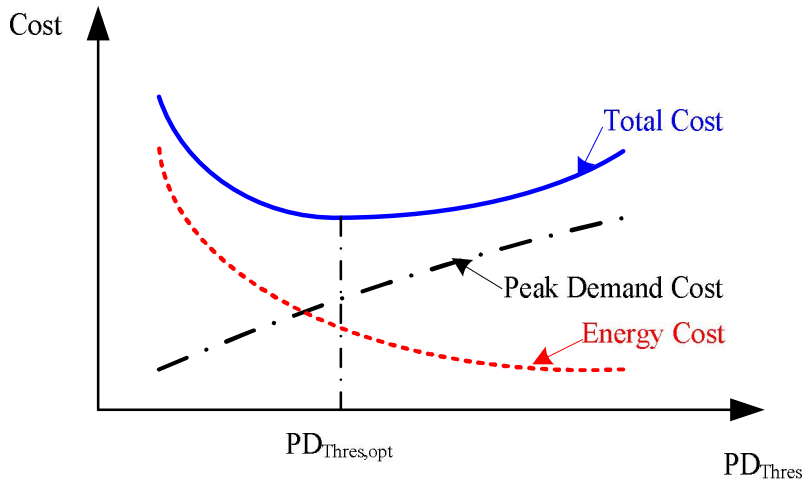

Figure 8.2. Peak demand and energy cost variation with the threshold

The saving of the total monthly electricity cost can be established as follows.

$$CS_{tot} = \hat{\alpha} \times \Delta PD_{mon} - \hat{\beta} \times \sum_{i=1}^{N} \Delta E_i \tag{8.1}$$

where CS_{tot} is the overall cost saving (HKD) after a demand limiting strategy implemented; α, β are the unit prices for electrical demand and energy separately; ΔPD_{mon} is the monthly peak demand reduction (kVA); and ΔE_i is the i^{th} day energy rise for reducing the daily peak demand $\widetilde{PD}_i$ by ΔPD_i after the implementation of demand limiting strategy.

The relationship between daily peak demand reduction ΔPD_i and related energy rise ΔE_i is described as

$$\Delta E_i = \begin{cases} f(\Delta PD_i); 0 < \Delta PD_i \le \Delta PD_{mon} \\ 0; \Delta PD_i \le 0 \end{cases} \tag{8.2}$$

where $f(\cdot)$ represents a non-negative function.

The optimal monthly peak demand reduction $\Delta PD_{mon,opt}$, which maximizes the monthly cost saving CS_{tot}, is determined after the $f(\cdot)$ function identified. With $\Delta PD_{mon,opt}$ known, suitable threshold $PD_{Thres,opt}$ is calculated as below.

$$PD_{Thres,opt} = \widetilde{PD}_{mon} - \Delta PD_{mon,opt} \tag{8.3}$$

8.2. Outline of the Control Strategy

The basic idea of the proposed strategy is shown as Figure 8.3. Five different modules are used in this strategy. The monthly peak demand prediction module (Module I) and the optimal demand reduction prediction module (Module II) are used to compute the suitable monthly peak demand threshold $PD_{Thres,opt}$. In Module I, the monthly peak demand value $PD_{mon,pre}$ is predicted based on the similarities of same month peak demand in different years. Module II is used to estimate the optimal monthly peak demand reduction $\Delta PD_{mon,opt}$ based on the electricity price structure and the identified function (8.2). The daily power profile *P* is predicted using Module III in cooperation with the predicted hourly cooling load and estimated central chilling system overall coefficient of performance (COP). With $PD_{Thres,opt}$ and *P* known, the amount of the daily peak demand reduction is determined. The pre-cooling lead time will be estimated based on the determined reduction amount in Module IV. Module V, i.e. PI demand limiting algorithm, is a specific control approach to realize limiting the daily peak demand under the identified threshold $PD_{Thres,opt}$ via varying the indoor room temperature set-points. The details of the essential modules will be described in the following sections.

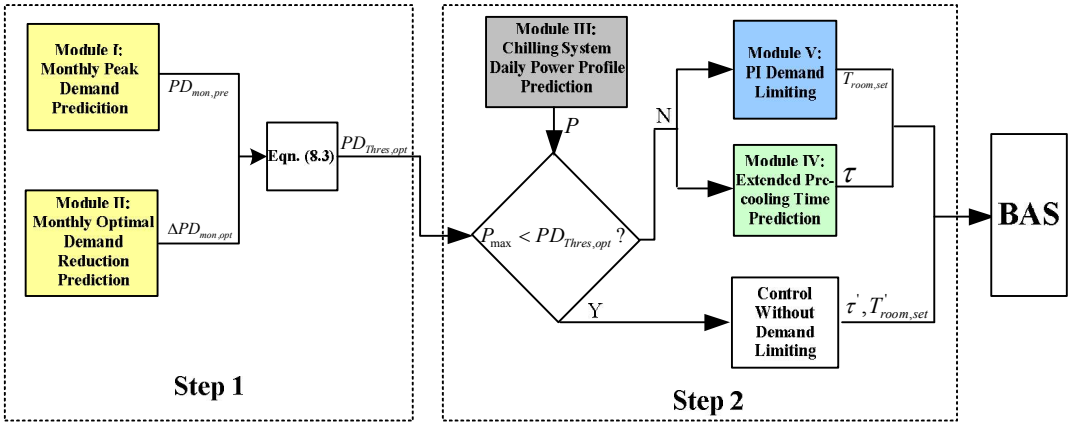

Figure 8.3 Basic idea of the developed demand limiting strategy

8.2.1 Module I for Monthly Peak Demand Prediction

The module is used to predict the monthly peak demand $PD_{mon,pre}$ based on the peak demand similarity of the same month in different years. The recorded data of the same months in previous years are used to compute the peak demand of current month, shown as (8.4).

$$PD^{[j]}_{mon,pre} = \sum_{k=1}^{n} a_k \times PD^{[j]}_{prv,k} \tag{8.4}$$

Where $PD_{prv,k}$ is the monthly peak demand of previous k^{th} year; a_k is the related weighted factor which can be identified by least square method using history data; and superscript *j* represents the month index.

8.2.2 Module II for Optimal Monthly Demand Reduction Prediction

This module aimed to estimate the optimal monthly demand reduction $\Delta PD_{mon,opt}$ that maximizes the monthly cost savings CS_{tot}. As shown in (8.1), $\Delta PD_{mon,opt}$ can be identified after the specific electricity price structure and the relationship between the daily energy rise ΔE_i and the daily peak demand

reduction ΔPD_i are identified. The electricity price used in this study is from power company CLP and the details are presented in section 8.2.4.

A multinomial function is adopted to describe the relationship between ΔE_i and ΔPD_i, shown as (8.5).

$$\Delta E_i = \sum_{j=0}^{m-1} b_j \times (\Delta PD_i)^j \tag{8.5}$$

where the coefficients b_j can be identified using least square method with historic data.

Substitute (8.5) to (8.1), and the following equation is established.

$$CS_{tot} = \hat{\alpha} \times \Delta PD_{mon} - \hat{\beta} \times \sum_{i=1}^{N} \sum_{j=0}^{m-1} b_j \times (\Delta PD_i)^j ; (\Delta PD_{mon} \le \sum_{i=1}^{N} \Delta PD_i \le N \times \Delta PD_{mon}) \tag{8.6}$$

Considering the constraint, (8.6) is reformed into

$$CS_{tot} \in [CS_{tot,lower}, CS_{tot,upper}] \tag{8.7}$$

where

$$CS_{tot,lower} = \hat{\alpha} \times \Delta PD_{mon} - \hat{\beta} \times N \times \sum_{j=0}^{m-1} b_j \times (\Delta PD_{mon})^j$$

$$\mathrm{CS}_{tot,upper} = \hat{\alpha} \times \Delta PD_{mon} - \hat{\beta} \times \sum_{j=0}^{m-1} b_j \times (\Delta PD_{mon})^j$$

The monthly peak demand reduction $\Delta PD_{mon,opt}$ is therefore located in the range as follows.

$$\Delta PD_{mon,opt} \in [\Delta PD_{mon,lower}, \Delta PD_{mon,upper}] \tag{8.8}$$

where $\Delta PD_{mon,lower}, \Delta PD_{mon,upper}$ are the values that maximize the cost saving $CS_{total,lower}$ and $\mathrm{CS}_{total,upper}$ separately and they are obtained by solving the following equations.

$$\frac{d(CS_{tot,lower})}{d(\Delta PD_{mon})} = 0; \frac{d(CS_{tot,upper})}{d(\Delta PD_{mon})} = 0 \tag{8.9}$$

8.2.3 Module III for Hourly Power Profile Prediction

In the overall power profile prediction, the hourly cooling load prediction Q_{pre} of next day is firstly yielded. For calculating the related power consumption, a simplified approach for computing the central chilling system overall coefficient of performance (COP) is proposed. With the Q_{pre} and COP_{sys} known, the power consumption P_{pre} is computed as follow.

$$P_{pre} = \frac{Q_{pre}}{COP_{sys}} \tag{8.10}$$

I) Model-based Cooling Load Prediction

Hourly cooling load is predicted using a weather prediction model and a simplified building model. The weather prediction module, developed by Zhou et al. [2009], is used to predict the hourly weather data (including the solar radiation I_{global}, outdoor air temperature T_{amb} and relative humidity RH_{amb}) of the coming day cooperating with the daily weather forecast from the local observatory. After the weather data are predicted, the simplified building model developed by Wang and Xu [2006] is used to estimate the building cooling load. Due to the fact that the used simplified building model has been introduced in previous chapter, this section mainly presents the weather prediction module.

The weather prediction module outputs the hourly predicted solar radiation $I_{global,k}$, outdoor air temperature $T_{amb,k}$ and relative humidity $RH_{amb,k}$ predictions, where k indicates k^{th} hour. Note that k varies from 1,…, 24.

The solar radiation hourly prediction $I_{global,k}$ is calculated by (8.11), where b_1, b_2 and b_3 are the coefficients, which can be obtained using the recursive least square algorithm [Q. Zhou et al., 2009]; T_{max} and T_{min} are the daily maximum and minimum temperatures respectively which are usually available in the weather forecast from a local observatory; and $T_{amb,k}$ is the predicted ambient temperature. I_0 is daily extraterrestrial solar radiation constant for a particular region shown as (8.12), in which D is the day index number in a year; I_{const} is a solar constant (1370Wm^{-2}); and C_{m} is the average cloud coverage of the coming day based on the cloud amount forecasted.

$$I_{glabal,k} = I_0 \times (b_1 + b_2\sqrt{\frac{T_{amb,k} - T_{\min}}{T_{\max} - T_{\min}}} + b_3\sqrt{1 - \frac{C_m}{8}}) \tag{8.11}$$

$$I_0 = I_{const} \times [1 + 0.033 \times \cos(2\pi \times \frac{D}{365})] \tag{8.12}$$

The outdoor air temperature (or relative humidity) at the k^{th} hour in the coming day, i.e. $T_{amb,k}$ (or $RH_{amb,k}$), is predicted based on the measured temperature (humidity) at the same hour in the last several days. Usually previous five-day measured data are used. Since the prediction of $T_{amb,k}$ and $RH_{amb,k}$ follows the same procedure, x is used to denote T_{amb} or RH_{amb} in the following description.

Assume previous five-day measurements of x at the k^{th} hour are denoted as $x_k^{[-4]},\ldots, x_k^{[0]}$ where the superscript $[i]$ denotes the previous $(-i)^{\text{th}}$ day and $i = 0$ is the current day. Then, define $X_k^{[j]}$ as (8.13). The newly generated data sequence $X_k^{[-4]},\ldots, X_k^{[0]}$, is approximated by an exponential function, shown as (8.14), where the empirical constants $d_{1,k}$ and $d_{2,k}$ can be determined by the least square

regression [Q. Zhou et al., 2009]. Equation (8.14) describes a first-order grey dynamic model (GM) proposed by Deng [1989]. The predicted value of X at the k^{th} hour of the coming day, denoted as $\overline{X}_k$ is given by (8.15), and correspondingly the predicted value of x is calculated by (8.16). The empirical constants $d_{1,k}$ and $d_{2,k}$ is updated every day in order to reduce approximation errors.

$$X_k^{[j]} = \sum_{i=-4}^{j} x_k^{[i]} \tag{8.13}$$

$$X_k^{[j]} = [X_k^{[-4]} - \frac{d_{2,k}}{d_{1,k}}] \times e^{d_{1,k}(j+4)} + \frac{d_{2,k}}{d_{1,k}} \tag{8.14}$$

$$\overline{X}_k = [X_k^{[-4]} - \frac{d_{2,k}}{d_{1,k}}] \times e^{5d_{1,k}} + \frac{d_{2,k}}{d_{1,k}} \tag{8.15}$$

$$\overline{x}_k = \overline{X}_k - X_k^{[0]} \tag{8.16}$$

The study in [Q. Zhou et al., 2009] shows that the prediction accuracy of $\overline{x}_k$ can be improved by the calibration (8.17), where x_k is the calibrated value of $\overline{x}_k$; the variable x_{avg} is defined as (8.18); δ_h and δ_l are the scale factors, defined by (8.19). In Equation (8.18), x_{min} and x_{max} are the forecasted maximum and minimum value of x from the observatory; and $\overline{x}_{\min}$ and $\overline{x}_{\max}$ in (8.19) are the minimum and maximum in the predicted sequence $\overline{x}_k$, k =1,…, 24.

$$\hat{x}_k = \begin{cases} x_{avg} + \delta_h \left[\overline{x}_k - x_{avg} \right], & When\ \overline{x}_k \geq x_{avg} \\ x_{avg} - \delta_l \left[x_{avg} - \overline{x}_k \right], & When\ \overline{x}_k < x_{avg} \end{cases} \tag{8.17}$$

$$x_{avg} = \frac{x_{\min} + x_{\max}}{2} \tag{8.18}$$

$$\delta_h = \frac{x_{\max} - x_{avg}}{\overline{x}_{\max} - x_{avg}}; \delta_l = \frac{x_{avg} - x_{\min}}{x_{avg} - \overline{x}_{\min}} \tag{8.19}$$

II) Central chilling system overall Coefficient of Performance

The overall *COP* is calculated by (8.20), where *PLR* is the part load ratio calculated by the central chilling system supplied cooling Q_{sup} and its rated cooling capacity Q_{rated}, i.e. $\mathrm{PLR} = \mathrm{Q}_{\mathrm{sup}} / Q_{rated}$. The supplied cooling is equal to the predicted cooling load, thus $\mathrm{PLR} = Q_{pre} / Q_{rated}$. $c_0,\ldots,c_n$ are the coefficients that can be identified with historic recorded data.

$$COP = c_n \times PLR^n + \ldots + c_1 \times PLR + c_0 \tag{8.20}$$

8.2.4 Module IV for Pre-cooling Duration Estimation

This module aimed to estimate the extended pre-cooling duration τ_i based on the required daily peak demand reduction ΔPD_i. The larger demand reduction ΔPD_i need more cooling stored in advance and therefore a lengthier pre-cooling τ_i.

A polynomial function is employed to depict the relationship between τ_i and ΔKVA_i, shown as (8.21).

$$\tau_i = \sum_{j=0}^{m-1} \hat{e}_j \times (\Delta PD_i)^j \tag{8.21}$$

where the coefficients $\hat{e}_j$ can be identified using least square regression algorithm with the trial data obtained in the commissioning..

8.2.5 Module V for Limiting Daily Peak Demand

The idea of the PI demand limiting algorithm for reducing the daily peak demand is shown as Figure 8.4.

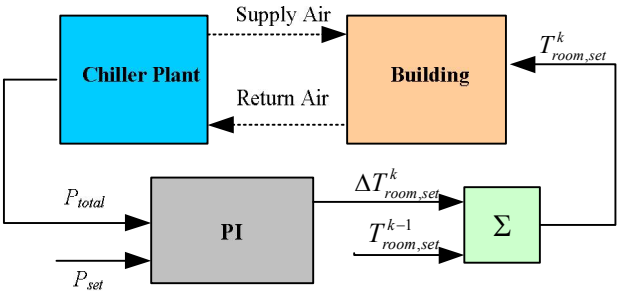

Figure 8.4. The schematics of PI demand limiting algorithm

In this algorithm, the PI controller is used to maintain the overall power consumption of the chiller plant P_{tot} at its set-point P_{set} by adjusting the room temperature set-point in a limited range, e.g. [22.5℃, 25.5℃]. With considering the control deviation, the P_{set} is calculated as $P_{set} = PD_{Thres.opt} + \hat{\sigma}$. $\hat{\sigma}$ represents the control deviation. The output of the PI controller is the variation of room temperature set-point $\Delta T^{k}_{room,set}$. Superscript k represents the instant time interval. The variation is used to generate the current room temperature set-point with the previous set-point, *i.e.* $T^{k}_{room,set} = T^{k-1}_{room,set} + \Delta T^{k}_{room,set}$.

Through adjusting the room temperature set-point, the cooling stored in the extended pre-cooling can be released to lower down the instant cooling demand. The reduced load demand subsequently lowers down the overall power consumption. The detailed process is as follows. As the overall power is increasing, the room temperature set-point will be raised up which decrease the system power consumption due to the reduction of instant cooling demand. Meanwhile, the stored cooling will be released to satisfy the part of reduced instant cooling demand which further reduces the required amount of mechanical cooling from central chilling system. The room temperature will stop rising until the reduced power reaches its set-point P_{set}. In

contrast, as the overall power is decreasing, the room temperature set-point will be lowered down which increases the system power consumption due to the increased cooling load demand. The room temperature set-point will stop falling as the increased power reaches the demand set-point. Meanwhile, the reduced room temperature set-point will lower down the temperature of building thermal mass including building envelopes and indoor furniture. In this case, the building thermal mass is charged again and certain amount of cooling is stored compared with the case when a higher room temperature maintained. The restored cooling is helpful to lower down the rising power in the following period. To sum up, the overall power consumption is controlled to be maintained at a constant set-point by adjusting the room temperature set-point in which the cooling stored in building thermal mass will be released as overall power increases and the building thermal mass will be charged as overall power lower decrease. Note that the amount of the cooling stored in off-peak period has a significant impact on the amount of daily peak demand reduction. More cooling stored, more daily peak demand reduction can be achieved.

Since the room temperature set-point is only allowed to be varied in a limited range mainly due to the consideration of the indoor thermal comfort, the amount of daily peak demand reduction is as well limited. Therefore a suitable value should be assigned to P_{set} which should be reachable and guarantee an acceptable indoor thermal comfort. The parameters for PI controller can be obtained in the commissioning period.

8.3. Validation Case Studies

The proposed optimal start control strategy was validated using the dynamic simulation platform built in chapter 3. The Validation of PI demand limiting algorithm is firstly performed in section 8.3.1. The validation of the whole developed strategy as well as other modules was conducted in the following sections.

8.3.1 Validation of Module V for Limiting Daily Peak Demand

The PI demand limiting algorithm is used to maintain the overall power consumption at its peak demand set-point P_{set} by adjusting the room temperature set-point. For testing its performance, the comparison has been made between the three days in July with PI demand control implementations and the same days without them. In this study, the results from the days without demand limiting controls were taken as baselines. More specifically, the base case was the room temperature set-point was fixed at 24℃ in occupation period and the pre-cooling time was set to 0.5hr which was adequate to cool down the indoor room temperature to a desired level, e.g. 24 ℃. In the PI demand limiting control, the proportional and integral parameters were assigned values *P=0.007* and *I=2* minute. The room temperature of occupation period was allowed to vary in the range [22.5℃, 25.5℃] for restraining the overall power consumption. The pre-cooling period varied from 1 hr to 9 hrs and the temperature set-point in these extended pre-cooing periods was set to be 22.5℃. For assuring the equivalent indoor thermal comfort, the predicted mean vote (PMV) module in the multi-zone building model [TRNSYS, 2004] was adopted to evaluate

the thermal comfort difference after the PI demand control was implemented. The PMV module fully considered the influential factors including temperature, air velocity, clothing level, occupant metabolic rate, and etc. A pre-defined result range from PMV module, i.e. [-0.8, 0.8], indicated an acceptable indoor thermal comfort. A trial and error method was employed to search for the proper P_{set}. If the accumulated time of PMV result exceeding the defined range was larger than that in the base case, the set-point P_{set} for the PI control would be raised up until finally it was nearly the same as that in the base case. Table 8.1 presented the acquired data.

Table 8.1. Data obtained using trial and error method

No.	Pre-coo -ling Time (hr)	Control type	P_{set} (kW)	E_i (10^5 kW)	PD_i (10^4 kVA)	ΔE_i (10^4 kWh)	ΔPD_i (10^3 kVA)	Accum -ulated time (min.) (PMV<-0. 8)	Accum -ulated time (min.) (PMV>0.8)
Day 1	9	PI	11500	1.5951	1.2113	2.82	3.09	1	5
	6	PI	12400	1.5312	1.2993	2.18	2.21	0	5
	3	PI	13200	1.4603	1.3783	1.47	1.42	0	4
	0.5	Base Case	N/A	1.3132	1.5203	0	0	0	5
Day 2	8	PI	11400	1.5240	1.2003	2.61	2.80	0	6
	5	PI	12300	1.4603	1.2892	1.97	1.91	0	6
	2	PI	13000	1.3827	1.3575	1.20	1.23	0	3
	0.5	Base Case	N/A	1.2632	1.4803	0	0	0	5
Day 3	7	PI	10800	1.4407	1.1403	2.11	2.80	0	6
	4	PI	11900	1.3967	1.2493	1.67	1.71	0	6
	1	PI	12500	1.3144	1.3063	0.847	1.14	0	5
	0.5	Base Case	N/A	1.2297	1.4203	0	0	0	5

It should be noted that the actual daily peak demands after the demand control implementation still had certain differences from their set-points P_{set}. For instance, the 9 hours pre-cooling in the day one finally reduced the daily peak demand from 15951 kVA in base case to12113 kVA which had about a 600 kVA deviation from its

set-point 11500 kVA. It is mainly caused by the parameters configuration in the PI control. Inappropriate settings may result in poor control accuracy and reliability.

The detailed comparison results of the first day between 9 hours pre-cooling PI demand control and the related base case in terms of indoor room temperature T_{room}, system power consumption P_{sys} and PMV results were presented in the following Figure.

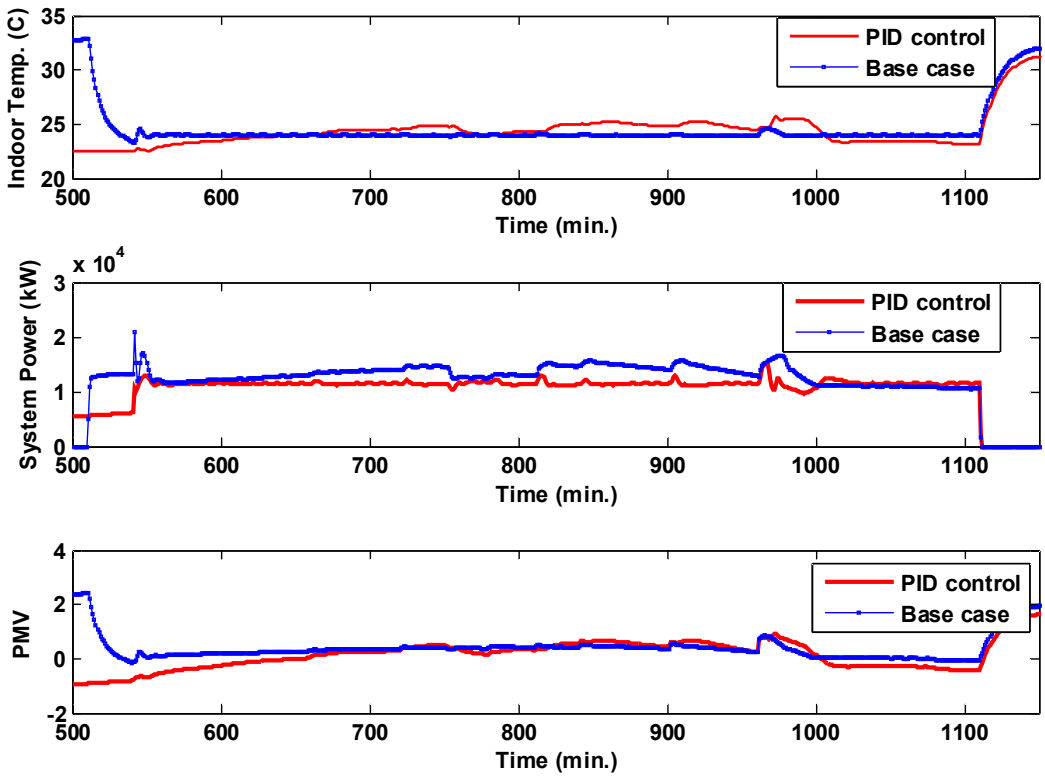

Figure 8.5. Comparisons between the PI demand control and the base case

It is observed that the PI demand control can effectively lower down the daily peak demand to a desired level without great change in indoor thermal comfort as they are compared with those from the base case.

8.3.2 Validation of Module IV for Pre-cooling Duration Estimation

Based on the data in Table 8.1, the coefficients in (8.21) were identified, shown as (8.22). The relationship between pre-cooling time and the demand reduction can be described well by the established linear equation with an R square value 0.97.

$$\tau_i = 0.0037 \times \Delta PD_i - 2.5222 \tag{8.22}$$

where τ represents the pre-cooling duration.

For further validating the proposed linear relationship in (8.22), more data of different days had been yielded using the same trial and error method adopted for generating the data in Table 8.1. The results calculated from (8.22) were of good accuracy in estimating the related pre-cooling duration τ_i based on the required demand reduction ΔPD_i, shown as Figure 8.6. More than 85% of the estimated pre-cooling durations had less than 15% relative errors compared with the actual values.

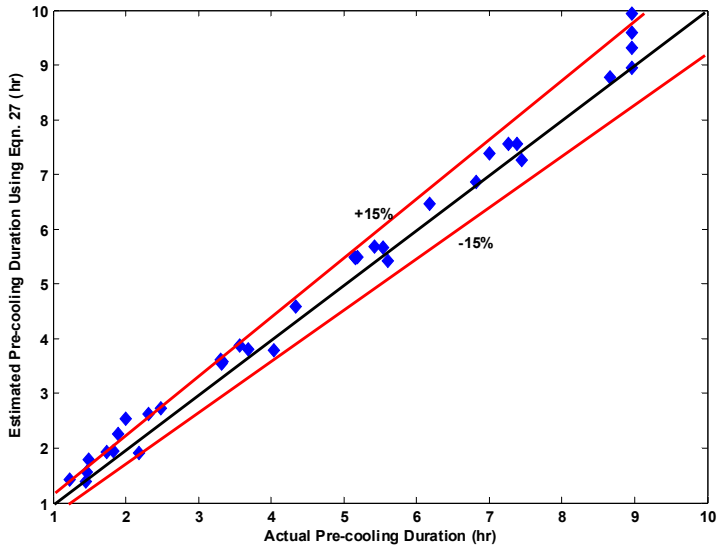

Figure 8.6. Comparison between the actual pre-cooling duration and the estimated ones

8.3.3 Validation of Module I for Monthly Peak Demand Prediction

For validating the proposed monthly peak demand prediction module, 22 years operating data of the chilling system overall power consumption has been generated using the test platform introduced in Section 3. The first three years data were used to identify the coefficients in Equation (8.7) and the rest were used for validating the module by comparing them with the calculated result from (8.7). The parameters were identified as a_1=1.3668, a_2=-0.3536. Figure 8.7 is the validation results using the identified coefficients. More than 92% of the data were located in the relative error range [-15%, 15%] which indicated an acceptable accuracy of the predicted results.

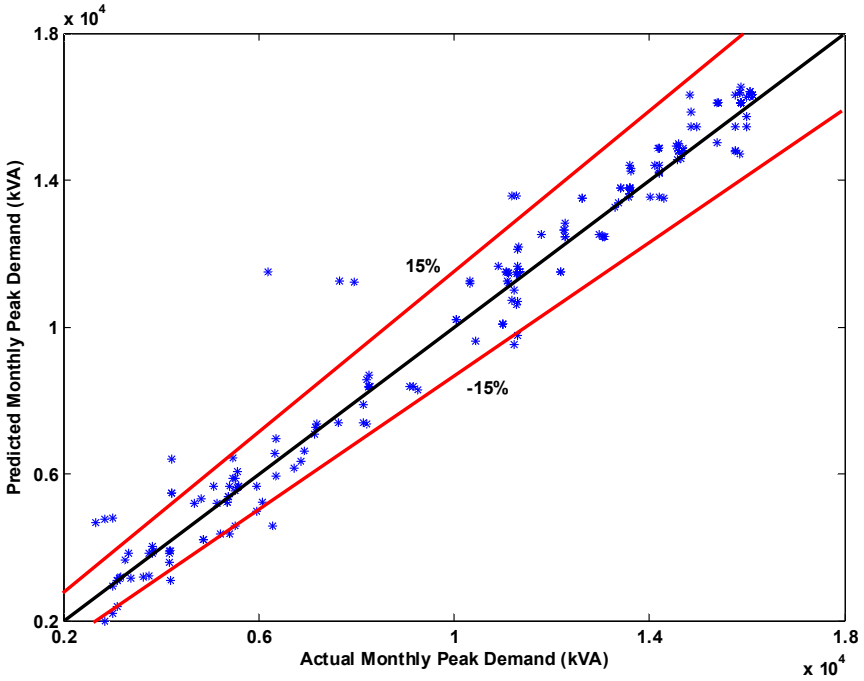

Figure 8.7. Comparison between actual monthly peak demands and the predicted ones

8.3.4 Validation of Module II for Optimal Monthly Demand Reduction Estimation

a) Identification of Unit Price for Electrical Demand and Energy

The electricity price structure from CLP is depicted in Table 8.2. There are four different tariff types for the end-users in total. Each of them, except the first one, is mainly comprised of two items. One is the cost for the monthly peak demand; and the other is the cost for the overall energy consumption in a whole month. In addition, the prices for the on-peak and off-peak periods are different. The on-peak prices are much higher than those of off-peak, which is in attempt to encourage part of the on-peak load to be shifted into off-peak period.

Table 8.2. Electricity price structure from CLP

Tariff Type	**Composing Items**			
	Demand Part (HKD/kVA)		**Energy Consumption Part (Cent/kWh)**	
	On-peak Period	Off-peak Period	On-peak Period	Off-peak Period
General Service Tariff	0.0	0.0	96.3(First 5000 kWh)	
			95.3(Exceeding part)	
Bulk Tariff (monthly no less than 20,000 kWh)	66.5(First 650)	0.0(Less than the on-peak peak)	68.9(First 200,000)	61.4
	63.5(Exceeding part)	26.0(Lager than the on-peak peak)	67.4(Exceeding part)	
Large Power Tariff (monthly no less than 3000 kVA)	117.0(First 5000)	0.0(Less than the on-peak peak)	52.4(First 200kWh/kVA)	42.9
	112.0(Exceeding part)	33.0(Lager than the on-peak peak)	50.4(Exceeding part)	
Ice-storage Air-conditioning Tariff	66.5(First 650)	0.0(Less than the on-peak peak)	68.9(First 200,000)	61.4
	63.5(Exceeding part)	26.0(Lager than the on-peak peak)	67.4(Exceeding part)	

The on-peak period in CLP refers to the time span from 9:00 a.m. to 9:00 p.m. of

normal workday and the rest as well as the public holiday is the off-peak period. The different end-users are qualified to take diverse tariffs according to the requirements. For instance, the buildings with monthly peak demand larger than 3000kVA can take the third tariff (i.e. large power tariff) which may charge less in the electricity bill than the first two tariffs. If the buildings equipped with the ice or chilled water-storage storage system, they are eligible to take the last tariff which appears more favorable in the monthly peak demand charge compared with that of the large power tariff.

For developing the demand limiting strategy, the third tariff (i.e. the large power tariff) is selected. In this case, the price for the first on-peak 5000 kVA is 117 HKD/kVA; and the demand part exceeding 5000 KVA in the on-peak period will be charged 112 HKD/kVA. If the monthly peak demand in the off-peak period is larger than the monthly on-peak peak demand, extra cost will be charged for the exceeding part, i.e. 33 HKD/kVA. For the energy consumption cost, it is also divided into two parts, i.e. on-peak part and off-peak part. The load of the first 200 kWh/kVA in the on-peak period charges 52.4 Cent/kWh and the exceeding part charges 50.4 Cent/kWh. All the energy consumed in the off-peak period will be charged at a constant price, i.e. 42.9 Cent/kWh. The tariff is described as (8.23).

The off-peak load does not need to take into calculation in this study because the number of operating chillers in off-peak period is always much less than that in on-peak period, which makes the off-peak peak demand smaller than the on-peak one. Thus, (8.24) is used for calculating the actual monthly bill.

$$C_{mon} = \underbrace{5000 \times 117 + (PD_{mon,on} - 5000) \times 112 + (PD_{mon,off} - PD_{mon,on}) \times 33}_{Demand\ Cost} + \underbrace{200 \times PD_{mon,on} \times 0.524 + (E_{mon,on} - 200 \times PD_{mon,on}) \times 0.504 + E_{mon,off} \times 0.429}_{Energy\ Cost} \quad (8.23)$$

$$C_{mon} = \underbrace{5000 \times 117 + (PD_{mon,on} - 5000) \times 112}_{Demand\ Cost} + \underbrace{200 \times PD_{mon,on} \times 0.524 + (E_{mon,on} - 200 \times PD_{mon,on}) \times 0.504 + E_{mon,off} \times 0.429}_{Energy\ Cost} \quad (8.24)$$

where C_{mon} represents the total monthly electricity bill; and $E_{mon,on}$, $E_{mon,off}$ are the monthly overall energy consumptions in the on-peak and off-peak periods respectively.

A simplification can be made for the bill calculation if we ignore the slight price difference between the first limited part and the exceeding part, e.g. the unit demand price for the first 5000 kVA is 117 HKD and the part in excess is charged 112 HKD/kVA. Such simplification will not affect the final monthly bill comparison results between the one with developed limiting strategy implementation and that of the base case. The bill difference is mainly from the tradeoff between reduced peak demand cost and increased energy cost as they take the same simplified price structure. Therefore, the parameters $\hat{\alpha}, \hat{\beta}$ are assigned the values as follows.

$$\hat{\alpha} = 112;\ \hat{\beta} = 0.504 \quad (8.25)$$

b) Identification and Validation of the Relationship between Energy Rise and Demand Reduction

After the parameters $\hat{\alpha}$ and $\hat{\beta}$ identified, the relationship between the daily

energy rise ΔE_i and the daily peak demand reduction ΔPD_i need to be determined for the optimal monthly peak demand reduction $\Delta PD_{mon,opt}$ prediction. The data from Table 8.1 can also be used for identifying the coefficients in (8.5). Based on the data, a linear equation is established with a 0.90 R square value in description of the relationship between energy rise and related demand reduction, shown as (8.26).

$$\Delta E_i = 8.35 \times \Delta PD_i + 1764.2 \tag{8.26}$$

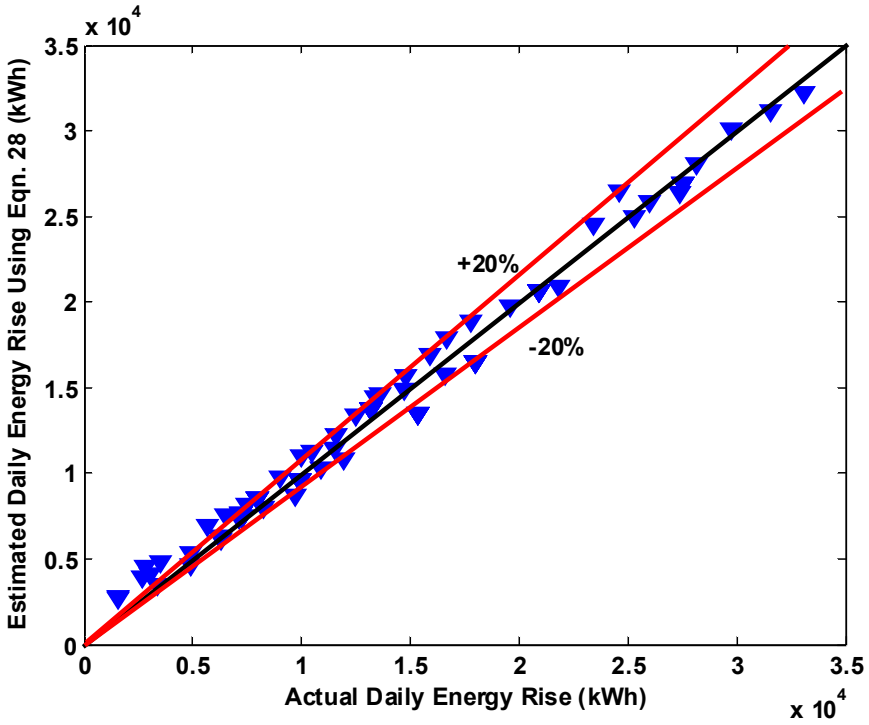

Figure 8.8. Comparison between actual daily energy consumptions and the estimated ones

For validating the developed relationship, the generated data employing trial and error method in previous section 8.3.1 were used. The comparison results showed that (8.26) was capable of obtaining an estimated energy rise with acceptable accuracy. More than 85% of the energy rise estimations located in the relative error range [-20%, 20%], shown in Figure 8.8.

c) Identification of Optimal Monthly Demand Reduction

Substitute (8.25) and (8.26) to (8.7), the following equation is established.

$$CS_{tot} \in [2.6 \times \Delta PD_{mon} - 23119, 107.8 \times \Delta PD_{mon} - 889.2] \tag{8.27}$$

Since $d(CS_{tot}) \big/ d(\Delta PD_{mon})$ is in the range [2.6, 107] which indicates the linear function CS_{tot} is monotonic increase, the optimal monthly demand reduction $\Delta PD_{mon,opt}$ should be assigned the largest value. As equation (8.22) shown, the maximum peak demand reduction can be obtained as the longest pre-cooling duration taken. In the study, 9 hour was set as the upper limit of the pre-cooling duration. Thus, optimal monthly demand reduction is $\Delta PD_{mon,opt} = 3114.1 kVA$.

8.3.5 Validation of Module III for Hourly Power Profile Prediction

The model-based cooling load prediction algorithm had already been validated by Zhou and Wang in [2009]. Hence, the coefficients identification of equation (8.20) and the related validation were of major concern in this section. One week simulation data had been adopted for identifying the coefficients using least square regression method. The other three weeks data were used for the related validation.

It was found that a quadratic function was able to well depict the relationship between part load ratio *PLR* and the central chiller system overall COP. The identified coefficients in (8.20) are shown as $c_2 = -4.2417, c_1 = 5.8675, c_0 = 0.1199$.

The comparison results between the calculated system overall COP using (8.20)

and the actual ones are shown in Figure 8.9. More than 95% of the data were located in the relative error range [-10%, 10%] which indicated a good accuracy of the calculated COP results.

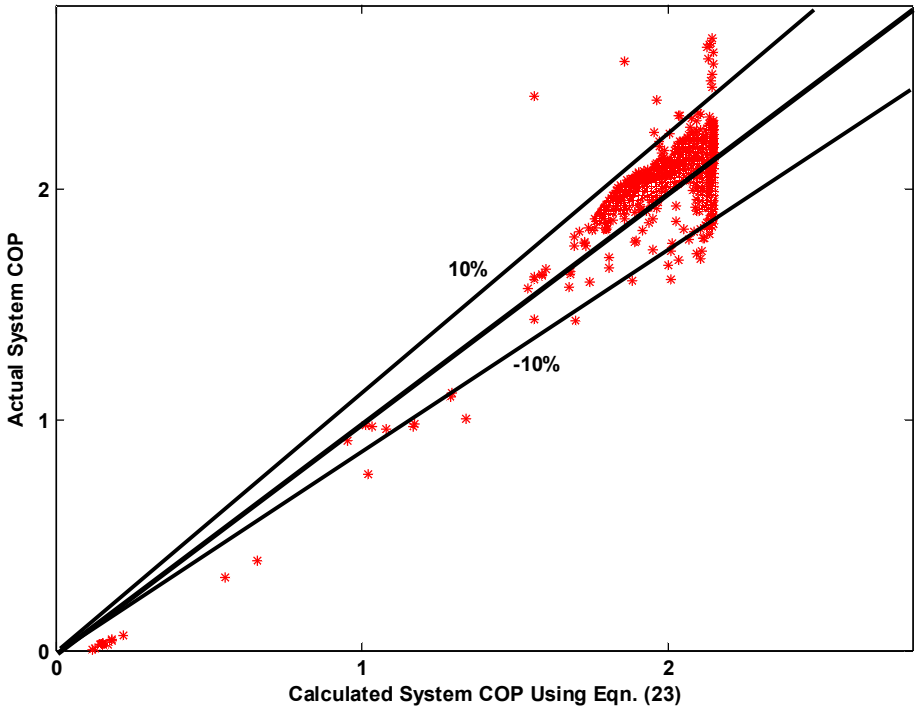

Figure 8.9. Comparison between the actual system COPs and the calculated ones

8.3.6 Validation of the Demand Limiting Strategy

As the estimated optimal monthly demand reduction $\Delta PD_{mon,opt}$ and monthly peak demand prediction $PD_{mon,pre}$ known, the demand limiting threshold $PD_{Thres,opt}$ is obtained using (8.3). With the predicted daily peak demand PD_i from module III, the difference between PD_i and $PD_{Thres,opt}$ will determine the implementation of module IV and V. If they were needed for a particular day, the estimation of the pre-cooling duration τ_i is attained from module IV and the varying room temperature set-point

$T_{room,set}$ in the occupation period is outputted from the module 5, i.e. PI demand limiting algorithm. Meanwhile, the indoor thermal comfort is successively evaluated by the PMV model.

Table 8.3. Variable values used in the case study

Variables	Values (10^4kVA)
$PD_{mon,pre}$	1.605
$\Delta PD_{mon,opt}$	0.3114
$PD_{Thres,opt}$	1.294
$\hat{\sigma}$	-0.06
P_{set}	1.234

For validating the entire developed strategy in terms of monthly cost savings, simulations of three continuous months (i.e. July, August and September) had been conducted. Firstly, the results from the base case with constant 24℃ room temperature set-point were obtained and set as baselines. Secondly, the proposed demand limiting strategy was implemented and the obtained monthly electricity bill and PMV results were compared with those in base case. The comparison results from these three months were similar to each other and the comparison results from August were selected as an example to show the effectiveness of the developed strategy. The estimated values from the individual module used in this study were shown as Table 8.3.

The comparison results are shown as the first two cases in table 8.4. The total

monthly cost saving with proposed demand limiting strategy implementation achieved 8.51% compared with that from base case. The cost saving was the tradeoff result between energy cost rise and peak demand reduction. The energy cost increased by $5.0048*10^4$ HKD because of the extended pre-cooling implementations and the demand cost decreased by $2.9792*10^5$ HKD after the implementation of the developed demand limiting strategy. With further test whether the maximum monthly cost saving had been achieved, the P_{set} was manipulated to be varied in a large rang, shown as case 3 to case 11. It is observed that with the decrease of the P_{set}, the relative percentage of monthly cost saving accordingly increased compared with that in base case. However, the occupants' thermal comfort may be sacrificed if an extremely low P_{set} was taken (e.g. P_{set}=10500 in case 3). The accumulated time of PMV in excess of 0.8 in case 3 was much larger than that in base case. The case 5 with P_{set} equaled 11500 actually achieved the largest cost saving (i.e. 10.45% or $3.05*10^5$ HKD) with similar indoor thermal comfort to that in base case. The developed strategy did not achieve such account cost saving mainly because of the setting of the monthly peak demand set-point P_{set}. Thus, a suitable P_{set} is greatly important for maximizing the monthly cost saving and guaranteeing the acceptable indoor thermal comfort. If it was set excessively large, limited cost saving was achieved, see case 11. In the opposite, if it was set excessively small, the occupants' thermal comfort was sacrificed greatly, see case 3.

Table 8.4. Comparisons between results from base case and those from proposed demand limiting control with different P_{set}

Case	Control Type	P_{set} (kW)	E_{mon} (10^6 kWh)	PD_{mon} (10^4 kVA)	CS_E (10^4HKD)	CS_{PD} (10^5HKD)	CS_{tot} (%)	Accumulated Time (min.)(PMV <-0.8)	Accumulated Time (min.)(PMV> 0.8)
1	Base Case	N/A	2.5558	1.5529	0	0	0	0	5
2	PI	12340	2.6747	1.2983	-5.005	2.9792	8.51	0	6
3	PI	10500	2.8181	1.1497	-11. 15	4.7169	12.36	1	35
4	PI	11000	2.7646	1.1759	-8.8613	4.4111	12.1	1	24
5	PI	11500	2.7568	1.2196	-8.5305	3.8996	10.45	1	5
6	PI	12000	2.7382	1.2641	-7.7309	3.3785	8.94	0	5
7	PI	12500	2.6726	1.3123	-4.9147	2.8151	7.97	0	6
8	PI	13000	2.6589	1.3621	-4.3307	2.2325	6.17	0	4
9	PI	13500	2.6124	1.4221	-2.3344	1.5298	4.45	0	2
10	PI	14000	2.5723	1.4844	-6.1502	8.0192	2.54	0	0
11	PI	14500	2.5843	1.5020	-1.1272	5.9517	1.66	0	0

8.4. Summary

This paper presented a demand limiting control strategy for optimizing the monthly cost savings of commercial buildings with acceptable indoor thermal comfort. A suitable demand threshold for demand limiting is firstly calculated based on the predicted monthly peak demand and the estimated optimal monthly demand reduction. For restraining the daily peak demand under the threshold, a specific PI demand limiting algorithm is proposed. Case studies have proved that

(i). The developed demand limiting strategy can save up to 8.5% of the total monthly cost by adjusting the indoor room temperature set-points. Meanwhile,

the indoor thermal comfort had not been compromised comparing it with that in the base case.

(ii). The monthly peak demand prediction module is capable of obtaining a result with acceptable accuracy based on the historic data.

(iii). The results from the established linear relationship between the pre-cooling duration and daily demand reduction (i.e. Equation (8.19)) are of satisfactory accuracy. So is the linear relationship between daily energy rise and daily demand reduction (i.e. Equation (8.23)).

(iv). The identified quadratic relationship between system overall COP and the part load ratios can well depict the actual situations.

(v). The PI demand control algorithm is capable of lowering down the daily peak demand if a suitable demand set-point used.

Therefore, the developed demand limiting strategy can result in considerable amount of monthly cost savings and guarantee acceptable indoor thermal comfort meanwhile. It is suitable for the practical application for reducing the monthly electric bill.

CHAPTER 9 IN-SITU IMPLEMENTATIONS OF THE ONLINE CONTROL STRATEGIES

This chapter presents the in-situ implementation of the online control strategies developed in previous chapters for the optimal control of the multiple-chiller system. The developed optimal control strategies are compiled into related software packages and they are executed on a management and communication platform based on intelligent building integration and management system (IBmanager). The optimization results from these packages are used to enhance control robustness and energy efficiency. Section 9.1 addresses the implementation architecture of the developed software packages. In section 9.2, the basis of the management and communication platform, i.e. IBmanager, is firstly introduced. Secondly, the main functions and interfaces of the developed platform are addressed. A summary of this chapter is provided in Section 9.3.

9.1 Implementation Architectures of the Developed Control Software Packages

The online control software packages of optimal control strategies were programmed using the application program of Matlab. All optimal control strategies (i.e., control functions) in the same package were programmed as subroutines, and were compiled as DLL modules which are convenient for the implementations in

IBmanager. In these online control packages, the practical constraints, such as minimum up/down time for the chiller sequencing control, have been taken into consideration. The in-situ implementation architecture of the online control software packages is shown in Figure 9.1. The packages developed in this thesis are executed in a dedicated PC station interfaced with the main station of the chiller plant control system. The interface or protocol for the communications between control software packages and the main station is provided by the contractors. It should be mentioned that the executions of these standalone control software packages are in parallel with the executions of control strategies provided by the HVAC&BMS contractors.

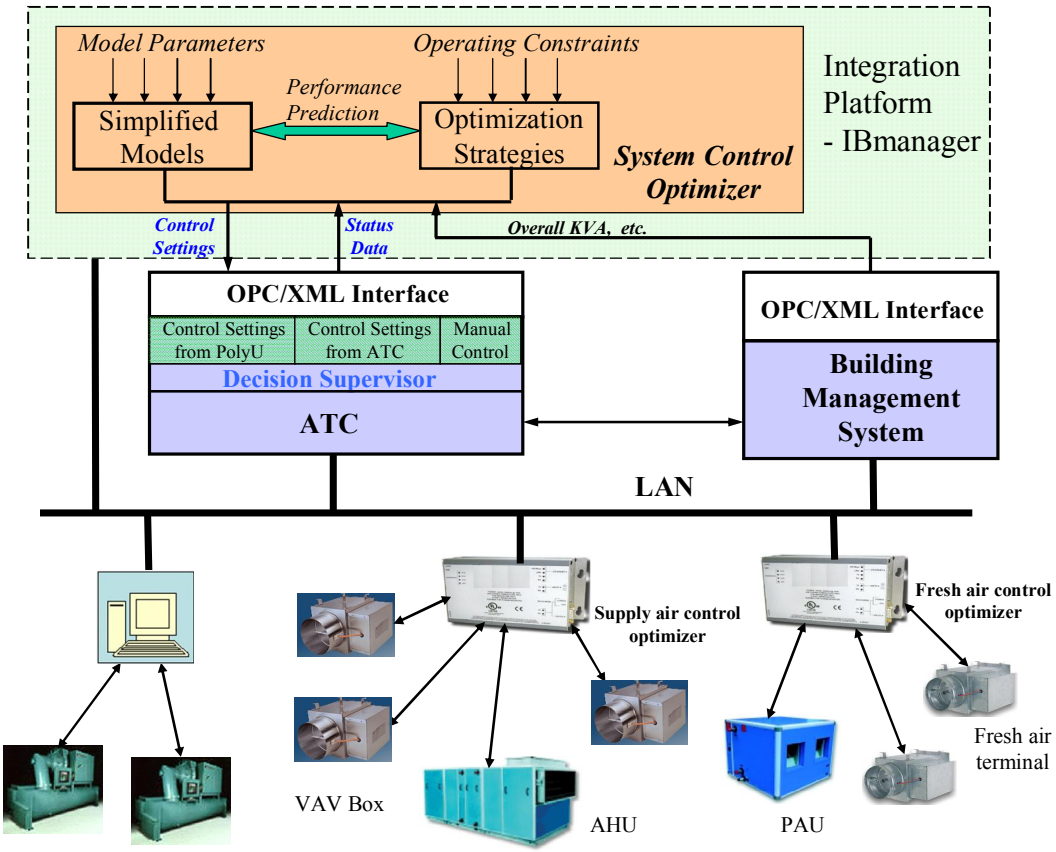

Figure 9.1 In-situ implementation architectures of online control software packages.

A decision supervisor in the chiller control system is designed for the operators to set whether the settings given by the online control software packages developed are used or not. For instance, when the chiller sequencing control is of concern, the related control software packages will provide the optimized operating number of chillers and the decision supervisor will determine to use it or not. This implementation approach provides conveniences in further improving the performances of optimal control strategies developed in this thesis by offering adequate update space and freedom.

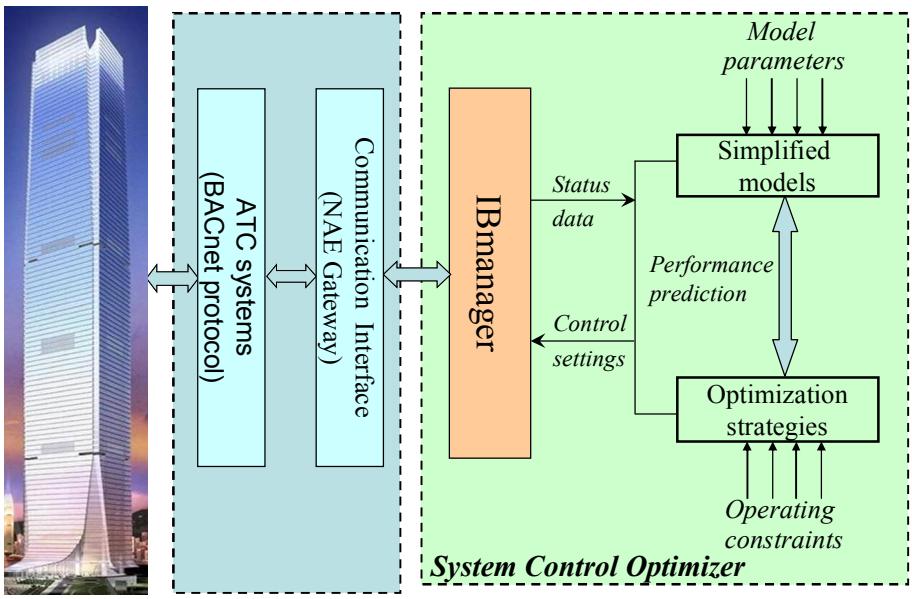

Figure 9.2 Interface between the management and communication platform and the ATC system.

The interface used for the interoperation of the management and communication platform based on IBmanger and ATC (Automatic Temperature Control) system is shown in Figure 9.2. It was developed based on a trial version of the BACnet SDK

(Software Development Kit) since the network of the BMS system was based on the BACnet protocol. IBmanager can read the system operation data through a NAE linked with local controllers, and BA outstations linked with sensors, actuators, etc. Meanwhile, IBmanager can send the optimized control settings to the ATC systems through the NAE for the practical control of the HVAC system to improve their operating efficiency.

9.2 An Overview of the Management and Communication Platform

9.2.1 Brief Introduction of IBmanager

IBmanager is the basis of the developed management and communication platform, which was developed in The Hong Kong Polytechnic University. This open IBMS (Intelligent Building Management System) integration and management platform allows the integration and management of building automation systems from different vendors as well as remote monitoring and management services. The IBmanager using the middleware and web services technologies provides convenience for integrating full scale building automation and industrial automation (IA) systems. Different subsystems can be integrated in IBmanager for diverse functions, such as data acquisition, network communication, automation and information management. IBmanager, like other mature commercial software, provides software interfaces for the supervision, management and customized development. Figure 9.3 shows the interface connection and function blocks of IBmanager, which is divided into several parts, i.e., OPC (OLE for Process Control)

servers, historical database, BMS function components, BMS HMI (human machine interface) based on the Local Area Network (LAN) version, web services server and building management web server. The OPC servers can be installed in various PCs (Personal Computers) in the LAN. The BMS function components are used to execute the tasks of real-time data access, alarms & events process, historical data access, scheduling, parameter optimization of control strategies, performance/fault diagnosis of HVAC systems, etc. The LAN-based BMS HMI realizes the full BAS functions in the LAN applications. The COM/DCOM interfaces are converted to web services interfaces by the web services server. The Active Service Pages (ASP) and dynamic link library (DLL) files are deployed in the building management web server to communicate with the web services server and provide the user access interface (web pages) to users. There are several essential functions for BASs, such as real-time data sharing, alarm/event, historical data and trending, scheduling and network management. The real-time data access is accomplished by OPC DA (Data Access) server. The OPC HDA (historical data access) is used to realize historical data access. The alarms & events are carried out by OPC AE (Alarm & Event). The above mentioned functions can be wrapped as public web services interfaces for the communication and integration on the Internet.

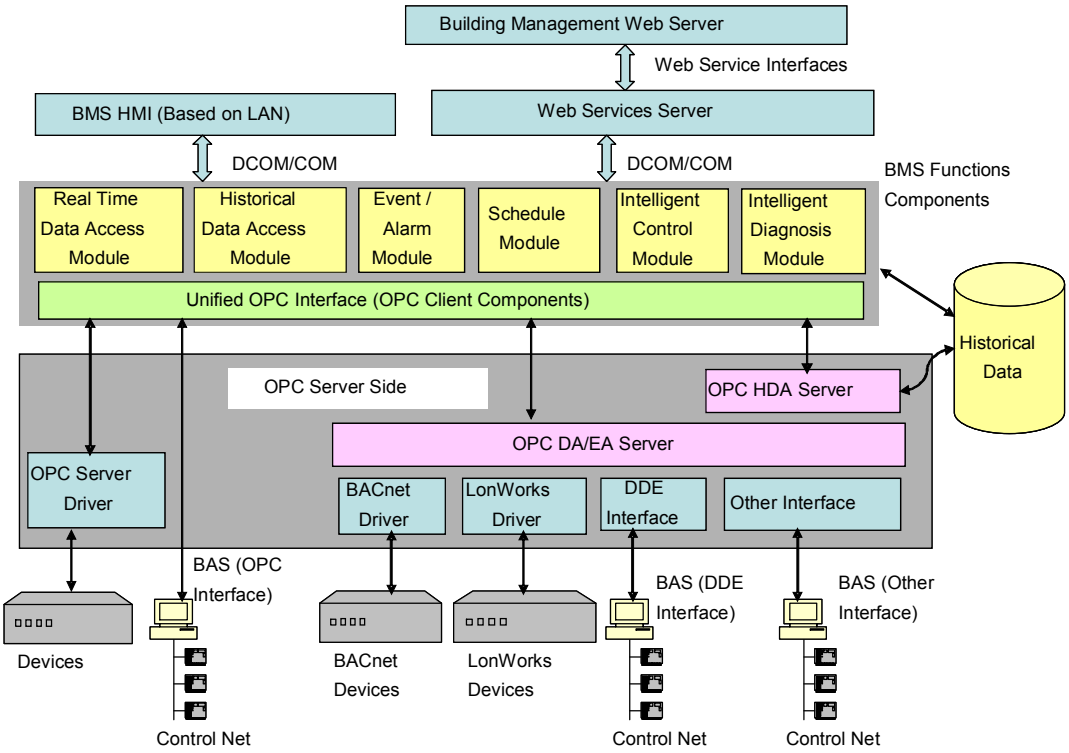

Figure 9.3 Interface connection and function blocks of IBmanager.

The typical applications of IBmanager can be divided into the following three categories:

• *Internet-based centralized management platform integrating multiple (vendor) systems:* It is used to support centralized services and management on Intranet/Internet;

• *Supervision, integration and development platform for BA and IA systems:* It is utilized to integrate field control stations of different vendors (protocols);

• *Supporting and management platform for independent online applications:* It can add third-party or complicated application programs of added-value services to BA systems.

9.2.2 Main Functions and Interfaces of the Platform

Figure 9.4 shows the home page of the developed platform denoted as IBMS (intelligent building management system). It is mainly used for the application of the online control software packages to achieve reliable and energy efficient control and operation of the chiller plant in the super high-rise building presented in Chapter 3. Six main functions constitute this platform and they are *access management*, *history data*, *system setting*, *system configuration*, *system maintenance* and *real-time monitoring*.

Figure 9.4 Home page of the IBMS in the ICC site.

Access Management is used to define the authority levels of different users. The users consist of supervisory user, advanced users and usual operators. The supervisory one has the highest authority and can manage the authority levels of the other users.

History Data is to write the system operation data into the database. These recorded operation data can be used to fit parameters, train model and diagnose faults. *System Setting* is to conFigure the system in terms of the protocols used in building automation systems and/or the building management systems. *System Configuration* is to set the data points of IBmanager based on the field installation information provided by the MVAC&BMS contractors. It can also set the parameters for different control strategies. *System Maintenance* is to provide the related log services. *Real-Time Monitoring* is to monitor the system and component operation, etc. With the assistance of the friendly human machine interface, some operation data can be monitored with visualization while others can be monitored in the form of tables.

Figures 9.5 shows the monitoring interfaces of the real-time operation data with visualization for the chiller group. The main operation data including chilled water supply and return temperatures, etc. can be read from these monitoring interfaces. It provides the convenience for the operators to quickly estimate whether the system/corresponding component operate normally. Since the operation status of each individual chiller plays a significant role on the overall system energy efficiency, the major measurements of each chiller are monitored and displayed on a separate interface, shown as Figure 9.6.

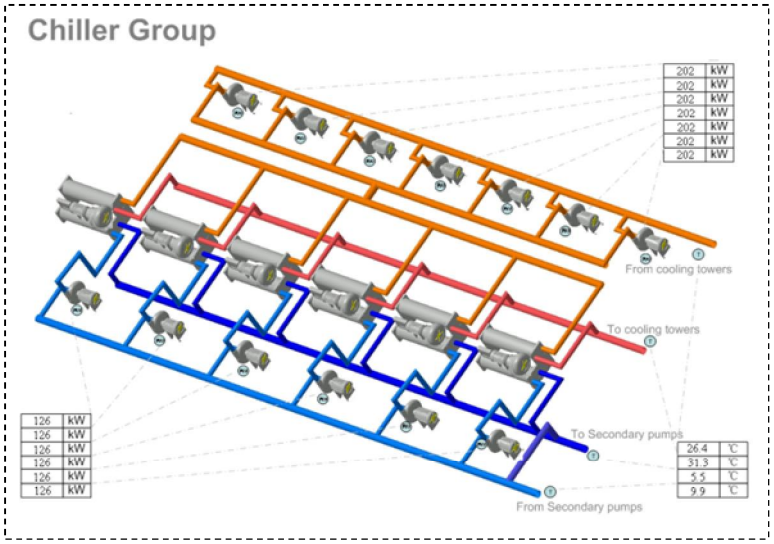

Figure 9.5 Monitoring interface of the chiller operation status.

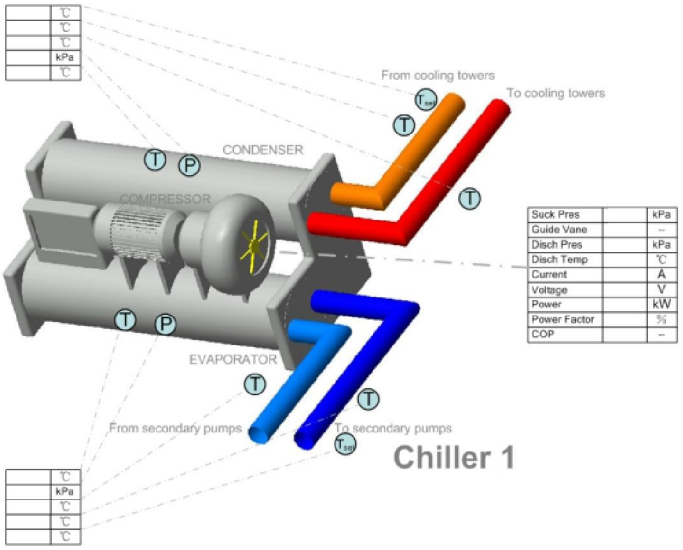

Figure 9.6 Monitoring interface of the individual chiller operation status.

9.3 Summary

The in-situ implementation and test of the developed online optimal control strategies are of great significance to validate their operational performances in practice. Many practical issues including data communication, interface, etc., need to

be seriously considered for the implementation of the online control software packages in real building systems. In this chapter, the implementation architectures of the online control software packages as well as the essential interfaces used for communication and interoperation of the platform and ATC system is firstly introduced. Next, the basis of the developed management and communication platform which is used to implement the online control software packages of optimal control strategies is addressed briefly. At the end, an overview of the application software system including its main functions and interfaces which is used in the super high-rise building is provided. The system presented in this chapter is being tested and evaluated in the super high-rise building.

CHAPTER 10 SUMMARY AND RECOMMENDATIONS

Optimal control strategies of multiple-chiller systems have significant impacts in enhancing the control and operation robustness as well as improving the energy and cost efficiency of HVAC systems. It is therefore highly desirable to develop robustness enhanced and cost efficient control strategies for building air-conditioning systems, especially for complex building air-conditioning systems. The presented thesis has addressed this need through making the following contributions.

Conclusions on Main Contributions

i. The main contributions of this thesis are the development and validation of the online optimal control strategies for multiple-chiller systems. The software tools and implementation guidelines for applying these online optimal control strategies for enhancing robustness and cost efficiency have also been provided.

ii. Another contribution of this thesis is the development of a dynamic simulation platform for the multiple-chiller systems, which was used for testing and analyzing the control reliability, environmental and energy performances of the developed optimal control strategies under dynamic working conditions prior to their site implementation.

iii. The data fusion technique has been used to develop an algorithm for obtaining a more accurate and reliable cooling load measurement through combining the complementary advantages of two different types of load measurements. This algorithm resolves the long lasting practical problem of inaccurate direct cooling load measurement.

iv. The strategy for chiller sequencing control with robustness enhanced has been developed. In this strategy, the chiller sequencing control performance can be improved due to two main improvements. One is that the direct cooling load measurement is replaced by the more accurate and reliable cooling load fused measurement. The other one is the used chiller maximum cooling capacity is from a simplified model according to chiller operating conditions instead of a constant one.

v. The optimal start strategy takes the chiller operating number as an optimizing variable as well as the pre-cooling lead time for the first time. The case studies confirmed the chiller operating number is important for optimizing the chiller plant energy consumption in the start period. The developed strategy can successfully determine the optimal number of operating chiller and estimate its associated pre-cooling lead time, which lead to the minimal energy consumption of chiller plant in the start period.

vi. The developed demand limiting strategy is capable of greatly reducing the monthly electricity bill by taking into both the peak demand cost reduction and energy cost rise into consideration. The developed specific PI demand limiting

strategy is of satisfactory performance in restraining the daily peak demand to a pre-defined threshold.

Performance Summary of the Cooling Load Fused Measurement

For resolving the practical problem of inaccurate building cooling load measurement, a data fusion algorithm had been developed to combine the complementary advantages of two different types of cooling load measurements, i.e. cooling load direct measurement and cooling load indirect measurement. The case study results showed that the impacts of the sensor measurement noise, outliers and systematic errors in cooling load direct measurement had been greatly alleviated or eliminated. Thus, a more accurate and reliable fused measurement was generated using the developed fusion algorithm. An associated confidence degree for systematically evaluating the quality of fused cooling load was as well yielded. The confidence degree can be used as an indicator of sensor measurement faults existence by showing a lasting low value. The cooling load fused measurement with improved accuracy and reliability is of great significance in strengthening the performance of chiller automatic controls, e.g. chiller sequencing control.

Performances Summary of the Chiller Sequencing Control

Chiller sequencing control aims to switch on right number of operating chiller for satisfying the varying building cooling load. However, such control in practice is

usually of unsatisfactory performance due to the inaccurate cooling load measurement.

The developed chiller sequencing control strategy was based on the fused cooling load measurement and the chiller maximum cooling capacity calculated from a simplified model. The case studies results showed that the proposed control strategy greatly enhanced the robustness of chiller sequencing control and provided a better indoor thermal comfort environment with less energy consumption if compared with the conventional control strategy based on the direct cooling load measurement and constant chiller maximum cooling capacity.

Performances Summary of the Data Fusion Based Online Sensor Fault Diagnosis Method

For ensuring the healthy sensor operations in the cooling load direct measurements, a data fusion based online sensor fault diagnosis method was developed. The continuous low confidence degree from the data fusion engine was used to trigger the fault diagnosis process. For those faults occurring in the chilled water flow meter and supply temperature sensor, the associated Moffat distances were calculated to isolate them by checking the consistence between the sensor measurements and their expected values. If the distance was larger than unity, the faults existed. For those faults in chilled water return temperature sensor, a confidence reconstruction approach was taken for diagnosing. The small value of the reconstructed confidence degree implied the faults existence in the return temperature measurement.

Case studies had been performed to assess the performance of the developed sensor fault diagnosis method. The results showed that it can efficiently diagnose the faults no matter when they occurred separately or together. It should be noted that the moving window length and the uncertainty bounds used in the strategy needed to be assigned proper values. Otherwise, the false diagnosis results ratio would increase largely.

Performances Summary of the Model-based Optimal Start Control Strategy

For minimizing the energy consumption of the central chilling system in the start period, a model-based optimal start control strategy has been developed and validated. The chiller operating number had been taken into consideration for the first time. The pre-cooling lead time would be shortened with the increase of chiller operating number. If less than necessary chillers were switched on, the insufficient supplied cooling would take forever to cool the indoor room temperature down to a desired level.

The developed model-based optimal start control strategy has been tested on the constructed dynamic simulation platform. The results showed that it was capable of selecting optimal number of operating chiller and accurately estimating its related pre-cooling period which result in less chiller plant energy consumption compared with other options.

Summary of Performance of the Demand Limiting Control Strategy

A demand limiting strategy for optimizing the monthly cost saving of the complex central chilling system was presented. It comprehensively considered the tradeoff between the cost saving from the demand reduction and the cost rise from the increased energy consumption after a demand limiting control is complemented. There were two main steps in the presented strategy. The first one was to estimate a suitable monthly peak demand threshold. An excessively high threshold would result in limited cost saving or even increased monthly bill, while an inappropriately low one may greatly sacrifice occupants' thermal comfort. The second step was to limit the peak demand of particular day to the settled threshold by utilizing the thermal mass of building, i.e. PI demand limiting algorithm in this study.

The performed cases studies demonstrated the proposed demand limiting control strategy can greatly reduce the monthly electricity bill of the central chilling system with no sacrifice of the occupants' thermal comfort meanwhile. The results as well confirmed the importance of proper peak demand threshold selection and proper parameter setting in the PI demand limiting algorithm.

Recommendations for Future Work

Major efforts of this thesis are made on the development of the optimal control strategies for the chiller operation in multiple-chiller systems. It would be very desirable and valuable to make further efforts on the following three aspects related to

the research presented in this thesis.

- In-situ implementation and validation of the developed optimal control strategies on complex building central chilling systems are needed. The feedback information is valuable for updating them to obtain desirable and satisfactory performances in practice. It is a time and energy consuming task to validate the proposed strategies in the practical commercial building. Therefore, essential efforts are required in the future.

- The fixed chilled water and cooling water supply temperature were used in the study. For maximizing the operating efficiency of the overall air-conditioning system, optimized chilled water and cooling water supply temperatures are required, which could be developed based on the power consumption tradeoff between different components. For example, the optimized chilled water supply temperature will completely consider the power consumptions of chiller group and pumps. The rise of chilled water supply temperature result in the decrease of chiller group power but an increased water pump power due to the growing chilled water flow rate demand.

- For demand limiting research in the future, the control of phase change material (PCM) can be integrated to discuss the potential of demand reduction due to the usage of PCM. PCM has the great capacity of heat absorbing or cooling releasing when material phase changes. This particular feature can be perfectly used to curb peak demand cost by taking advantage of the great

difference between on-peak and off-peak electric price. The PCM can be charged to store the cooling in the off-peak period, while the stored cooling can be controlled to release when peak load occurs in the on-peak period.

APPENDIX A--- WALL ABSORBED RADIATION CALCULATION

The I_{global} is comprised of two parts: the direct normal radiation I_{dn} and the horizontal diffusive radiation I_{dif} which is usually obtained by multiplying a proportion factor φ with the global radiation I_{global}

$$I_{global} = I_{dn} + I_{dif} \tag{A1}$$

$$I_{dif} = \varphi \times I_{global} \tag{A2}$$

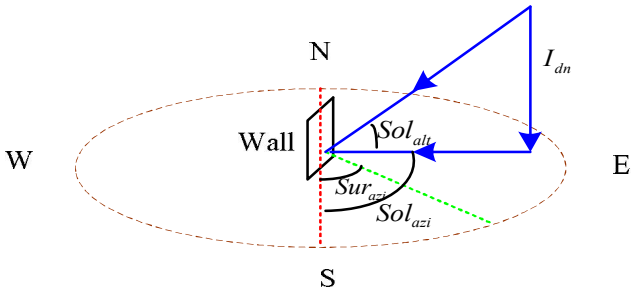

Figure A1. Radiation absorbed by the wall

Figure A1 is used to explain the calculation of the wall absorbed radiation W_{Rad}, shown as

$$W_{Rad} = \frac{I_{global} \times (1-\varphi) \times \cos(Sol_{alt}) \times \cos(Sol_{azi} - Sur_{azi})}{\sin(Sol_{alt})} + I_{dif} \tag{A3}$$

where Sol_{alt} is the solar altitude; Sol_{azi} is the solar azimuth and Sur_{azi} is the wall surface azimuth which is the angle between the south orientation and the normal line of the wall surface.

APPENDIX B --- DLL SOFTWARE PACAKAGES

```
**************************************************************************
```

DLL CODE OF DATA FUSION METHOD USED FOR MERGERING TWO LOAD MEASUREMETNS

Developer: Sun Yongjun, June, 2008
Department of Building Services Engineering
The Hong Kong Polytechnic University

```
**************************************************************************

function CL_output = entry(CL_input)

**************************************************************************
****
% Inputs
%
% Includes three parts: measurements, parameters and previous results
%
% % measurements
% 01-06         : Pev           % Evaporating temperature(C)
% 07-12         : Pcd           % Condensing temperature(C)
% 13-18         : Pcom          % chiller power (kw)
% 19-24         : FR            % Flow rate of chiller 1 to 6 (l/s)
% 25            : Tchin         % chilled water return temperature(C)
% 26            : Tchout        % Chilled water supply temperature(C)
% 27-30         : reserve for future use
%
% % preveous results
% 31-50         : pre_direMeas          % previous N direct measurements
% 51-70         : pre_indrMeas          % previous N indirect measurements
% 71            : last_fuseMeas         % previous fused measurement
% 72            : last_confDegr         % previous confidence degree
% 73            : last_direMeas         % direct measurement at one step ahead
% 74            : last_indrMeas         % indirect measurement at one step ahead
% 75-80         : reserve for future use
%
% % parameters
% 81            : E_mn          % The threshold for distinguishing the outliers for
%                                   the experimental data of 5 chillers(kW)
% 82            : E_f_mean      % The value for calibrating the CL_im for the
%                                   experimental data of 5 chillers(kW)
```

```
% 83            : deta          % value identifying the threshold for system error
% 84            : beta1         % decreasing rate confid. degree of outlier
% 85            : beta2         % decreasing rate confid. degree of system error
% 86-91         : LOSSES        % loss
% 92-97         : Alpha         % loss factor
% 98-99         : reserve for future use
%
%
*****************************************************************
****
% Outputs
%
% 01            : fused measurement
% 02            : confidence degree
% 03-05         : reserve for future use
% 06-25         : pre_direMeas          % previous N direct measurements
% 26-45         : pre_indrMeas      % previous N indirect measurements
% 46            : current direct measurement
% 47            : current indirect measurement
% 48-60         : reserve for future use
%
%
*****************************************************************
****
%
% variables
% CL_indirect      : current indirect measurement
% Curr_NM            : number of operating chillers
% CL_indir          : indirect measurement for each chillers (6 items)
% Para_DF            : vector to store fusion algorithm
% CL_direct         : current direct measurement
% CL1                 : vector (2 items) to store current direct/indirect meas.
% MWindow            : moving window
% MLast               : vector (2 items) to store last direct/indirect meas.
% CLprv               : vector (2 items) to store last fused meas. and confd. deg

% measurements
Pev        = CL_input(1:6);
Pcd        = CL_input(7:12);
Pcom       = CL_input(13:18);
FR1          = CL_input(19);
FR2          = CL_input(20);
FR3          = CL_input(21);
FR4          = CL_input(22);
```

```
FR5          = CL_input(23);
FR6          = CL_input(24);
Tchin      = CL_input(25);
Tchout    = CL_input(26);


% preveous results
pre_direMeas       = CL_input(31:50);
pre_indrMeas       = CL_input(51:70);
last_fuseMeas     = CL_input(71);
last_confDegr     = CL_input(72);
last_direMeas     = CL_input(73);
last_indrMeas     = CL_input(74);

% parameters
E_mn              = CL_input(81);
E_f_mean       = CL_input(82);
deta              = CL_input(83);
beta1             = CL_input(84);
beta2             = CL_input(85);
LOSSES           = CL_input(86:91);
Alpha            = CL_input(92:97);


% filtering the foul inputs
Pev_thre=10;
Pcd_thre=10;
FR_thre=0;
Tchin_thre=0;
Tchout_thre=0;
for i=1:6
      if Pev(i)<Pev_thre
          Pev(i)=Pev_thre;
      end
      if Pcd(i)<Pcd_thre
          Pcd(i)=Pcd_thre;
      end
end

if FR1<FR_thre
      FR1=FR_thre;
end

if FR2<FR_thre
```

```
    FR2=FR_thre;
end

if FR3<FR_thre
    FR3=FR_thre;
end

if FR4<FR_thre
    FR4=FR_thre;
end

if FR5<FR_thre
    FR5=FR_thre;
end

if FR6<FR_thre
    FR6=FR_thre;
end

FR=FR1+FR2+FR3+FR4+FR5+FR6;

if Tchin<Tchin_thre
    Tchin=Tchin_thre;
end

if Tchout<Tchout_thre
    Tchout=Tchout_thre;
end

% constant parameters
Cp          = 4.187;       % specific heat of water(kW/kg.C)
Cpl         = 1.265;       % liquid refrigerant R134a specific heat(kW/kg.C)
Hf0         = 200.000;     % enthalpy at reference state R134a (kJ/kg)
Cpg         = 0.8925;      % gaseous refrigerant specific heat R134a(kW/kg.C)
Hfg0        = 197.9;       % latent heat at reference state pressure R134a (kJ/kg)
ON_OFF_Threshold = 50;     % Power threshold for judging chiller on-off status
RZ          = 73.4143;          % gas constant times the compressibility
                                % factor of the refrigerant R134a (kJ/(kg.C))
Gamma       = 1.072;            % Mean isentropic coefficient of R134a;
Gm1G        = (Gamma-1.0)/Gamma;
Ac1         = 17.4;             % Parameters for pressure and temp. convertion
Bc1         = -3297.2;          % for R134a

% Indirect cooling load of six chillers
```

```
Tev=zeros(1,6);
Tcd=zeros(1,6);
Win=zeros(1,6);
H0=zeros(1,6);
H2=zeros(1,6);
Hcomp=zeros(1,6);
H4=zeros(1,6);
Mref=zeros(1,6);
CL_indirect = 0;
Curr_NM         = 0;              % Currently operating number of chiller
CL_indir        = zeros(1,6);
for i = 1:6
      if Pcom(i) <= ON_OFF_Threshold                % chiller is off or not
            CL_indir(i) = 0;
      else
            % Evap. and cond. temp. obtained from corresponding pressure
            Tev(i)    = -273.15+Bc1/(-Ac1+log(Pev(i)));
            Tcd(i)    = -273.15+Bc1/(-Ac1+log(Pcd(i)));
            Win(i)    = (Pcom(i)-LOSSES(i))/Alpha(i);
            H0(i)     = Hf0+Hfg0+Cpg*Tev(i);
            H2(i)     = Hf0+Hfg0+Cpg*Tcd(i);
            Hcomp(i)= RZ*(Tev(i)+273.15)/Gm1G...
                  *(power((Pcd(i)/Pev(i)),Gm1G)-1)/1000;
            H4(i)     = Hf0+Cpl*Tcd(i);
            if Hcomp(i)>0 & H0(i)-H4(i)>0
                  Mref(i)         = Win(i)/Hcomp(i);
                  CL_indir(i) = Mref(i)*(H0(i)-H4(i));
            else
                  CL_indir(i)=0;
            end
            % calculating the number of operating chillers
            Curr_NM = Curr_NM+1;
      end
      CL_indirect = CL_indirect+CL_indir(i);
end

% Specifying the value of the DF parameters
Para_DF = [E_mn,E_f_mean,beta1,beta2,deta];
Para_DF(1) = Curr_NM*Para_DF(1);
Para_DF(2) = Curr_NM*Para_DF(2);
Para_DF(5) = Curr_NM*Para_DF(5);

% Direct cooling load
CL_direct     = Cp*(Tchin-Tchout)*FR;
```

```
CL1              = [CL_direct; CL_indirect];
MWindow          = [pre_direMeas; pre_indrMeas];
CLprv            = [last_direMeas; last_indrMeas];
MLast            = [last_fuseMeas; last_confDegr];
[CL_fusion,CL_degree,MWindow]=DataFusion(MWindow,CL1,MLast,CLprv,Para_
DF);
MLast            = [CL_fusion; CL_degree];
CLprv            = [CL_direct; CL_indirect];

% Outputs
CL_output            = zeros(1,60);
CL_output(1)       = CL_fusion;
CL_output(2)       = CL_degree;
CL_output(6:25) = MWindow(1,:);
CL_output(26:45)= MWindow(2,:);
CL_output(46)      = CL_direct;
CL_output(47)      = CL_indirect;

% End of the function
%
% sub-function
%
function [CL_fusion_k,CL_degree_k,MWindow] = ...
      DataFusion(MWindow,CL1,MLast,CLprv,Para_DF)

% parameters for data fusion
NW          = 20;                 % length of the moving window
E_m         = Para_DF(1);     % The threshold for distinguishing
                                  % the outliers(kW) Fitted from the Cal_E_mn.m
E_f_mean = Para_DF(2);    % The value for calibrating the CL_im(kW)
beta1      = Para_DF(3);      % incling rate for reliable degree of outlier
beta2      = Para_DF(4);      % incling rate for reliable degree of system error
deta1      = Para_DF(5);      % The value for identifying the transient interval
deta2      = deta1;
E_f_low = E_f_mean-2*deta1;         % lower limit of system error(kW)
E_f_upp = E_f_mean+2*deta2;         % upper limit of system error(kW)

% initialize the moving window

% data length
Dlength = NW;
for i = 1:20
      if abs(MWindow(1,i)) < 1e-2
            Dlength = Dlength-1;
```

```
    end
end
if Dlength < 1-1e-2          % No data at all
    MWindow(1,1)= CL1(1);
    MWindow(2,1)= CL1(2);
    CLfusion       = MWindow(1,1);
    CLdegree       = 1;
    CL_fusion_k = CLfusion;
    CL_degree_k = CLdegree;
else
    % previous results
    CLfusion       = MLast(1);
    CLdegree       = MLast(2);
    CL_dm            = CL1(1);
    CL_im            = CL1(2);
    DCL_dm_k       = CL_dm-CLprv(1);
    DCL_im_k       = CL_im-CLprv(2);
    e_k              = abs(DCL_im_k-DCL_dm_k);
    % In case of measure error
    if e_k > E_m
        CL_fusion_k = CLfusion+DCL_im_k;
        CL_degree_k = beta1*CLdegree;
    else
        % in case of measure noise
        % update the moving window
        if Dlength > NW-1
            MWindow = [MWindow(:,2:end),[CL_dm; CL_im]];
        else
            MWindow (:,Dlength+1)= [CL_dm; CL_im];
        end
        S_measure     = sum(MWindow(1,:));
        DCL_im          = MWindow(2,2:end)-MWindow(2,1:end-1);
        N1               = size(MWindow,2);
        CL_fusion_k = (S_measure+[1:N1-1]*DCL_im')/N1;
        tv1              = CL_fusion_k;

        DCL_dm          = MWindow(1,2:end)-MWindow(1,1:end-1);
        S_m              = sum(abs(DCL_dm));
        S_c              = sum(abs(DCL_im));
        % reliable degree
        CL_degree_k = 1-(1-beta1)*abs(S_c-S_m)/((N1-1)*E_m);
        tv2              = CL_degree_k;

        % store the fused data sequence
```

```
            E_fk            = CL_fusion_k-CL_im;
            %
            if E_fk <= E_f_low | E_fk >= E_f_upp
                CL_fusion_k = CL_im+E_f_mean;
                CL_degree_k = beta2*CLdegree;
            end

            % during the intervals
            if E_fk > E_f_low & E_fk < E_f_low+deta1/10
                lamda           = (E_fk-E_f_low)/deta1;
                CL_fusion_k = lamda*tv1+(1-lamda)*(CL_im+E_f_mean);
                CL_degree_k = lamda*tv2+(1-lamda)*(beta2*CLdegree);
            end
            if E_fk < E_f_upp & E_fk > E_f_upp-deta2/10
                lamda           = (E_f_upp-E_fk)/deta2;
                CL_fusion_k = lamda*tv1+(1-lamda)*(CL_im+E_f_mean);
                CL_degree_k = lamda*tv2+(1-lamda)*(beta2*CLdegree);
            end
        end
    end

% End of the subfunction

**************************************************************************
        DLL CODE OF DATA FUSION BASED CHILLER SEQUENCING CONTROL


                        Developer: Sun Yongjun, June, 2008
                    Department of Building Services Engineering
                        The Hong Kong Polytechnic University
**************************************************************************
function SeqCtrl_output = entry(SeqCtrl_input)

% 06/05/2008
%
**************************************************************************
****
% Inputs
%
% Includes three parts: measurements, parameters and previous results
%
% % measurements
% 01-06         : Pev           % Evaporating pressure(kPa)
% 07-12         : Pcd           % Condensing temperature(kPa)
```

```
% 13              : CL_fusion % Fused cooling load(kW)
% 14              : CL_degree % Fused cooling load quality
% 15              : trnTime      % Current system time(minutes)
% 16              : Tchout       % Chilled water supply temperature (C)
% 17-20          : reserve for future use
%
% % previous results
% 21             : OTime                    % previous action occuring time (minute)
% 22             : Num_previous             % current number of operating chiller
% 23             : Pre_oper                 % previous action:1 indicates staging one
%                                                 and -1 indicates destaging one
% 24-28         : reserve for future use
%
% % parameters
% 29             : A=3150             % The parameter for determining the maximum
cooling
%                                          capacity of single chiller
% 30             : T_err=0.5          % The allowed temperature deviation (C)
% 31             : Tset=5.5           % Chilled water supply temperature setpoint (C)
% 32             : OPeriodThreshold=30    % Time limit for same action orientation
% 33             : CPeriodThreshold=40    % Time limit for opposite action orientation
% 34             : Deadband=5               % the band for preventing chiller from
%                                               repeatedly switching
% 35-39         : reserve for future use
%
**********************************************************************
****
% Outputs
%
% 01             : the number of operating chillers in next time instant (Num_previous)
% 02             : the time of action occured last time (OTime)
% 03             : the switching action of last time (Pre_oper)
% 04             : Chiller maximum cooling capacity    (kW)
% 5-8            : reserve for future use
%
%
**********************************************************************
****
%
% variables
% CAP                              : Maximum cooling capacity of single chiller (kW)
% ONum                             : number of chillers that could be changed
% Period                           : time length between the current time and the
%                                      last action occuring time
```

```
% Q_load                          : fused cooling load (kW)
% Q_state_threshold              : threshold for staging one more chiller (kW)
% Q_Destate_threshold           : threshold for destaging one more chiller (kW)

% measurement inputs
Pev               = SeqCtrl_input(1:6);
Pcd               = SeqCtrl_input(7:12);
CL_fusion      = SeqCtrl_input(13);
CL_degree      = SeqCtrl_input(14);
trnTime         = SeqCtrl_input(15);
Tchout           = SeqCtrl_input(16);

% filtering the foul data
Pev_thre=10;
Pcd_thre=10;
CL_fusion_thre=0;
CL_degree_thre=0;
Tchout_thre=0;
for i=1:6
      if Pev(i)<Pev_thre
          Pev(i)=Pev_thre;
      end
      if Pcd(i)<Pcd_thre
          Pcd(i)=Pcd_thre;
      end
end

if CL_fusion<CL_fusion_thre
      CL_fusion=CL_fusion_thre;
end

if CL_degree<CL_degree_thre
      CL_degree=CL_degree_thre;
end

if Tchout<Tchout_thre
      Tchout=Tchout_thre;
end

% previous results
OTime                 = SeqCtrl_input(21);
Num_previous       = SeqCtrl_input(22);
Pre_oper             = SeqCtrl_input(23);
```

```
% parameters
A               = SeqCtrl_input(29);
T_err       = SeqCtrl_input(30);
Tset        = SeqCtrl_input(31);
OPeriodThreshold            = SeqCtrl_input(32);
CPeriodThreshold            = SeqCtrl_input(33);
DeadBand                      = SeqCtrl_input(34);

% A = 3150;% the parameter to determine the maximum cooling capacity of chiller
% Tset = 5.5;%Temp. setpoint
% T_err = 0.5;              % temperature deviation allowed

%parameters for pressure and temp. convertion for R134a
Ac1=17.4;
Bc1=-3297.2;
% R134a thermophysical parameters
Cpl         = 1.265;       % liquid refrigerant R134a specific heat(kW/kg.C)
Cpg         = 0.8925;     % gaseous refrigerant specific heat R134a(kW/kg.C)
Hfg0        = 197.9;       % latent heat at reference state pressure R134a (kJ/kg)
RZ = 73.4143;             % gas constant times the compressibility factor of the
refrigerant R134a

[Pev_oper,N_oper] = min(Pev);
Tev(N_oper)=-273.15+Bc1/(-Ac1+log(Pev(N_oper)));
Tcd(N_oper)=-273.15+Bc1/(-Ac1+log(Pcd(N_oper)));
Tev_oper = Tev(N_oper);
Tcd_oper = Tcd(N_oper);
CAP0 =
(A*Pev_oper)*(Hfg0+Cpg*Tev_oper-Cpl*Tcd_oper)/(RZ*(273.15+Tev_oper));
%considering the real CAP with respect to the CL_degree
if Tchout <= Tset+T_err
      if   CL_degree>=0.8
            CAP = CAP0;
      else
            CAP = CAP0*1.02;
      end
else
      CAP = CAP0;
end

%
**********************************************************************
*
%     Updated Chiller sequence Control
```

```
%
**********************************************************************
*
% OPeriodThreshold = 30/60;      % the time period (hour) for two operations with
same direction
% CPeriodThreshold = 40/60;       % the time period (hour) for two operations with
opposite directions
% DeadBand = 5;
% calculate the Q_load
Q = CL_fusion;
if Q < 0
      Q_load = 0;
else
      Q_load = Q;
end
% % calculate the number of chillers in operation
%
% OTime = history.OTime;
% Pre_oper = history.Pre_oper;
%
% % the number of chillers in operation

Period = trnTime-OTime;          % the period
if Period<0
      Period=Period+24;
end
% the threshold for switching on/off a chiller
Q_state_threshold = Num_previous*CAP*(1+DeadBand/100);
Q_Destate_threshold = (Num_previous-1)*CAP*(1-DeadBand/100);

% determine the number of chillers should be in operation

% open a chiller
if Q_load > Q_state_threshold & Num_previous < 6
%         ONum = 1;       % start from the second one
%         % which one should be open
%         while CH(ONum).ONOFF >= 1 & ONum<6
%               ONum = ONum+1;
%         end
              ONum=Num_previous+1;
      % open the chiller
      if ONum <= 6
            if Period >= OPeriodThreshold & Pre_oper==1
%                       CH(ONum).ONOFF = 1;
```

```
            %at the beginning of the state or destate the chiller power
            %consumption can not indicate the supplied cooling
            Pre_oper=1;
            OTime = trnTime;
            Num_previous = Num_previous+1;
        elseif Period>= CPeriodThreshold & Pre_oper==-1
            %at the beginning of the state or destate the chiller power
            %consumption can not indicate the supplied cooling
            Pre_oper=1;
            Num_previous = Num_previous+1;
            OTime = trnTime;
        end
    end
end
% close a chiller
if Q_load < Q_Destate_threshold & Num_previous > 1
      ONum=Num_previous;
    % close the one
    if ONum >= 2
        if Period >= OPeriodThreshold & Pre_oper==-1
            Pre_oper=-1;
            Num_previous = Num_previous-1;
            OTime = trnTime;
        elseif Period >= CPeriodThreshold & Pre_oper==1
            Pre_oper=-1;
            Num_previous = Num_previous-1;
            OTime = trnTime;
        end
    end
end

% Outputs
SeqCtrl_output          = zeros(1,8);
SeqCtrl_output(1)       = Num_previous;
SeqCtrl_output(2)       = OTime;
SeqCtrl_output(3)       = Pre_oper;
SeqCtrl_output(4)       = CAP;
```

REFERENCES

Abu-el-zeet, Z. H. and Becerra, V. M., 2002, Combined Bias and Outlier Identification in Dynamic Data Reconciliation, Computers and Chemical Engineering V26 (6): 921-935.

A.L. Dexter and D. Ngo. 2001. Fault diagnosis in HVAC systems: a multi-step fuzzy model-based approach. Int J HVAC R Res 7 (1), pp. 83–102.

ASHRAE, 2007, ASHRAE Handbook--HVAC Applications, Atlanta: American Society of Heating, Refrigerating and Air-Conditioning Engineers, Inc.

Braun, J.E, 2007, Near-optimal control strategies for hybrid cooling plants, HVAC&R Research 13(4):599-622.

B.G. Liptak, 1975, Reducing the operating cost of buildings by use of computers. ASHRAE Trans., 83, Pt. I,419-35.

Crawley, D.B., L.K. Lawrie, C.O. Pedersen, and F.C, Winkelmann. 2000, EnergyPlus: energy simulation program. ASHRAE Journal 42(4):49-56.

Comstock MC, Braun JE. 1999. Development of analysis tools for the evaluation of fault detection and diagnostics in chillers. Report HL99-20. Purdue University, Ray W. Herrick Laboratories, West Lafayette, IN

Chen T.Y, 2001, Real-time predictive supervisory operation of building thermal systems with thermal mass, Energy and buildings, 33, pp. 141-150.

Chang Y.C., Lin J.K. and Chuang M.H., 2005, Optimal chiller loading by genetic algorithm for reducing energy consumption, Energy and Buildings, 37, pp. 147–155

Ding G. L., Fu L., Performance analysis and improvement of air-to-water chiller for application in wide ambient temperature range, Applied Thermal Engineering 25(2005) 135-145.

Duta M. and Henry M.P., 2005, The fusion of redundant SEVA measurement, IEEE Transactions on Control systems Technology, Vol. 13 (2), pp.173-84

D. Ngo and A.L. Dexter. 1999. A robust model-based approach to diagnosing faults in air-handling units. ASHRAE Trans 105 (1), pp. 1078–1086.

Du Z.M. and Jin X.Q. 2007, Detection and Diagnosis for Sensor Fault in HVAC Systems, Energy Conversion and Management, V48 (3): 693-702

Grewal, M.S. 2001. Kalman Filtering: Theory and Practice using Matlab. New York, Chichester, Wiley.

Gregor P. Henze, 2005, Energy and Cost Minimal Control of Active and Passive Building Thermal Storage Inventory, Solar Energy Engineering, Vol. 127, pp. 343-351.

G.S. Huang, S.W. Wang, F. Xiao, Y.J. Sun, 2009, A data fusion scheme for building automation systems of building central chilling plants, Automation in Construction (2009) 18 (3) 302-309.

G..S. Huang, S.W. Wang, Y.J. Sun, 2008, Enhancing the reliability of chiller sequencing control using fused measurement of building cooling load, HVAC&R Research 14 (6) 941-958.

Guo Z. et al., 2005, Parametric Analysis of Active and Passive Building Thermal Storage Utilization, Solar Energy Engineering, Vol. 127, pp.37-46

Honeywell, 1997, Engineering manual of automatic control for commercial buildings, Honeywell SI Edition

Henze, G. P., Dodier, R. H., and Krarti, M., 1997, Development of a Predictive Optimal Controller for Thermal Energy Storage Systems, HVAC&R Res., 3(3), pp. 233–264.

Haves P., 1999, Overview of Diagnostic Methods, Proceedings of diagnostics for commercial buildings: from research to practice, San Francisco, CA.

H. Peitsman and V.E. Bakker. 1996. Application of black-box models to HVAC systems for fault detection. ASHRAE Trans 102 (2), pp. 628–640.

H.W. Stanford, HVAC water chillers and cooling towers: fundamentals, application, and operation, New York, Marcel Dekker, 2003.

H. Yoshida, T. Iwami, H. Yuzawa and M. Suzuki. 1996. Typical faults of air-conditioning systems and fault detection by ARX model and extended kalman filter. ASHRAE Trans 102 (1), pp. 557–564.

I.H. Yang, M.S. Yeo and K.W. Kim. 2003. Application of artificial neural network to

predict the optimal start time for heating system in building Energy Conversion and Management, Vol 44 (17): 2791-2809

J.E. Seem, P.R. Armstrong and C.E. Hancock, 1989. Algorithms for predicting recovery time from night setback. ASHRAE Transactions, Vol. 1-4:439-446.

John E. Seem, 1995, Adaptive Demand Limiting Control Using Load Shedding, HVAC&R Research, Vol. 1, No. 1, pp. 21-34.

J.E. Seem, P.R. Armstrong and C.E. Hancock, 1989. Algorithms for predicting recovery time from night setback. ASHRAE Transactions, Vol. 1-4:439-446.

J. Flórez, 1987.Adaptive control of central heating systems: part 1: optimum start time control. Applied Mathematical Modeling, Vol. 11, No. 2, pp. 89-95.

J.I. Levenhagen, D.H. Spethmann, 1992. HVAC controls and systems. McGraw-Hill, Inc.

J.L. Deng, 1989, Introduction to grey system theory, The Journal of Grey System, Volume 1, pp. 1-24.

J.M. House, H. Vaezi-Nejad and J.M. Whitcomb. 2001. An expert rules set for fault detection in air handling units/discussion. ASHRAE Trans 107 (1), pp. 858–871.

J.M. Gordon, K.C. Ng, H.T. Chua, 2000, Cool Thermodynamics, Cambridge International Science Publishing, U.K.

Jun Xu et al., 2005, An Optimization-Based Approach for Facility Energy Management with Uncertainties, HVAC&R RESEARCH, 11(2), pp.215-237.

Kwan, C, 2001, Investigation of sensor topology for sequential control of chiller plants for efficient operation and control, MSc Dissertation, Department of Building Services Engineering, Hong Kong Polytechnic University.

K.H. Drees and J.E. Braun, 1996, Development and evaluation of a rule-based control strategy for ice storage systems, HVAC& R Res., Vol. 2 (4), pp. 332–335.

K.H. Lee and J.E. Braun, 2008a, Development of methods for determining demand-limiting set-point trajectories in buildings using short-term measurements, Building and Environment, Volume 43, Issue 10, pp. 1755-1768.

K.H. Lee and J.E. Braun, 2008, 2008b, Evaluation of methods for determining

demand-limiting setpoint trajectories in buildings using short-term measurements, Building and Environment, Volume 43, Issue 10, pp. 1769-1783.

K. Ogata. 1996. Modern Control Engineering. Third Edition, Prentice Hall.

Lawrence Berkeley Laboratory, 1982, DOE-2 Engineering Manual Version 2.1C Berkeley, CA, Lawrence Berkeley Laboratory

Lam J.C, 2000, Energy analysis of commercial buildings in subtropical climates, Building and Environment, 35(1):19–26.

Lu, L., W.J. Cai, Y.C. Soh, and L.H. Xie, 2005, Global optimization for overall HVAC systems-Part II problem solution and simulations. Energy Conversion and Management 46(7-8):1015-28.

M.A. Piette, S.K. Kinney and H. Philip, 2001, Analysis of an information monitoring and diagnostic system to improve building operation, Energy Build 33 (8), pp. 783–791

Massie, D., P. Curtiss, and J. F. Kreider, 2004, Neural Network Optimal Controller for Commercial Ice Thermal Storage Systems, ASHRAE Transactions, Vol. 110, Pt. 2, pp. 361-369.

Moffat R.J., 1982, Contributions to the theory of single sample uncertainty analysis, ASME J. Fluid Eng. 104 (1982) 250-260.

Nassif, N., S. Kajl, and R. Sabourin, 2005, Optimization of HVAC control system strategy using two-objective genetic algorithm. HVAC&R Research 11(3):459-86.

Ozyurt, D. B. and Pike, R. W., 2004, Theory and Practice of Simultaneous Data Reconciliation and Gross Error Detection for Chemical Processed, Computers and Chemical Engineering, V28(3): 381-402.

Q. Zhou, S.W. Wang, X.H. Xu and F. Xiao. 2009. A Gray-Box Model of Next-day Building Thermal Load Prediction for Energy-Efficient Control. International Journal of Energy Research (in print).

Ruhm K.H., 2006, Sensor fusion and data fusion-mapping and reconstruction, Measurement, Vol. 40, Issue 2, pp. 145-157

R.K. Schneider, 1981. HVAC Control Systems, New York; Wiley

R.N. Brown, 2005, Compressors: selection and sizing, 3rd Edition, Amsterdam, Elsevier.

R.R. Hackner, J.W. Mitchell, W.A. Beckman, 1984, HVAC system dynamics and energy use in buildings-Part I, ASHRAE Transactions 90 (213) 523–535.

Sun, J., and A. Reddy, 2005, Optimal control of building HVAC&R systems using complete simulation-based sequential quadratic programming (CSB-SQP). Building and Environment 40(5):657-69.

Soderstrom T.A., D.M. Himmelblau and T.F. Edgar. 2001. A mixed integer optimization approach for simultaneous data reconciliation and identification of measurement bias. Control Engineering Practice, 9: 869-876.

S.W. Wang, 1999, Dynamic simulation of a building central chilling system and evaluation of EMCS online-line control strategies, Building and Environment, 33 (1), pp 1-20

S.W. Wang, Y.M. Chen. 2004. Sensor validation and reconstruction for building central chilling systems based on Principal Component Analysis, Energy Conservation and Management 45, pp. 673–695

S.W. Wang, X.H. Xu. 2006. Simplified building model for transient thermal performance estimation using GA-based parameter identification. International Journal of Thermal Sciences, Volume 45, pp. 419-432.

T. B. Jackson, 1976. Optimum start control- Why now? Build. Serv. Eng., 44, A24-44.

T. M. Rossi and J.E. Braun, 1997, A statistical rule-based fault detection and diagnostic method for vapor compression air conditioners. Int J Heat Ventil, Air Cond Refrig Res 3 (1), pp. 19–37.

TRNSYS. 2004. TRNSYS 16 Documentation, http://sel.me.wisc.edu/trnsys

Urbanski, M. K. and Wasowski, J., 2003, Fuzzy Approach to the Theory of Measurement Inexactness, Measurement, V34(1): 67-74.

Wang S.W., Chen Y.M., 2004, Sensor Validation and Reconstruction for Building Central Chilling Systems Based on Principal Component Analysis, Energy

Conversion and Management 45 673-695.

Wang, S.W., J.B. Wang and J. Burnett, 2000, Mechanistic model of centrifugal chillers for HVAC system dynamics Simulation, Building Service Engineering Research and Technology, 21(2): 73-83

Wang S.W. and J.T. Cui, 2005, Sensor-fault detection, diagnosis and estimation for centrifugal chiller systems using principal-component analysis method, Applied Energy, 82(3):197-213.

Wang S.W. and Wang J.B., 1999, Law-Based Sensor Fault Diagnosis and Validation for Building Air-conditioning Systems, HVAC&R Research, Vol.5 (4), pp.353-378

Wang S.W. and Wang J.B, 2002, Automatic sensor evaluation in BMS commissioning of building refrigeration systems, Automation in Construction, Vol.11(1), pp. 59-73

Wang, S.W., and Z.J. Ma, 2008, Supervisory and optimal control of building HVAC systems: A review. HVAC&R Research 14(1):3-32.

W.Y. Lee, J.M. House and D.R. Shin, 1997, Fault diagnosis and temperature sensor recovery for an air-handling unit [J], ASHRAE Trans 103 (1), pp. 621–633.

X.H. Xu. 2005. Model-Based Building Performance Evaluation and Diagnosis, PhD dissertation, Department of Building Services Engineering, The Hong Kong Polytechnic University.

Xu, X.H., F. Xiao and S.W. Wang, 2008, Enhanced chiller sensor fault detection, diagnosis and estimation using wavelet analysis and principal component analysis methods. Applied Thermal Engineering, vol. 28 (2-3), pp. 226-237

Xu P, Haves P, Zagreus L. and Piette M., 2006, Demand shifting with thermal mass in large commercial buildings (field tests, simulation and results), Lawrence Berkeley National Laboratory, CEC-500-2006-009

Y.C. Chang, J.K. Lin, M.H. Chuang, 2005, Optimal chiller loading by genetic algorithm for reducing energy consumption, Energy and Buildings 37(2), pp 147–155

Yu F.W. and Chan K.T. Performance evaluation of air-cooled chiller plants for

improving design and operation. CIBSE National Conference 2002, October, Paper No. 23, 2002.

Y. Jiang, W.F. Zhu. 1999. Sensor fault detection in heating, ventilation and air-conditioning systems, Journal of Tsinghua University (Sci and Tech), 39 (12) 54–56, 61.

Zaheer-uddin, M., and G.R. Zheng, 2000, Optimal control of time-scheduled heating, ventilating and air conditioning processes in building, Energy Conversion and Management 41(1):49-60.

Z.J. Ma, 2008, Online Supervisory and Optimal Control of Complex Building Central Chilling Systems, PhD dissertation, Department of Building Services Engineering, The Hong Kong Polytechnic University